AFWAL - TR - 81 - 3176

HEAT TRANSFER MEASUREMENTS IN COLD WIND TUNNELS

H. L. Moody and K. Jechel
PDA ENGINEERING
1560 Brookhollow Drive
Santa Ana, California 92705

September 1982

Final Report for period May 1980 - October 1981

FLIGHT DYNAMICS LABORATORY
AIR FORCE WRIGHT AERONAUTICAL LABORATORIES
AIR FORCE SYSTEMS COMMAND
WRIGHT-PATTERSON AIR FORCE BASE, OHIO 45433

DISCLAIMER NOTICE

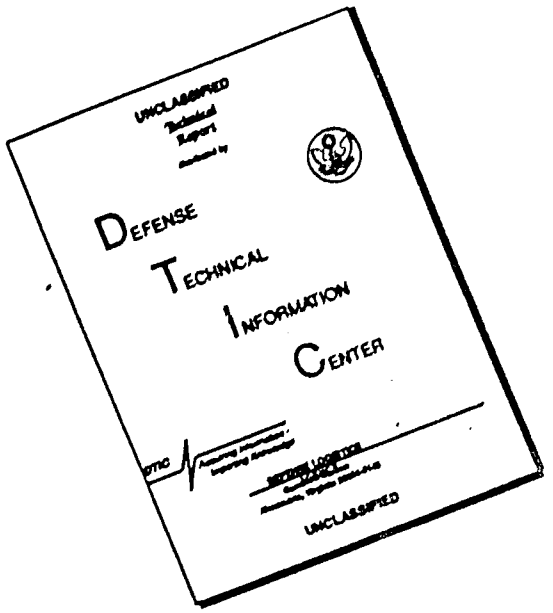

THIS DOCUMENT IS BEST QUALITY AVAILABLE. THE COPY FURNISHED TO DTIC CONTAINED A SIGNIFICANT NUMBER OF PAGES WHICH DO NOT REPRODUCE LEGIBLY.

NOTICE

When Government drawings, specifications, or other data are used for any purpose other than in connection with a definitely related Government procurement operation, the United States Government thereby incurs no responsibility nor any obligation whatsoever; and the fact that the government may have formulated, furnished, or in any way supplied the said drawings, specifications, or other data, is not to be regarded by implication or otherwise as in any manner licensing the holder or any other person or corporation, or conveying any rights or permission to manufacture, use, or sell any patented invention that may in any way be related thereto.

This report has been reviewed by the Office of Public Affairs (ASD/PA) and is releasable to the National Technical Information Service (NTIS). At NTIS, it will be available to the general public, including foreign nations.

This technical report has been reviewed and is approved for publication.

RICHARD D. NEUMANN
Tech Mgr, Aero Heating Gp.

J. CHRISTOPHER BOISON
Chief, High Speed Aero Perf. Branch

FOR THE COMMANDER

JOHN R. CHEVALIER
Colonel, USAF
Chief, Aeromechanics Division

If your address has changed, or if you wish to be removed from our mailing list, or if the addressee is no longer employed by your organization, please notify AFWAL/FIMG, W-PAFB, OH 45433 to help us maintain a current mailing list.

Copies of this report should not be returned unless return is required by security considerations, contractual obligations, or notice on a specific document.

UNCLASSIFIED
SECURITY CLASSIFICATION OF THIS PAGE *(When Data Entered)*

REPORT DOCUMENTATION PAGE		READ INSTRUCTIONS BEFORE COMPLETING FORM
1. REPORT NUMBER AFWAL-TR-81-3176	2. GOVT ACCESSION NO. AD-A135740	3. RECIPIENT'S CATALOG NUMBER
4. TITLE *(and Subtitle)* HEAT TRANSFER MEASUREMENTS IN COLD WIND TUNNELS		5. TYPE OF REPORT & PERIOD COVERED Final Report 1 May 1980 to 26 October 1981 6. PERFORMING ORG. REPORT NUMBER PDA TR 5530-00-02
7. AUTHOR(s) H. L. Moody and K. Jechel		8. CONTRACT OR GRANT NUMBER(s) F33615-80-C-3002
9. PERFORMING ORGANIZATION NAME AND ADDRESS PDA Engineering 1560 Brookhollow Drive Santa Ana, California 92705		10. PROGRAM ELEMENT, PROJECT, TASK AREA & WORK UNIT NUMBERS 62201F, 2307, 2307N4, 2307N441
11. CONTROLLING OFFICE NAME AND ADDRESS Flight Dynamics Laboratory (AFWAL/FIMG) Air Force Wright Aeronautical Laboratories (AFSC) Wright-Patterson Air Force Base, Ohio 45433		12. REPORT DATE September 1982 13. NUMBER OF PAGES 162
14. MONITORING AGENCY NAME & ADDRESS*(if different from Controlling Office)*		15. SECURITY CLASS. *(of this report)* UNCLASSIFIED 15a. DECLASSIFICATION/DOWNGRADING SCHEDULE

16. DISTRIBUTION STATEMENT *(of this Report)*

Approved for public release, distribution unlimited.

17. DISTRIBUTION STATEMENT *(of the abstract entered in Block 20, if different from Report)*

18. SUPPLEMENTARY NOTES

19. KEY WORDS *(Continue on reverse side if necessary and identify by block number)*

Instrumentation
Heat Transfer
Cold Wind Tunnels

20. ABSTRACT *(Continue on reverse side if necessary and identify by block number)*

Investigations were performed on instrumentation concepts for the purpose of acquiring heat transfer and recovery temperature measurements on models to be tested in cold wind tunnels. The problem in cold wind tunnels is the recovery and model initial (or ambient) temperature can be of the same level so that the temperature excursion during test is generally negligible. (continued)

DD FORM 1 JAN 73 1473 EDITION OF 1 NOV 65 IS OBSOLETE

Unclassified

Block 20. Abstract (continued)

A literature search was performed from which 13 candidate instrumentation concepts were identified for further investigation. Detailed analysis and design efforts were performed on the candidates to identify measurement errors, fabrication, data reduction procedures and costs. Based on technical merit and cost, four sensors were selected for cold wind tunnel applications. These sensors include the 2-D foil (Gardon) and wafer thermopile calorimeters, liquid crystals and thermal phosphors. Hybrid designs using thin film resistance thermometers are recommended for the later two sensors. To cause a temperature excursion during model test, internal heating of the model with hot fluid is selected for the 2-D foil and wafer sensors. A resistively heated metallic film applied to the model surface is selected for the liquid crystals and thermal phosphors.

PREFACE

This report was prepared by PDA Engineering, Santa Ana, California for the Air Force Wright Aeronautical Laboratory (AFWAL), Wright-Patterson AFB, Dayton, Ohio, under Contract No. F33615-80-C-3002. The report documents the technical effort which was performed from 1 May 1980 to 26 October 1981 on heat transfer measurement sensors for use in cold wind tunnels. Mr. Richard Neumann of AFWAL/FIMG provided technical direction.

Mr. Henry Moody was the PDA Program Manager and principal investigator for this effort. Mr. Kurt Jechel supported the literature search.

TABLE OF CONTENTS

LIST OF ILLUSTRATIONS

LIST OF TABLES

1.0 INTRODUCTION AND SUMMARY

A large number of supersonic ground test facilities, operated by government agencies and private industry, are available for experimental research and vehicle design development. Many of these facilities originally were designed for aerodynamic testing and, as a result, use cold gas supplies for cost effectiveness. The heat transfer potential produced in these facilities is very low for unheated/uncooled models, which serverely restricts their capability to perform heat transfer experiments. The objective of the program was to evaluate techniques that can be used to acquire heat transfer data in these cold gas facilities in a cost effective manner. Heat transfer data acquisition in cold gas facilities not only will increase facility capabilities, but also will extend the range of Mach number and Reynolds number conditions over which heat transfer data can be measured.

The technical plan that was followed in the program is presented in Figure 1. The technical effort involved three major tasks. In the first task, Measurement Concept Reivew, an exhaustive literature search and engineering design analysis was performed to identify potential measurement concepts. From this task, thirteen concepts were identified for further review. These concepts are summarized in Table 1. The second task, Concept Evaluation, involved detailed engineering and cost reviews of each selected concept. The cost and performance of each concept were compared to "conventional" thin skin measurement techniques that have been extensively used in hot wind tunnel facilities. Four concepts were identified that offer the capability of acquiring high quality heat transfer measurements in a cost-effective manner. These sensors include

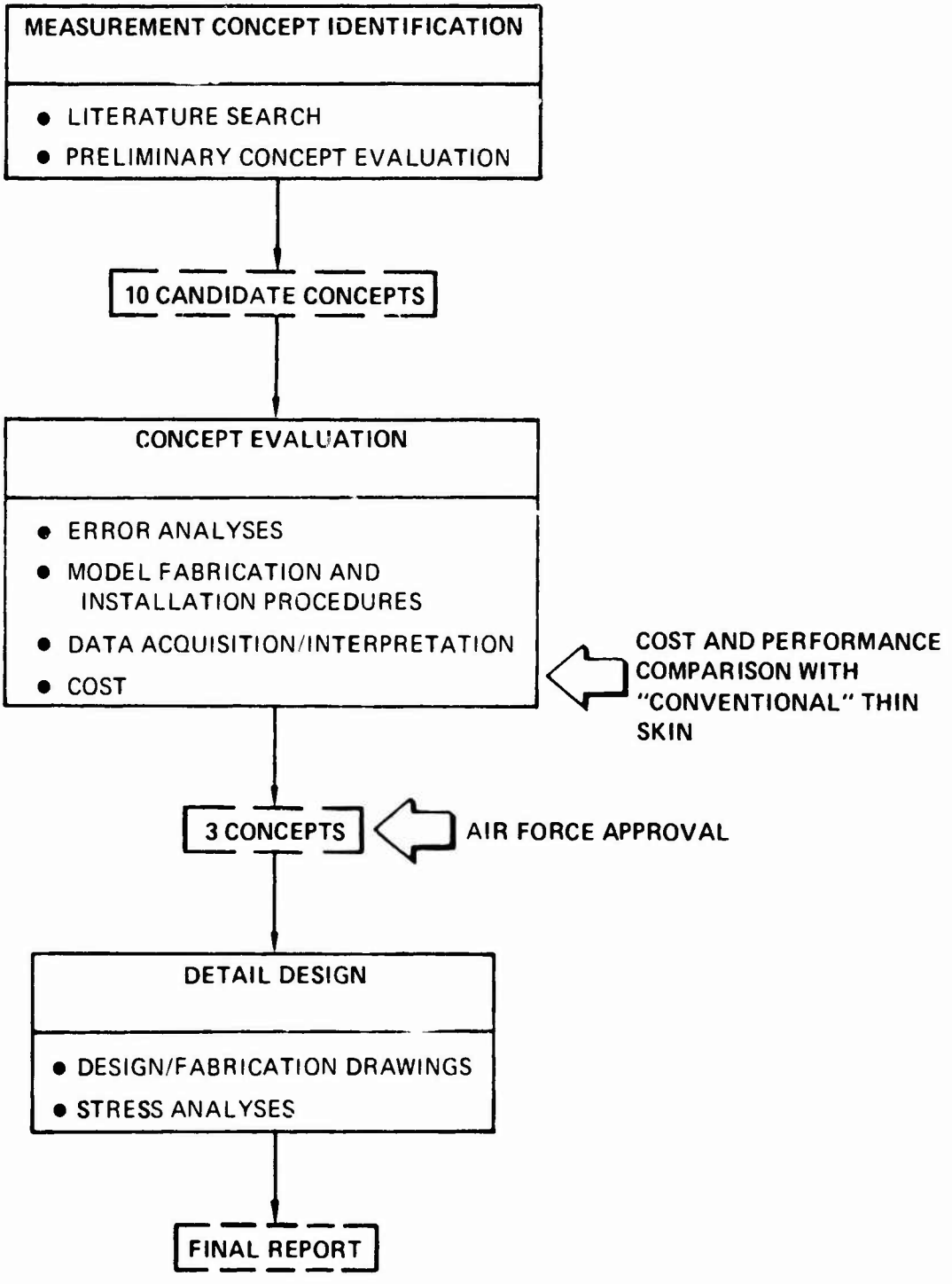

Figure 1. Program Plan

Table 1. Heat Transfer Measurement Concepts of Cold Wind Tunnels

INSTRUMENT / CALORIMETER	CONVENTIONAL T/C	THERMOPILE	THIN FILM RESISTOR	SEMICONDUCTOR T/C	THERMISTOR	PYROELECTRIC	LIQUID CRYSTALS	THERMAL PHOSPHORS	IR SCANNER	PHASE CHANGE PAINTS	LOW TEMP. ABLATORS
1-D Thin Skin	(1)				x						
2-D Foil	(2)	x									
Semi-Infinite Solid	(3)		(5)	(6)	(8)	(9)	(10)	(11)	(12)	(13)	x
Wafer	x	(4)		(7)							
Null Point	x										
Slug	x				x						
Resolution Enhancement		may not be required		may not be required		may not be required					cooling for stblty.
External quartz Lamps	(x)	(x)	x	(x)	(x)	(x)	(x)	(x)	(x)	(x)	
Self-Heating			(x)		x						
Metalized Resistance Heater	(x)			x	(x)		(x)	(x)	(x)	(x)	
Microwave	x	x		x	x	x					
Hot Fluid	(x)	(x)	x	x	x	x					

(x) Recommended for further investigation.

the 2-D foil (Gardon) and wafer thermopile calorimeters, liquid crystals and thermal phosphors. Hybrid designs using thin film resistance thermometers are recommended for the later two sensors. To cause a change in temperature that is above ambient; internal heating of the model with hot fluid is selected for the 2-D foil and wafer sensors. A resistively heated metallic film applied to the model surface is selected for the liquid crystals and thermal phosphor sensor concepts.

The investigations that were performed in the program are presented in the following paragraphs. The technical features of the cold wind tunnel that were used in the investigations are presented in Paragraph 2.0. The instrumentation design analyses are described in Paragraph 3.0. The sensors are compared on technical merit and cost effectivenses in Paragraph 4.0.. Paragraph 5.0 presents the sensor recommendations. The sensor design/fabrication drawings are presented in Appendix C. The literature search is presented in Appendix A and a computer code developed to analyze sensor thermal response is presented in Appendix B.

2.0 WIND TUNNEL FEATURES

The sensor concepts were investigated based on the following wind tunnel features that were derived from the Mach 3 facility users manual (AFFDL, Wright-Patterson Air Force Base, August 1977).

(1) The tunnel supply temperature can be below the ambient or room temperature value, therefore, as worst-case, supply temperature was assumed less than the initial model temperature.

(2) The facility cannot inject the model into the test section after the flow has stabilized. Therefore, the model is assumed to be in the flow during flow stabilization.

Because the model recovery temperature can be less than the initial model temperature, some type of auxiliary heating or cooling of the model is required for the measurement of convective coefficients. Auxiliary heating methods that have been identified as candidates include external quartz lamps, self-heating for resistance thermometers, metallized resistance heaters applied to the model surface, and the circulation of hot fluid in the model itself. Methods that were rejected included laser heating, microwave, and a model glove. Laser heating is localized, which can result in large model temperature gradients, thus effecting the thermal boundary layer. Microwave heating is complex relative to fluid heating, especially when trying to position and insulate RF coils in the 1.0-inch diameter model. A cooled or heated model glove that is removed after flow stabilization may require an extensive design program to prevent secondary shocks and tunnel flow blockage. Flow disturbances induced by the glove and/or glove removal

event must not significantly interfere with the model thermal distribution, thereby causing the model initial conditions to be ill-defined. Also, depending on model complexity, it may be required that the glove be designed for a particular model design which does not allow flexibility in model geometry.

Aerodynamic heating conditions were estimated for the AFWAL Mach 3 tunnel on an ogive-cylinder model at an angle-of-attack between 0 and 10°. The tunnel conditions were obtained from the facility user manual. The calculations were performed with the PDA NOHARE code.* The heat flux and recovery temperatures are presented in Figures 2 and 3. Figure 2 presents the model heating distributions for a near upper-limit in facility operating pressure, P_o = 570 psia. Figure 3 presents the model heating distributions for the lower level of facility operation, P_o = 70 psia. In both cases, the supply temperature was assumed to be 490°R. These heating distributions were used in the computer code to evaluate each candidate instrumentation system.

*Smith, D.H., et al, "Computer Codes for Nosetip Recession and In-Depth Thermal Analysis: NOHARE, NOSEC, NODGEN", PDA TR 5002-00-01, January 1976.

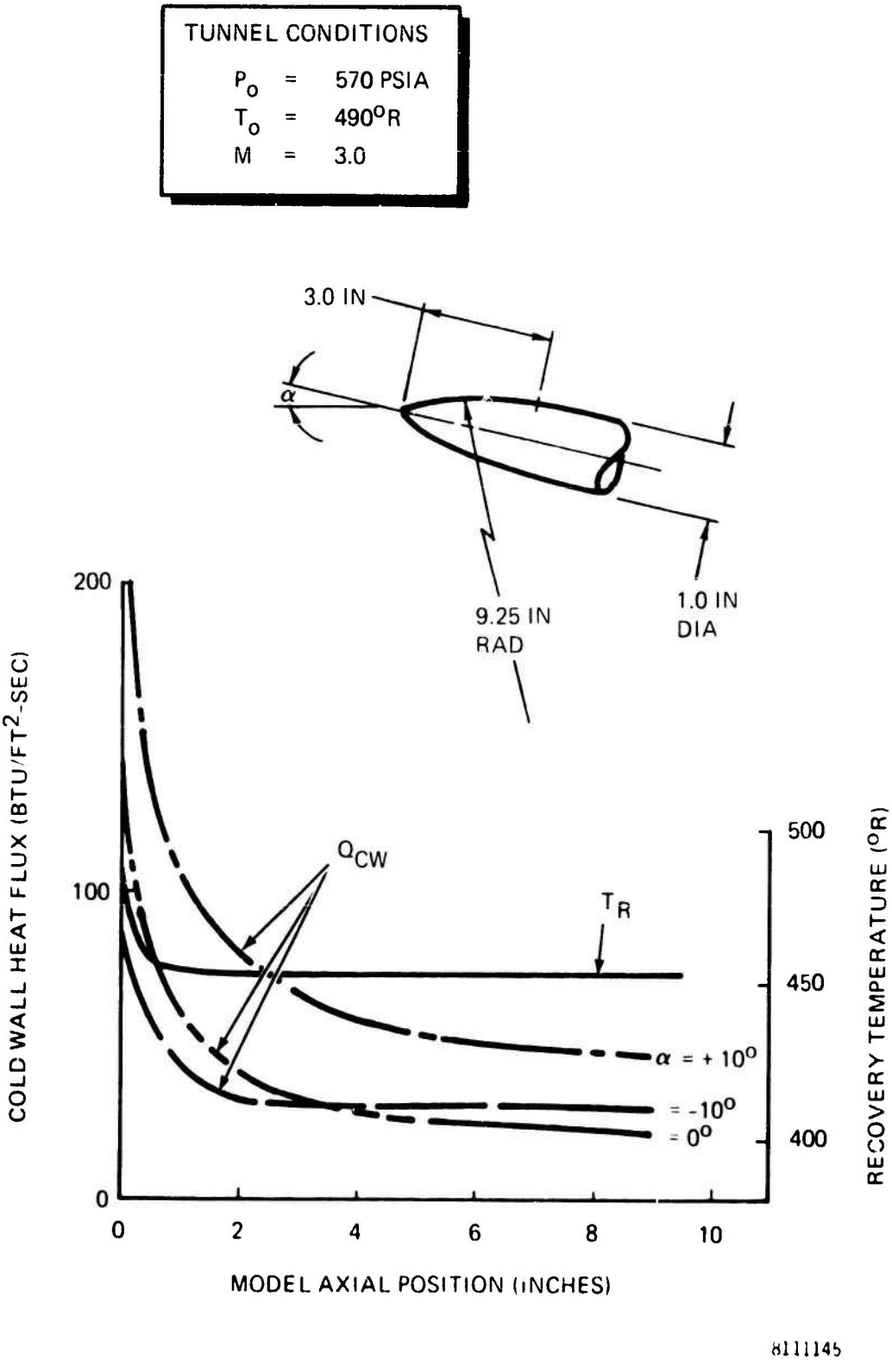

Figure 2. Model Convective Parameters, P_o = 570

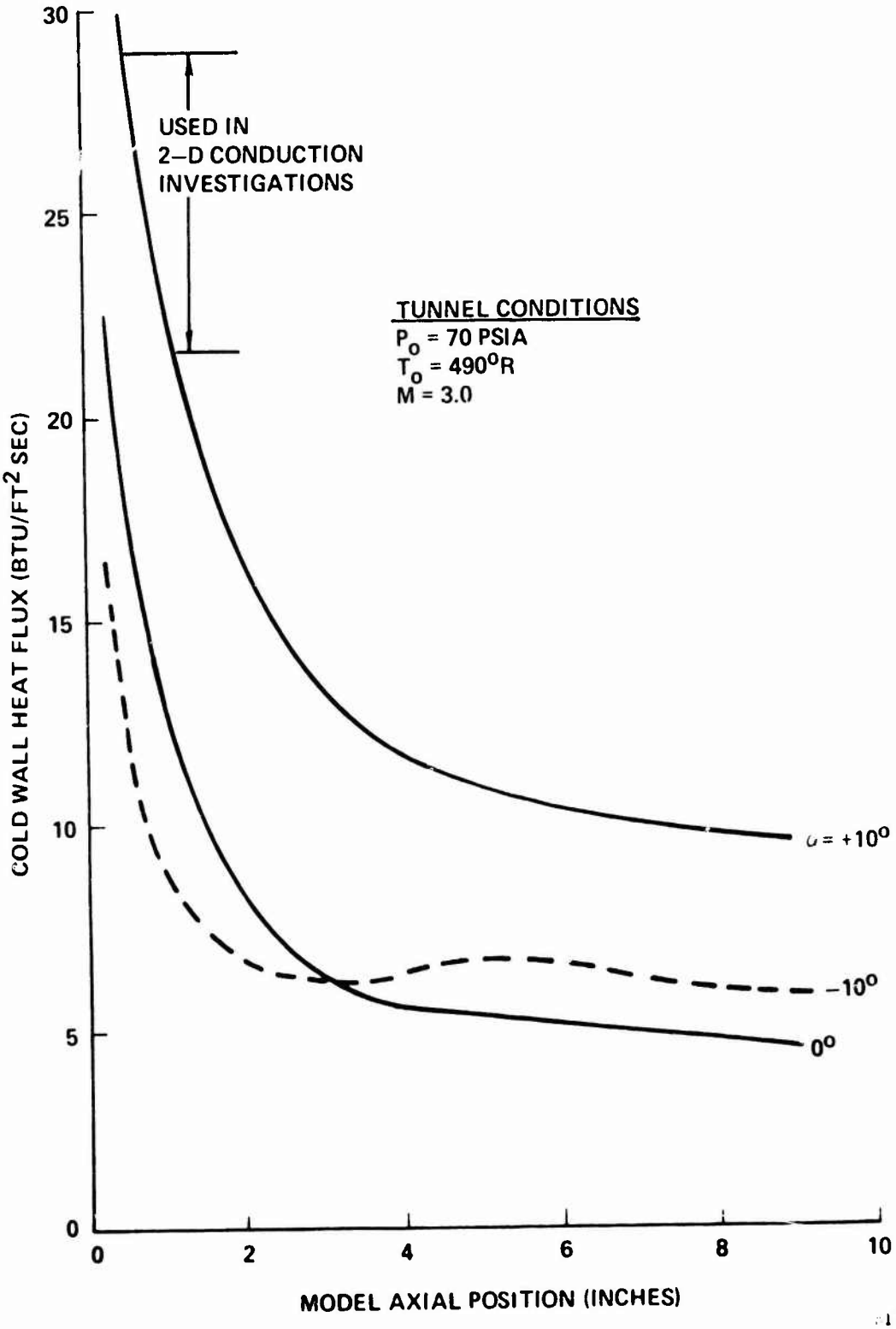

Figure 3. Parameters, P_o = 70

3.0 INSTRUMENTATION DESIGN STUDIES

3.1 1-D Thin Skin

This is the reference system to which all other instruments will be compared. The thin skin concept is designed so heat transfer is 1-D and conduction losses through the temperature measurement device are negligible. A schematic of the sensor is presented in Figure 4 and is similar in construction to the 2-D foil gage of Paragraph 3.2. In the design of the thin skin gage the metal thickness, δ, hole radius, R_o, and T/C diameter, d_{TC} are sized to minimize conduction losses. In contrast, the 2-D foil gage utilizes an additional T/C lead so that the radial temperature gradient from the foil center to the outer structure is measured. This gradient is sized for a given condition by varying the foil thickness, δ, and hole radius, R_o. Temperature can be measured using conventional T/C, semiconductor T/C, thermistors and/or resistance thermometers. In the selection of the measurement device, model fabrication methods and cost must be considered because of the small model size (1.0-inch diameter).

The model fabrication methods outlined in Reference DM-89* were selected for the 1-D thin skin. This involves casting the epoxy model (Stycast 2762FT) on a steel tube and machining the epoxy model about 0.003 inch below nominal radius. The steel tube provides model support and also a lead wire passage. At the locations where 1-D thin skin calorimeters are desired, holes of a diameter to be discussed, are drilled radially in the epoxy to join with the center steel tube. The model is then placed in

*References are listed in Appendix A, Literature Search

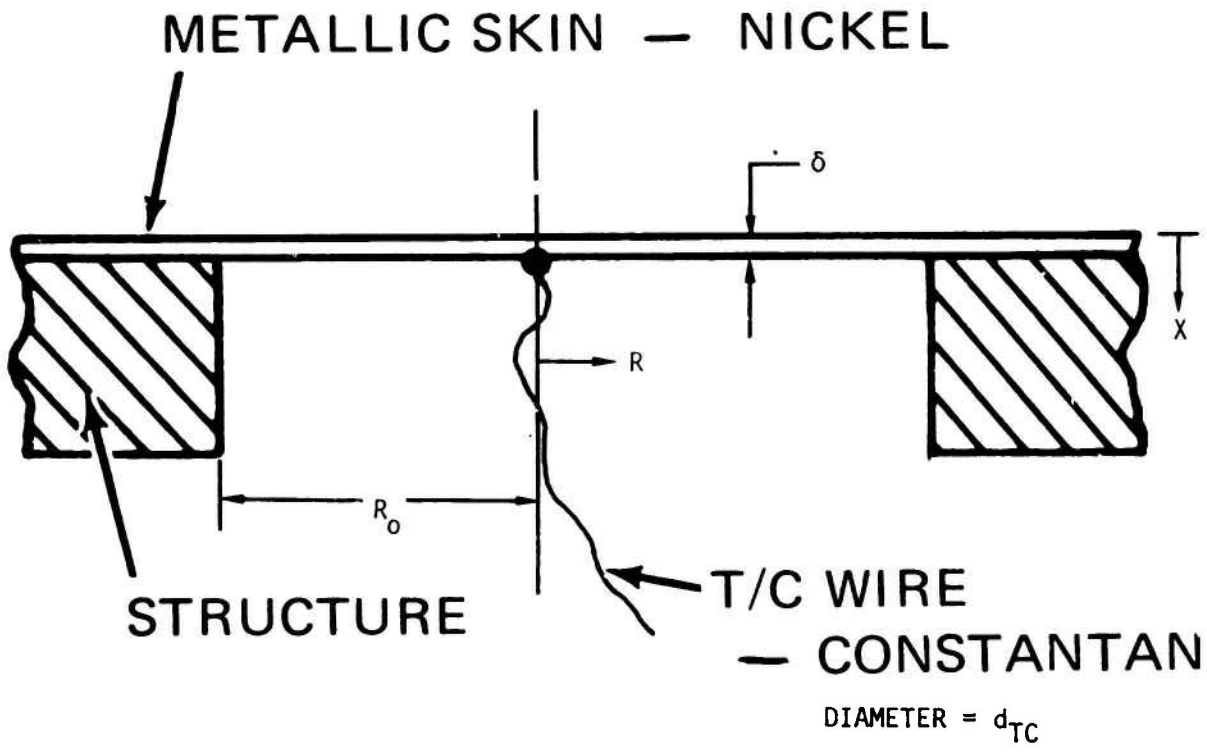

Figure 4. 1-D Thin Skin

a female mold with a small hole at the center of each radial hole to allow T/C wire pulling. A single constantan wire is then pushed through the small hole in the female mold into the center steel tube and out the aft end of the model. A small amount of excess constantan wire is left in the female mold. After all wires are located in the model and strain relieved by bonding them to the center tube, the assembly is heated and a wax (Cerrotru) is poured into the center tube to fill all the radial holes. Vacuum is applied during different stages in the wax pour to minimize air pockets. After the wax has hardened, the model is removed form the female mold. The surface is sanded or additional wax is added to result in a smooth surface, making sure that each constantan wire protrudes from the model surface. The model is then plated with approximately .001 to .0015 inch of electroless nickel using the techniques outlined in Reference DM-89. The exposed constantan wire is then removed and an additional .001 to .0015 inch of nickel is plated to form a smooth surface at the wire junction. The studies of DM-89 showed that nickel could be plated on the epoxy and wax material to form a smooth surface that is compatible at temperatures up to 810°R. After model plating, the model is heated to remove the wax.

It was concluded by reviewing the fabrication procedures with other temperature measuring devices, that the nickel-constantan T/C and possibly the thermistor are simpler to fabricate, and possibly lower in cost. The semiconductor T/C and resistance thermometer require access to the backface of the foil for installation which is difficult for the 1-inch in diameter x 9-inch in length ogive-cylinder model. This may require fabricating the model into two halves for installation. The

thermistor could possibly be fabricated using the above steps. This device, although more sensitive than the T/C, requires two lead wires instead of one, thus increasing lead wire conduction losses. The greater number of lead wires also doubles the probability of failure. The thermistor requires ceramic insulation with bead diameters typically 0.007 to 0.014-inch (DM-85), thus adding thermal mass in the sensor area. The nickel/constantan T/C, in comparison, adds very little additional thermal mass because wire diameters between 0.001 and 0.003-inch can be used. Both devices, however, are candidates for the 1-D thin skin gage.

A constant for the thin skin gage that must be evaluated either by direct laboratory calibration or from prior measurements is the product of density, specific heat and thickness of the nickel plate, $\rho C\delta$. The use of prior property data measurements and actual thickness measurement of the plate is relative to laboratory calibration, more cost effective, but somewhat less accurate. The method to be used for constant evaluation will depend on cost vs. desired accuracy for the particular application. In the sensor investigations that follow, laboratory calibration was selected because the model design and fabrication procedures could produce material properties that differ from handbook values. Laboratory investigations of recommended design and fabrication procedures should identify the applicability of handbook properties.

Because the tunnel supply temperature can equal the initial model temperature, auxiliary model heating (or cooling) will be required. By the very nature of the thin skin design, the T/C or thermistor is isolated from the adjacent model wall so that conduction is 1-D (i.e., minimal conduction losses to adjacent surfaces). Thus, internal model

heating is not attractive. Possible methods for external heating are quartz lamps or surface resistance heating. External quartz lamps could be placed in the outer regions of the test cell and focused on the model. Quartz lamps capable of producing up to 5 Btu/ft^{2}sec of radiant energy on the model can be commercially obtained (e.g., Ealing, Oriel, Klinger). Operation procedures with the quartz lamps would involve the following:

(1) Laboratory calibration of each thin skin T/C using a radiant heat source to determine the constant $\rho c\delta$ in the thin skin heat balance:

$$\alpha q_{rad} = \rho C\delta \frac{dT}{dt} \qquad (1)$$

The absorptivity of the sensor, α, is measured in the laboratory. The absorptivity and $\rho C\delta$ measurement can be performed, for example, at Hy-Cal or Medtherm.

(2) Wind tunnel calibration (with the tunnel off) of the incident model radiation from external quartz lamps. The $\rho C\delta$ measured in Step 1 and the measured model temperature response is used to calculate the incident heating q_{rad} in Equation 1. Note that heating need not be uniform on the model. To minimize errors, the lamp radiation must be reproducible or measured between wind-on and wind-off conditions.

(3) With lamps off, the tunnel is started. After the flow has stabilized, and the model has come to near thermal equilibrium, the 1-D thin skin T/C outputs are recorded to determine recovery temperatures, T_R. The lamps are then turned on and the transient temperature changes are measured along with the final quasi-steady-state temperature levels. The test is then terminated.

(4) The transient response of the thin circular sensor of Figure 4 where the temperature gradient in the X direction is negligible is:

$$\rho C \delta \frac{dT}{dt} = \frac{K\, d^2 T}{dr^2} + \frac{K}{r} \frac{dT}{dr} - \epsilon \sigma T^4 + h\,(T_R - T) + \alpha\, q_{rad} \quad (2)$$

Assuming that the temperature gradient in the radial direction and self-radiation are both negligible results in:

$$\rho C \delta \frac{dT}{dt} = h\,(T_R - T) + \alpha\, q_{rad} \quad (2a)$$

Equation 3 can be used to evaluate the convective heat transfer coefficient for relatively short test times (transient model response). For longer times, the model approaches steady state and the data reduction equation reduces to:

$$h\,(T - T_R) = \alpha\, q_{rad} \quad (3)$$

In the above equations, T is the instantaneous temperature. It must be noted that if the transient method is used, then shutters on the lamps will be required so that the initiation of radiant heating; i.e., the start of model heating is known. This is not required for the steady-state method.

Instead of external lamps, the model can be resistively heated by the passage of current through the nickel plate on the surface of the model. The nickel is plated on the surface with a portion of the surface "masked" to result in a plated nickel resistance element on the surface, so that when a voltage is applied across the resistor ends, a reasonable distribution of heating results over the model surface. For the model under consideration, 500 watts of electrical power will produce the same temperature conditions as the quartz lamp method with 2.5 Btu/ft^2 sec of indicent radiation. Operation with the resistance heater is similar to that of the quartz lamp, and is as follows:

(1) Determine $\rho C\delta$ in the same manner as for the quartz lamp method. (This step is not required if the steady-state solution, Equation 3, is applicable.)

(2) Measure the electrical heat dissipation as a function of temperature in the laboratory. Because the resistivity is temperature-dependent and varies with material purity (Reference DM-63), the nickel plate over each thin skin section should be calibrated. Calibration can involve waxing or greasing a reference calorimeter (e.g., wafer thermopile calorimeter made by Hy-Cal, Medtherm or RdF) on the model's external surface over the thin skin area so that essentially all the local heater power is conducted into the calorimeter. By applying power to the heater in steps and allowing the model to equilibrate, the electrical dissipation, q_{elect}, as a function of temperature, is measured and the constants C_1 and C_2 can be evaluated from:

$$q_{elect} = C_1(T - T_o) + C_2 \qquad (4)$$

(3) Same as Step 3 for the quartz lamp method.

(4) Same as Step 4 for the quartz lamp method, except q_{elect}, which is a function of temperature, is substituted for q_{rad}.

For the resistance heating method to measure temperature in the steady-state condition, two T/C lead wires will be required. That is, the nickel plate cannot be used as the other T/C lead because of the current required for heating. One T/C lead can, however, be used in the transient condition because the heater need not be functional after the model is brought to a satisfactory temperature. The requirement for two lead wires

makes the thermistor attractive, especially if the 1-D thin skin gage can be operated in steady-state, thus eliminating the effect of thermistor thermal mass (bead diameter ~ 0.007 inches vs. ~ 0.003 inches of nickel plate).

In the design of thin skin gages, T/C lead wire conduction, T/C thermal mass (not important in steady-state), and 2-D conduction effects need to be considered in order to determine the validity of using Equations 1, 2 and 3 to perform the data reduction. These were evaluated using the finite difference thermal model developed specifically for direct contact instruments (presented in Appendix B). The materials selected for the model were based on the experience in model fabrication described in DM-89. These materials and their properties (DM-89) were used to size the sensor. The material properties are presented in Appendix B. Important sensor parameters are T/C wire diameter, plate thickness, and radius of the thin skin section (i.e., hole in the epoxy structure). The analyses were applied to the operational steps as outlined above for both the quartz lamp and electrical resistance heating methods. In both cases, the tunnel conditions were q_{cw} = 20 Btu/ft^{2}sec, T_R = 478.8°R with the model initially at a constant temperature of 478.8°R. For the quartz lamp, q_{rad} = 2.5 Btu/ft^{2}sec. For electrical resistance heating:

$$q_{elect} = -.0078\ (T - T_o) + 2.5\ \text{Btu/ft}^2\text{sec}$$

where the constant .0078 was obtained from Reference DM-63 for nickel and the constant 2.5 was set equal to the quartz lamp power. The results of the analyses are presented in Figure 5. The error in the convective

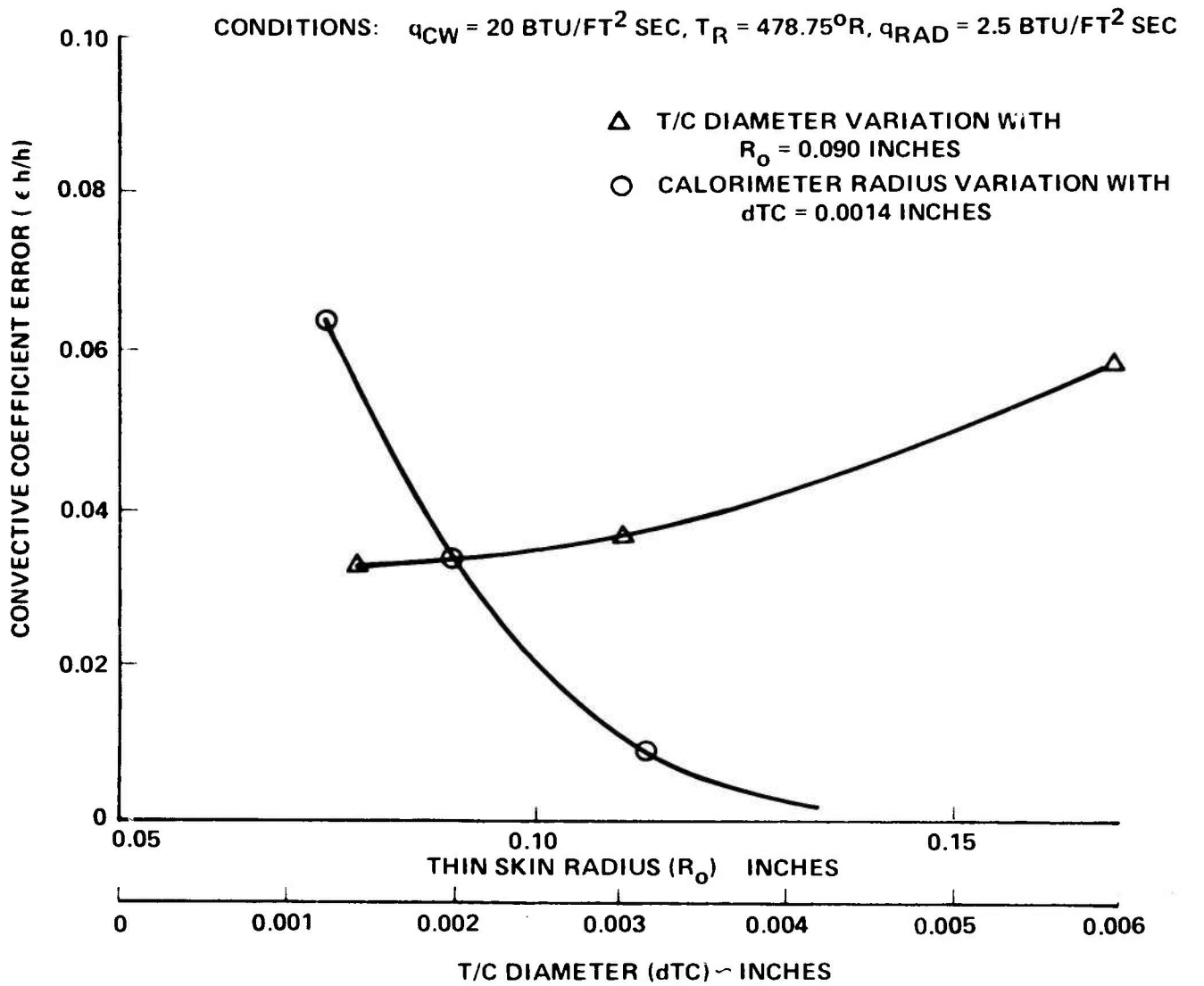

Figure 5. 1-D Thin Skin Design Study (Steady State Operation δ = .003")

coefficient, presented in Figure 5, was determined by applying Equations 1, 2 and 3 to the computer results to infer convective coefficient. These coefficients are then compared with the actual to determine the error. As can be noted from the figure, the error produced by 2-D conduction becomes significant for a thin skin radius less than 0.090 inches. The error produced by T/C lead wire conduction is reasonable for wire diameters less than 0.003 inches.

Error analyses were applied to a sensor design with a plate thickness of 0.003 inch, a T/C diameter of 0.003 inch and a thin skin section radius of 0.090 inch. These features reduce conduction errors to a reasonable level and do not make model fabrication difficult. That is, PDA has successfully fabricated similar models with wire diameters of 0.001 inches. Reference DM-63 has plated .003-inch thick nickel successfully. At the upper tunnel supply pressure (570 psia), the gas pressure on the ogive surface in the vicinity of where the 0.090-inch radius gage can be placed is 10 atm. This induces a shear stress of 2400 psi, which is less than the 24000 psi shear strength reported for plated nickel (Reference DM-63).

An error analysis was performed on the thin skin design to determine the accuracy of the quartz lamp and resistance heating methods. The error analysis considered T/C lead wire conduction, 2-D conduction to adjacent structure, thermal mass of T/C wire, effects of gradient in the convective coefficient, calibration, and temperature measurement. The Taylor series method of error propagation was applied as follows:

$$\frac{\varepsilon_h}{h} = \pm \frac{1}{h} \left\{ \sum_{i=1}^{n} \left(\frac{dh}{dP_i} \right)^2 \left(\varepsilon_{P_i} \right)^2 \right\}^{1/2} \qquad (5)$$

where εp_i is the uncertainty in parameter P_i.

The errors were estimated as follows:

(1) Indepth temperature gradient through .003-inch nickel plate with free air convection on inside surface of nickel is calculated to be $0.02^{\circ}R$.

(2) Laboratory calibration error in Step 1 for both quartz lamp = $\pm 3\%$ on the measurement of $\rho C\delta$ (Reference DM-35).

(3) For lamp heating, the total error, ε_h/h , produced by lead wire conduction, 2-D conduction to adjacent structure, and free convection in the tunnel calibration, Step 2, were predicted using a computer code to be a total of 3.4% for one 0.003-inch diameter lead wire.

(4) For resistance heating, the total error, ε_h/h , produced by T/C, 2-D conduction to adjacent structure, free convection in tunnel calibration, and nonuniform power dissipation over gage surface due to temperature gradients were predicted using a computer code to be a total of 6.8% for two 0.003-inch diameter lead wires.

(5) T/C temperature measurement error for both recovery and surface temperature is approximately .75% of the absolute temperature value (Reference OS-40), or $\pm 4^{\circ}R$ for the thin skin.

(6) Uncertainty in incident radiation for quartz lamp method: (a) intensity variation in lamp = 5% (Oriel Optics), (b) temperature measurement error of $\pm 4^{\circ}R$ produces an error of 5.7% in q_{rad} per Equation 1. Error due to $\rho C\delta$ measurements, free convection and conduction losses has been included in Item (1), above.

(7) The calibration of electrical dissipation (Step 2 for resistance heating) is 3% in the measured heat flux (Reference DM-36). The heat losses that occur during calibration are estimated to be 4%.

Using the above error estimates and Equations 1, 2, 3 and 4 in conjunction with the Taylor series (Equation 5), the errors presented in Table 2 were obtained.

Table 2. Heat Transfer Coefficient Error (q_{cw} = 20 Btu/ft^{2}sec, T_R = 478°R)

Heating Method	Data Reduction Method	Error, ε_h/h
Quartz Lamp	Transient, Eqn. 2	0.18
Quartz Lamp	Steady-State, Eqn. 3	0.14
Resistance	Transient, Eqn. 2	0.18
Resistance	Steady-State, Eqn. 3	0.15

From the computer analyses of error items 3 and 4 above, quasi-steady-state conditions were achieved in less than 5 seconds. Thus, tunnel run times less than 30 seconds appear to be satisfactory for the high tunnel supply pressures. This time will, of course, increase with lower tunnel supply pressures.

From the error analysis, both heating methods have essentially the same measurement uncertainty. The quartz lamp method has the undesirable feature of requiring tunnel modifications and is therefore likely to be more expensive than the resistance heater method. The

resistance heater method has the disadvantage of being more complex in model fabrication because of the electrical insulation and masking of the nickel foil required to form the resistance heater. However, before the resistance method is selected over the quartz lamp method, it is recommended that a small laboratory effort be performed to evaluate the quality of the resistance heater model (i.e., surface roughness between plated and masked regions, plate structural integrity, etc.). However, in this program, resistance heating was selected over external lamp heating because of lower costs that may be inherent in the former concept.

Use of a thermistor instead of a thermocouple to measure temperature would reduce the temperature measurement error. Because the thermistor has ceramic insulation over the sensor and relative to the T/C's greater thermal mass, operation of the thermistor in the steady-state condition (Equation 3) is desirable. Using a thermistor with a temperature mesurement uncertainty of $\pm 0.5^{\circ}R$ (Reference DM-85) to measure temperature in the steady-state condition, the convective coefficient measurement error is 8%. T/C models, similar to those required in the cold wind tunnel design have been fabricated (References DM-89 and -114), thus there is a good probability of fabricating high quality models. Fabrication of the thermistor model appears feasible but does not appear to have been performed. It is recommended that before the thermistor version is selected, that a laboratory test model be fabricated to determine nickel plate/thermistor bonding and surface uniformity.

Also the nickel-plated model has some restrictions on the temperature range over which it can operate. In Reference DM-89, difficulty was obtained in operating the plated model much over 810 R because of the difference in the coefficients of thermal expansion between nickel and the epoxy model. For the 1-D thin skin and other sensors (to be discussed) that use the nickel-plated concept, temperatures up to 660°R provide reasonable accuracy in measuring convective coefficients.

3.2 2-D Foil (Gardon Gage)

The 2-D foil concept is similar in construction to the 1-D thin skin except the former is designed so heat is transfered radially along the foil to the adjacent structure (or heat sink). Conventional data reduction techniques for the gage (References DM-2, DM-44 and DM-76) cannot be applied to the cold wind tunnel conditions because the heat flux incident in the foil is not constant over its surface (i.e., radial temperature gradient over the foil causes nonuniform convective heating when recovery temperature is on the same order as the surface temperature). This difference is shown in Figure 6 for the noted foil configuration and tunnel conditions. Figure 6 was calculated using the computer code developed for the thin skin.

The heat conduction equation for the steady-state condition with radial heat flow over the foil when the incident heat flux is a function of local temperature is:

$$\frac{d^2T}{dr^2} + \frac{1}{r}\frac{dT}{dr} = \frac{h}{\delta K}(T - T_R) \qquad (6)$$

where boundary conditions are: $r = 0$, $dT/dt = 0$, and $r = R_o$, $T = T_o$.

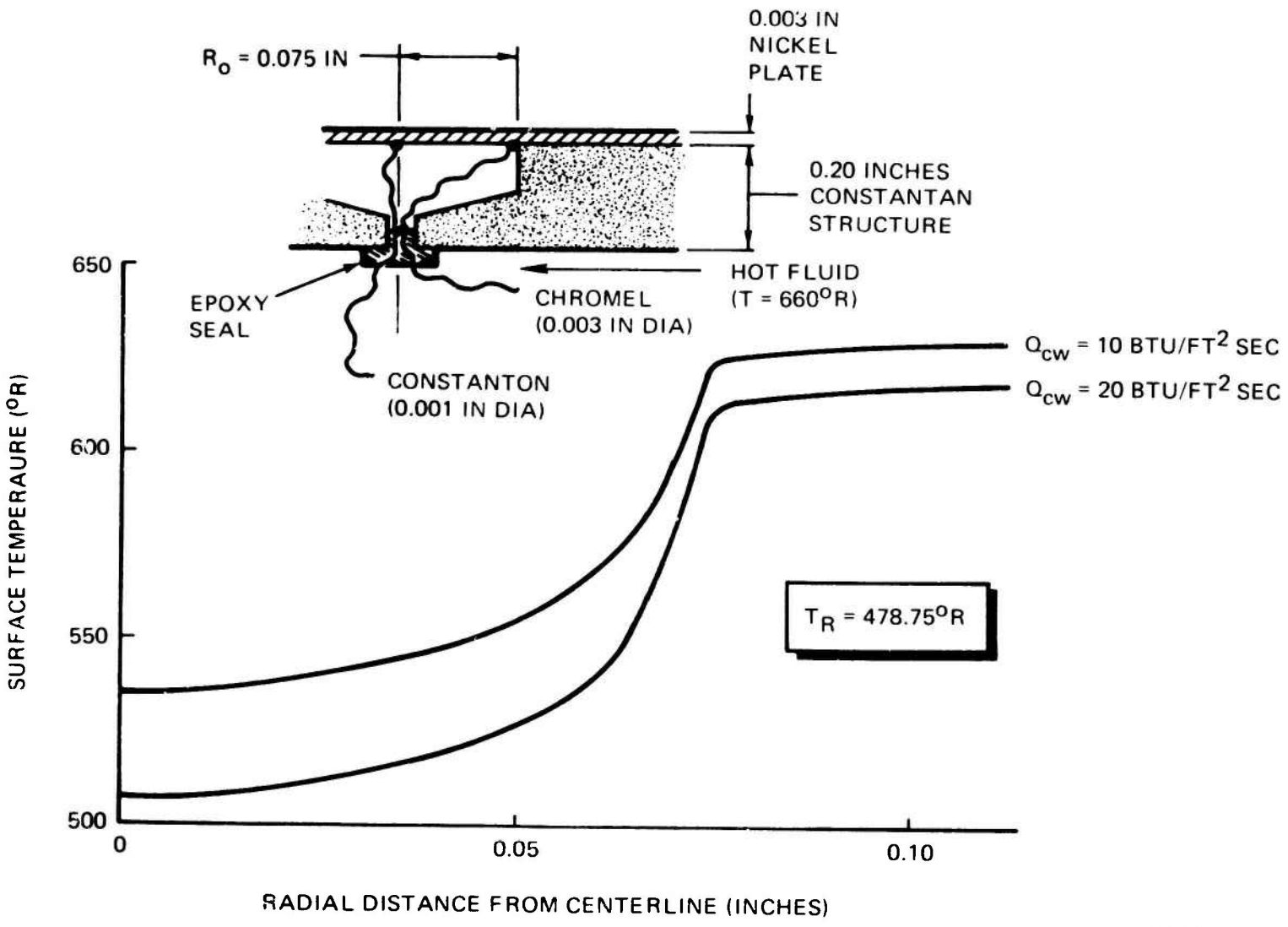

Figure 6. 2-D Foil Surface Temperature Gradient

Letting $y = T - T_R$ and $\lambda^2 = h/K\delta$, the above equation can be written as:

$$r^2 \frac{d^2y}{dr^2} + r\frac{dy}{dr} + \lambda^2 r^2 y = 0 \qquad (7)$$

which is Bessel's equation of the zero order and whose solution as outlined by Eckert and Drake* is:

$$y(r) = C_1 I_0(\lambda r) - C_2 K_0(\lambda r) \qquad (8)$$

By inspection of Equation 8, $K_0(\lambda r)$ is infinity at $r = 0$, therefore, C_2 must be zero. At $r = R_o$, $y = y_o$ then

$$C_1 = y_o / I_o(R_o \lambda) \qquad (9)$$

and temperature at the center of the disk (T_b at $r = 0$) is:

$$\frac{T_b - T_R}{T_o - T_R} = \frac{1}{I_o(R_o \lambda)} \qquad (10)$$

Use of the 2-D foil gage in the wind tunnel will require first calibrating the gage to determine the constant $R_o/\sqrt{K\delta}$ in Equation 10. That is

$$R_o \lambda = R_o \sqrt{\frac{h}{k\delta}}$$

This gage constant is determined using standard laboratory calibration procedures developed for commercially-available Gardon gages. Calibration involves a radiant heat source so the gage output ($T_o - T_b$) is related to the incident heating by

$$q_{rad} = \frac{4k\delta}{R_o^2} (T_o - T_b) \qquad (11)$$

*Eckert, E.R.G. and R. M. Drake, Heat and Mass Transfer, p. 50, McGraw-Hill, 1969.

The validity of using Equations 10 and 11 to evaluate convective coefficients in wind tunnels will depend on the ability to satisfy the assumptions used in generating the data reduction equations. These assumptions are 1) steady-state heat transfer, 2) one-dimensional heat flow in the radial direction and 3) a constant convective coefficient over the radius R_o. The ability of the gage in satisfying these assumptions was evaluated using the computer code described in Appendix B. The code was applied to the geometry and conditions shown in Figure 6. The model was initially at 478.8°R and at time = 0 the model was heated internally with water at 660°R. The code was first applied to laboratory calibration conditions with q_{rad} = 2.5 Btu/ft^2 sec to evaluate $R_o/\sqrt{K\delta}$, then to the wind tunnel condition with q_{cw} = 20 Btu/ft^2 sec. The results are presented in Table 3.

Table 3. 2-D Foil Design Studies
(δ = .003", R_o = .075", q_{cw} = 20 Btu/ft^{2}sec, T_R = 478.8°R)

Case	T/C Wire Diameter (in)	Laboratory Calibration, $\frac{R_o/\sqrt{K\delta}}{\sqrt{ft^2\text{-sec-}^\circ R/Btu}}$	Tunnel Operation, Measured h (Btu/ft^{2}sec°R)	$\varepsilon_{h/h}$ (%)
1) Equations 10 & 11 (Reference)	0.0	13.1	.0418	0.0
2) Computer Code (evaluate finite difference errors)	0.0	12.8	.0412	1.4%
3) Computer Code (design)	0.001	12.7	.0410	1.9%
4) Computer Code (design)	0.003	12.5	.0395	3.5%

For cold wind tunnel applications, a nickel foil thickness, δ = 0.003 inch, was selected to produce a structurally rugged model. The cavity radius, R_o = 0.075 inch, was selected to provide a reasonable

temperature difference, $T_o - T_b$ in Equations 10 and 11, and, at the same time, provide a spatial measurement resolution slightly better than the thin skin sensor (Section 2.1). From the computer results, it was concluded that steady-state heat transfer in the foil can be achieved within 10 seconds. One-dimensional radial heat flow is effected by the T/C wire located in the center of the gage with the resulting measurement error being a function of wire diameter. Table 3 presents the error induced by the T/C as a function of wire diameter. Case 1 in the table is the reference condition to which all other computations are compared and is the exact solution as obtained by Equations 10 and 11. Case 2 is the computer results applied to the gage with no T/C and represents the error induced by the numerical computer code. Cases 3 and 4 represent the errors induced by wires with diameters of 0.001 and 0.003 inch. These results are used in the error analyses (to be discussed) where it will be shown that the 0.003-inch diameter T/C is satisfactory.

Evaluation of fabrication and tunnel operation methods for the gage have been accomplished and are summarized below. The 2-D foil offers a number of advantages over the thin skin gage, as will be discussed.

The ogive-cylinder model is fabricated from a constantan structure over which nickel has been plated. The 2-D foil gage is formed in areas of the structure where radial holes have been machined in the constantan (see Figure 6). Model fabrication involves machining a constantan structure with a center hole for both lead wires and fluid flow (or a resistance heating element). The model is machined 0.003 inch below nominal radius. Radial holes are drilled from the outside surface to meet with the center hole. The radial holes are approximately 0.15 inch in

diameter. A chromel wire (.003-inch diameter) is welded to the outer edge of each radial hole to permit measurement of the model's surface temperature (T_o) during model operation. The model is placed in a female mold, similar to that used in thin skin model fabrication, and a single constantan wire (0.003-inch diameter) is placed in the center of each radial hole. Both the constantan and chromel wires are electrically insulated along their length. The wires are strain-relieved by epoxying their lead wires to the center of the model. Wax (Cerrotru) is then poured into the center, filling all the radial holes. The fabrication and plating procedures of the 1-D thin skin are now followed to form a 0.003-inch thick nickel plate over the entire model. The wax is melted and removed. Through the center hole, thin ceramic disks are used to cap the radial holes. The disks are then epoxied to seal the radial holes. For fluid heating, a tube is then installed in the model's central hole. This tube will provide the inlet for the hot fluid that will be used to heat the model. The annulus between the tube and constantan model will serve as the outlet. For resistance heating, an electrical heating probe is inserted in the central hole and the annulus filled with thermal grease to ensure uniform heat flow to the constantan structure.

The 2-D foil, as constructed, will measure surface temperature, T_o, at the outer edge of the radial hole by the voltage developed across the chromel lead wire and the constantan model body. The temperature difference between T_o and the center of the foil (T_o) is measured by the voltage developed across the constantan lead wire and the constantan model body. These temperatures can be related to convective coefficient by using Equation 10.

Operation procedures for the 2-D foil model should involve the following:

(1) Laboratory calibration of each calorimeter to determine the constant, $4K\delta/R^2$ in Equation 11, for the gage operating in an environment where the heat flux is essentially independent of surface temperature (i.e., radiation).

(2) With no fluid flow in the model or electrical heat dissipation, the tunnel is started and stabilized. After the model has come to nearly thermal equilibrium, the recovery temperatures are measured. Fluid (e.g., hot water) is then flowed through the model or the resistance heater is turned on and the model allowed to reach a second thermal equilibrium condition. The temperatures T_o and the difference (T_o - T_b) are measured. The test is then terminated.

(3) The convective coefficient is determined from Equation 10 using the gage constant obtained from the calibration run.

The constantan model will "smear" any large temperature variations that will occur as a result of heat flux gradients. This will only effect the measurement of local recovery temperature which, for the ogive-cylinder model, changes 10°R per inch of model length along the front part of the ogive (see Figure 2). This gradient is small and should induce a small error. "Smearing" will not effect the measurement of convective coefficients because the sensor measures heat flux only over the face of the foil and is essentially uneffected by conduction heat transfer in the model body. Thus, the measured convective coefficient is

an average over the face of the sensor.

Fluid heating (with water) will provide, relative to resistance, greater control of model temperatures, thus causing less likelihood of failing the nickel to constantan bond because of thermal expansion differences. Fluid heating, however, requires a sealed model with inlet and outlet connections. Resistance heating will require a thermal grease to enhance uniform model heating and a temperature controller to prevent model over-heating. An ullage volume will be required to handle thermal expansion of the grease. Selection of the heating method should be made using data provided by a preliminary laboratory investigation. In this program, fluid heating was selected because of greater temperature control.

An error analysis was performed on the 2-D foil gage using the procedures outlined in the thin skin section. The errors are summarized below and were estimated for q_{cw} = 20 Btu/ft^{2}sec and T_o = 478.8°R.

(1) Indepth temperature gradient through the 0.003-inch nickel plate with free air convection on the inside surface of the plate is 0.02°R.

(2) Laboratory calibration error in Step 1 above is ±3% (Reference DM-35).

(3) Recovery temperature measurement error is ±4°R (Reference OS-40) which produces, using Equation 10, an error on the convective coefficient of ±8.5%.

(4) Surface temperature measurement error, T_o, is ±4°R and also produces an error of ±8.5% on the convective coefficient.

(5) Temperature difference, $T_o - T_b$, is $\pm$0.75% of absolute or $\pm 2^{\circ}R$, whichever is greater (Reference OS-40). With this, the corresponding error in the convective coefficient is $\pm$5.6%.

(6) Conduction error because of T/C is 5.5% per Table 3.

(7) Error induced by the T/C wire not being at the center of the foil is based on a placement error of $\pm$0.010 inch during fabrication. From the computer output, Figure 6, the resulting error on convective coefficient is 1.7%.

Using the above error estimates in Equation 4 results in an RSS error of 14.3%. As can be noted in Table 3, using a small wire diameter does not reduce the error a significant amount because the measurement errors on T_R and T_o are dominating gage accuracy.

3.3 Semi-Infinite Model, Conventional T/C

A schematic of the semi-infinite model using a conventional T/C is shown in Figure 7. It may be noted in Table 1, that essentially all the instrumentation concepts can be used in the semi-infinite model configuration. For the conventional T/C the junction is formed at the intersection of the constantan wire and the nickel plate. By the very nature of the semi-infinite model, internal model heating is not applicable. Therefore, candidate heating methods are external quartz lamps or external electrical resistance heating.

Model fabrication procedures are similar to the 1-D thin skin except that no radial holes are required in the epoxy model. T/C wires are located in a female mold. Epoxy is then poured and cured. Plating follows the same procedures as outlined for the thin skin.

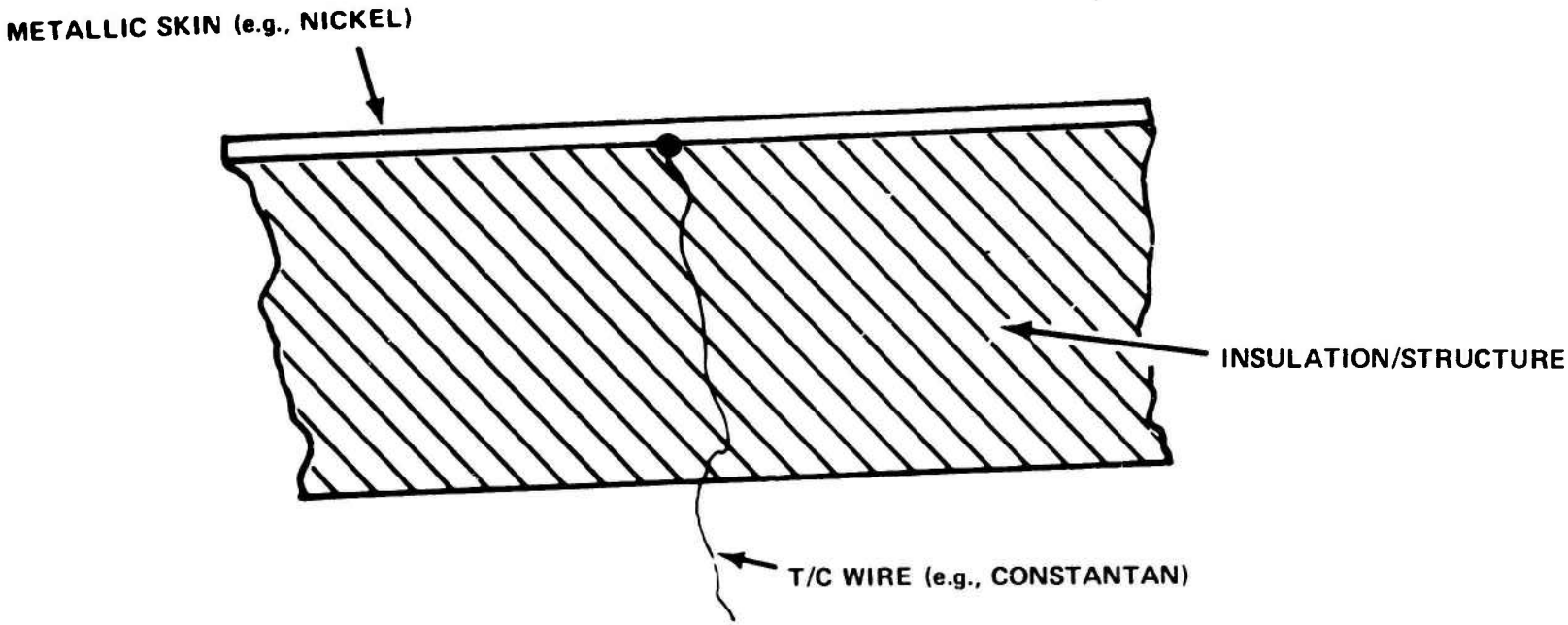

Figure 7. Semi-Infinite Model with Conventional T/C

For quartz lamp heating, one T/C wire will be required. For resistance heating, two T/C wires will be required because heating will be required at the same time model temperatures will be measured.

For the semi-infinite solid, the conduction equation is:

$$\frac{dT}{dt} = \frac{K}{\rho C}\frac{d^2T}{dx^2} = \alpha\frac{d^2T}{dx^2} \tag{12}$$

where the boundary conditions are at $t = 0$, $T = T_o$ = constant. For quartz lamp heating at $X = 0$,

$$-\frac{KdT}{dx} = q_{rad} + h(T_R - T) \tag{13}$$

and for resistance heating, the power dissipation is a linear function of temperature, that is:

$$q_{elect} = C_1(T - T_o) + C_2$$

then the boundary condition at $x = 0$ is:

$$-\frac{KdT}{dx} = C_1(T - T_o) + C_2 + h(T_R - T) \tag{14}$$

For the quartz lamp, the solution at $x = 0$ is:

$$\frac{\frac{q_{rad}}{h} + T_R - T_W}{\frac{q_{rad}}{h} + T_R - T_o} = \exp\left[\frac{h^2 t}{K\rho C}\right]\operatorname{erfc}\left[h\sqrt{\frac{t}{K\rho C}}\right] \tag{15}$$

For resistance heating, the solution at $x = 0$ is:

$$\frac{A + T_W}{A + T_o} = \exp\left[\frac{(C_1 - h)^2 t}{K\rho}\right]\operatorname{erfc}\left[(C_1 - h)\sqrt{\frac{t}{K\rho C}}\right] \tag{16}$$

where

$$A = \frac{hT_R + C_2 - C_1 T_0}{C_1 - h}$$

Operation procedures for the semi-infinite model should involve the following:

(1) Laboratory calibration of each T/C location using a radiant heat source to determine $K\rho C$ from

$$q_{rad} = \left(\frac{T - T_o}{2}\right)\sqrt{\frac{\pi\rho CK}{t}} \qquad (17)$$

(2) For the resistance heating case only, determine the constant in Equation 4 using the procedures outlined for the 1-D thin film resistance heater.

(3) For quartz lamp radiation only, determine q_{rad} in Equation 15 using procedures outlined for the 1-D thin film quartz heater.

(4) With no model heating, the tunnel is started and stabilized. After the model has come to near thermal equilibrium, the recovery temperature is measured at each T/C location. At time, t_1, the model is irradiated with quartz lamps or the resistance heater is turned on, depending on the heating method. The transient temperature response is recorded by each T/C. After sufficient data has been recorded, the test is terminated.

(5) Equations 15 or 16 are used with the above data to determine the convective coefficients.

The quartz lamps will require a shutter so that the lamps can be turned on and stablized to ensure that both q_{rad} in Equation 15 is constant and the time, t, can be precisely measured.

The computer code of Appendix B has been applied to the semi-infinite sensor to estimate the accuracy of the above data reduction equations. The model was Stycast 2762FT epoxy with a constantan T/C lead wire and nickel plate over the model's surface. Variables in the analysis were the thickness of the nickel plate and the diameter of the T/C lead wire. The code was applied to the laboratory calibration, tunnel calibration and tunnel test conditions to evaluate the convective coefficient measurement error. The thermal properties were obtained from Appendix B to this report. The tunnel conditions and incident power for lamp heating or resistance heating were the same as those used in the 1-D thin skin calculations. The results of the calculations are summarized in Table 4.

Table 4. Semi-Infinite T/C Sensor Design Analyses

External Heating Method	Plate Thickness (In)	T/C Diameter (In)	Equation 15 or 16 and 17 inferred Coefficient, h ($Btu/ft^2 sec$)	Measurement Error ε_h/h
Quartz Lamp	.003	.003	.0400	.043
Quartz Lamp	.005	.003	.0380	.091
Quartz Lamp	.003	.005	.0396	.053
Resistance	.003	.003	.0400	.043

In performing an error analysis on the semi-infinite model, it was found that the dominate error in the evaluation of convective coefficient was the temperature mesurement error (equal to $\pm 4^{\circ}R$ for T/C). For an electrical power dissipation of 5.0 Btu/ft^2sec for the tunnel condition of q_{cw} = 20 Btu and T_R = 478.8°R, the temperature uncertainty induces a 36% error in the convective coefficient. This error can be reduced by extending the test duration (now 5 seconds) or increasing heater power. Both of the parameters can only be changed to a limited extent. That is, the time over which the temperature is sampled must satisfy the condition that the model is a semi-infinite solid and the heater power is limited because of thermal expansion mismatches between the nickel plate and epoxy model.

Because of the expected measurement errors, the thermistor or thin film resistor is recommended instead of conventional T/C. The semi-infinite model with the thin film and thermistor are described in Paragraphs 3.5 and 3.8, respectively.

3.4 Wafer Thermopile

This concept can be used with either internal fluid heating or internal resistance heating. For both methods, the model instrumentation requirements are the same (e.g., number of sensors and T/C lead wires) as are the procedures for sensor installation.

For fluid heating, the model will entail two concentric steel tubes in the center of the model to permit fluid inlet/exit flow passages. For resistance heating, one center tube will be required for insertion of the electrical heating element. For both heating methods, model

fabrication will entail bonding wafer thermopiles to the external surface of the outer steel tube using a pad of epoxy insulation to place the wafer close to the eventual model's external surface, thus minimizing the thermal "smearing" that occurs in the relatively high thermal conductivity steel tube. The exact radial location is unimportant. A thin film resitance gage, a foil T/C or a conventional T/C is then waxed on the inside surface of a female mold contoured to the final model shape. These gages are located so they will be adjacent to a corresponding wafer when the steel tube is inserted into the female mold. The surface temperature gage lead wires are strain relieved by epoxying them to the steel tube. The female mold is then filled with epoxy (e.g., Stycast 2762FT) and cured. The assembly is heated to release the wax holding the temperature gages to the female mold and the model is removed. The model is finally coated with a thin coat of epoxy paint and ground to expose the surface temperature gages. This coat is applied to remove any surface imperfections caused by the wax which was used to mount the temperature gages.

Wafer thermopiles, suitable for the ogive-cylinder model are commercially available from RdF, Medtherm or Hy Cal. BLH Electronics fabricates thin film resistance thermometers and foil T/C gages that can be used for measuring surface temperatures.

For the ogive-cylinder design, an epoxy wall thickness of approximately 0.15 inch produces a reasonable surface temperature and allows sufficient room for the internal heater element or fluid passages. The wafer thickness is relatively unimportant but its width and length will dictate the spatial resolution in which surface heating distributions

can be measured. To be comparable with the 1-D thin skin sensor, the width and length should be less than 0.2 inch. Also, the wafer thermal conductivity should be near that of the epoxy to minimize 2-D conduction effects.

The above manufacturing methods should not influence gage calibration that is provided by the vendor. However, to ensure that calibration changes did not occur, the laboratory calibration procedures outlined for the 1-D thin skin gage to measure electrical heat dissipation is recommended for the first few fabricated models. Typical vendor calibration involves determining the sensor constant, K/L, by sandwiching the wafer between two conductors and passing a known heat flux, q_{con}. That is

$$q_{con} = \frac{K}{L}\Delta T \qquad (18)$$

where ΔT is the temperature differential measured by the thermopile. In the wind tunnel, the convective coefficient is evaluated when the model has reached temperature equilibrium with either the electrical heater in operation or hot fluid flowing in the center steel tubes. Data reduction simply involves

$$\frac{K}{L}\Delta T = h(T_W - T_R) \qquad (19)$$

where K/L is the gage constant, ΔT is the thermopile output, T_W is the surface temperature as measured by the surface gage and T_R is the recovery temperature.

Operating procedures for the thermopile model should involve the following:

(1) Laboratory calibration of wafer thermopiles, if necessary, using procedures outlined in 1-D thin skin resistance heating calibration.

(2) With no fluid or resistance heating in the model, the tunnel is started and stabilized. After the model has come to near thermal equilibrium, the recovery temperature is measured at each surface temperature gage location. Hot fluid is then circulated through the model or the resistance heater turned on until a second thermal equilibrium is reached. At this time, ΔT and T_w are measured. The test is then terminated.

(3) The data of Step 2 is then used in Equation 19 to evaluate the convective coefficient.

An error analysis was performed on the wafer thermopile using the procedures presented for the 1-D thin skin sensor. The thermopile errors were estimated as follows:

(1) Vendor calibration of the constant, K/L, is within $\pm 3\%$ (Reference DM-35).

(2) Surface temperature measurement error is $\pm 4^{\circ}R$ due to EMF output of conventional T/C (Reference OS-40).

(3) Surface temperature measurement error due to junction occupying a finite indepth volume in the model and lead wire conduction losses were analyzed by the computer code. For a junction diameter of 0.003

inch, q_{cw} = 20 Btu/ft^{2}sec, T = 478°R and fluid temperature = 660°R, computer results show that measurement error is ±4.2°R. This does not apply to the recovery temperature because it is measured when there is no thermal gradient in the model.

(4) Thermopile error in measuring ΔT will depend on the number of T/C junctions and the thickness and conductivity of the wafer. Therefore, the number of junctions and wafer thickness should be determined by the uncertainties that are inherent in other error sources. Thermopiles on the order of 0.050 inch thick with 10 to 40 junctions are common, resulting in errors that are lower than the calibration error in Item 1. Therefore, it was assumed as a worst-case that the thermopile error is equal to the 3% calibration error.

Using the above error estimates, the error in measuring the convective coefficient is ±0.10. This is slightly less than the error estimated for the 1-D thin skin sensor with T/C.

3.5 Thin Film Resistor/Semi-Infinite Solid

The thin film resistor has had extensive applications in aerospace (References DM-4, -35, -36, -41, -53, -63, -70, -88, -95 and -109). The sensor has been used primarily in shock tube applications because of its fast response times (less than 10 milliseconds per Reference DM-4).

The thin film sensor is a very thin temperature-sensitive resistance film deposited on an insulating substrate. Application of the resistive film can range from simple painting, epoxying, flame spraying, electroless deposition and electroplating to the methods used in the manufacture of microelectronic circuits: vacuum evaporation and sputtering (DM-63). The recent advances in microelectronic circuit manufacturing have made it possible to produce a thin film sensor that is cost-competitive with the simple methods and at the same time offers increased reliability, ruggedness and sensitivity. Materials that are most commonly used as the resistance element are platinum, nickel, aluminum, gold and iridium. The substrate is typically glass or quartz. The sensor can be ruggedized by the deposition of an SiO coating. The resistance element and protective coating thickness are typically 400 and 8000 A, respectively (DM-4).

The thin film sensor can be used in the cold wind tunnel application to measure the surface temperature of the model under transient and steady-state conditions. Use of the thin film in conjunction with the wafer thermopile has been described in Paragraph 3.4. In the following discussions, the thin film sensor is applied to measure the surface temperature of the semi-infinite model with the model heated by (1) self-heating, (2) quartz lamp, and (3) resistance heating of the metallic surface plate.

The thin film has been applied in cold wind tunnels wherein the resistance of the sensor is used to electrically heat the sensor and, by conduction, a portion of the model (Reference DM-53). In Reference DM-53, the thin film was applied to a quartz plate. A voltage was applied to the

film and the resulting transient temperature response was used to infer convective coefficient. The material properties and the "effective capacitance" of the sensor was determined analytically. A similar approach was investigated using the computer code described in Appendix B.

The self-heating approach that was analyzed involved the use of a thin film to measure the transient surface temperature response of the semi-infinite model when the thin film was heated by electrical current. This response and, therefore, the data reduction equation, is given by Equation 16. The accuracy of using Equation 16 to infer convective heating will depend primarily upon the ability to measure the constant $K\rho C$ of the model and the degree to which the assumption of 1-D heat conduction is satisfied. These two parameters were lumped into the data reduction technique of Reference DM-53 by defining an "effective capacitance." In the case at hand, a calibration test is recommended to define the effective ρCK . This calibration simply involves measuring the temperature response with the tunnel off and using Equation 16 to calculate ρCK . The computer code was applied to a Stycast 2762FT model (material properties presented in Appendix B) with a sensor radius of 0.05 inches. Electrical dissipation ws modeled by Equation 4 with C_1 = -.0078 $1/^{\circ}R$ and C_2 = 2.5 Btu/ft^2 sec. Tunnel test conditions were initial temperature, T_0, and recover temperature both equal to 478.8°R and q_{cw} = 20 Btu/ft^2sec. The transient temperature responses as measured by the sensor are presented in Figure 8 for both the calibration and tunnel conditions. The model's surface temperature distribution is presented in Figure 9. The sensor measures an average temperature over its surface and therefore Figure 8 is an average of Figure 9 based on area. Equation 16

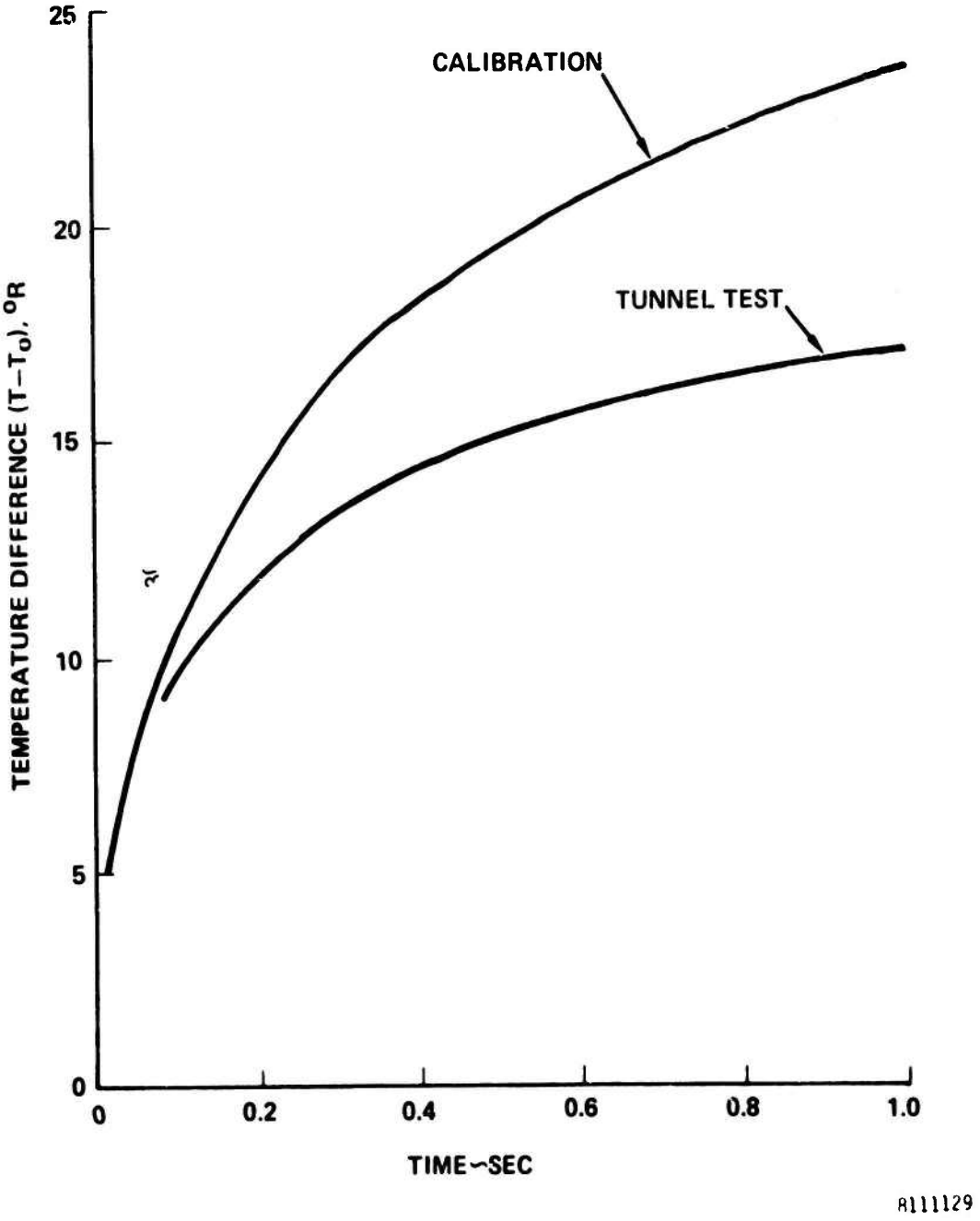

Figure 8. Thin Film Sensor Temperature Response

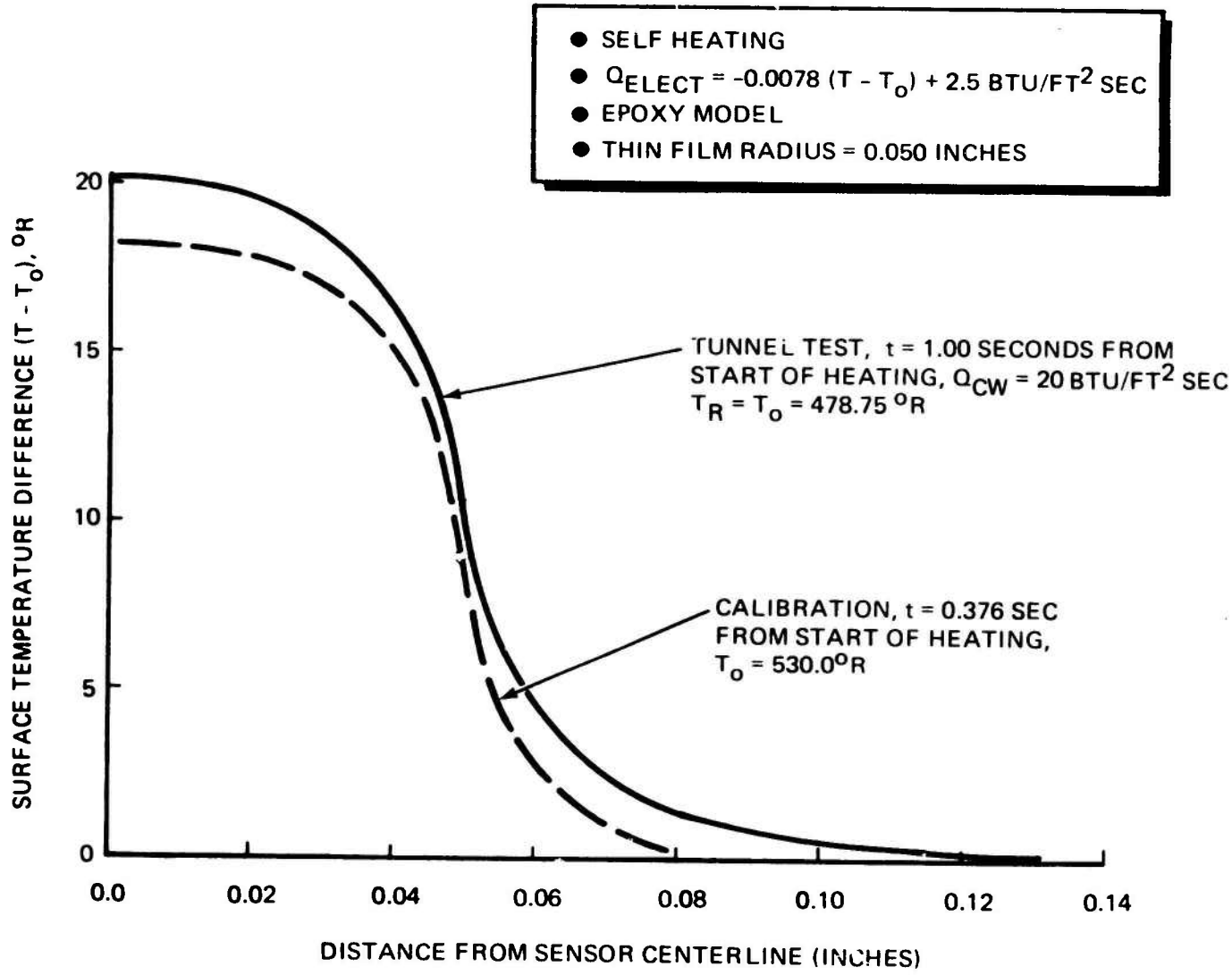

Figure 9. Surface Temperature Profile for Thin Film Resistor

was applied to the calibration predictions of Figure 8 to estimate the constant ρCK . Because of radial heat conduction, the constant was found to be highly dependent on the time period over which the constant was evaluated. The error in the convective coefficient that is calculated using the effective ρCK of Equation 16 and the measured temperatures of Figure 8 are presented in Table 5.

Table 5. Thin Film Sensor Conduction Errors (Self-Heating)

Calibration Test		Tunnel Test	
Time (sec)	Evaluated $\sqrt{\rho CK}$ $Btu/ft^2\text{-}^oR\text{-}sec^{1/2}$	Evaluated h Btu/ft^2sec	Error ε_h/h
0.376	0.00855	0.049	0.172
1.000	0.0125	0.068	0.627

As can be noted, the measured error is significant and highly dependent on the time at which the constant and convective coefficient is evaluated. Although some optimization can be made in q_{elect} , model material properties and data reduction times, the conduction error should still be large. Therefore, self-heating of the thin film sensor is not recommended.

The thin film sensor heated by quartz lamps or resistively heated by a nickel plate applied to the model's surface appears attractive. These heating methods eliminate the 2-D conduction-induced errors inherent in the self-heating method. The operating procedures of the thin film sensor are the same as the T/C semi-infinite solid (Paragraph 3.3). The error sources are described below. The noted errors

are ε_h/h.

(1) Laboratory calibration error in measuring ρCK from Equation 17 is $\pm$3%.

(2) Recovery and transient surface temperature mesurement error is $\pm 0.7^{\circ}R$ (Reference DM-95). For the tunnel conditions that were used in the above self-heating calculation, an error of 12.5% in the convection coefficient was obtained for both the recovery and transient surface temperature.

(3) The calibration of electrical dissipation constants, C_1 and C_2 of Equation 4, is 3% (Reference DM-35). Calibration heat losses are estimated to be 4%.

(4) For lamp heating, the error produced by free convection in tunnel calibration is 2%. Error produced by the $\pm 0.7^{\circ}R$ uncertainty in temperature during tunnel calibration is 4%. Intensity variation in lamp is 5%.

The above error sources result in a convective coefficient RSS error of 18.6 and 19.1% for electrical and quartz lamp heating, respectively. The errors can be reduced to some extent by increasing the heating level.

Model fabrication can be accomplished in two ways. One method is to install sensor plugs in pre-drilled holes in the model. Plugs similar to those of References DM-88 and -109, which are commercially available are examples. For this design, electrical heating is not

possible. Another method is to cast lead wires into the epoxy model and plate the surface with the thin film elements. A similar method was used in Reference DM-53.

3.6 Semi-Infinite Model, Semiconductor T/C

This type of T/C sensor was designed, fabricated and calibrated by Reference DM-22. The T/C is n-p germanium deposited on an insulator. The T/C is installed in a probe for insertion into a model. Probe sizes are small (.5 cm long x .3 cm diameter). Relative to conventional T/C, semiconductors have a very high measurement sensitivity, 2.0 mv/°C (vs. 0.061 mv/°C for chromel/constantan). Using the $\pm 4^{\circ}R$ temperature uncertainty of Reference OS-40 for conventional T/C, the corresponding uncertainty for the semiconductor is $\pm 0.1^{\circ}R$. However, Reference DM-22 found that the EMF generated at lead wire attachements is of the same order as the n-p junction and care must therefore be used to ensure that the lead attachments and n-p junction are isothermal.

The use of the seminconductor T/C will require installation of a T/C probe assembly in the model. Commercially-available semiconductor T/C probes could not be found at this time. In comparison to the thermistor (Sensor 8 of Table 1, which is commercially available), the semiconductor T/C does not offer any significant enhancement in sensitivity. Also the thermistor is compatible with the fabrication techniques required for plating nickel on epoxy models. This offers greater simplicity in model fabrication than does the discrete plug required for the semiconductor T/C. With these comparisons, the semiconductor T/C is concluded to offer no significant advantage over the thermistor. The semiconductor is therefore deleted as a candidate.

3.7 Semiconductor Thermopile

This type of sensor was developed by Schutle and Kohl (Reference DM-50). The sensor uses $AgSbTe_2$ as the active element arranged in a 45-element thermopile. The sensor resulted in a measurement sensitivity of 225 mv per watt/cm^2 of heat flux incident on the surface. This sensitivity is more than needed for the application at hand. A sensor with less elements and/or less sensitive EMF output when used in conjunction with a thermistor for measuring surface temperature could result in a very accurate method for measuring recovery temperatures and convective coefficients. Therefore, the errors, in comparison with the wafer thermopile using a conventional T/C, would essentially be (1) calibration errors (i.e., K/L of the instrument), (2) surface temperature measurement errors due to the junction occupying a finite indepth volume and (3) lead wire conduction losses. The operational procedures for the wafer thermopile using conventional T/C (Sensor 4) also apply to the semiconductor thermopile. The errors for the semiconductor sensor in measuring convective coefficient is estimated to be approximately 5% based on the thermopile error analyses (Paragraph 3.4).

The fabrication procedures outlined for the wafer thermopile using conventional T/C also apply to the semiconductor. Cost differences can, however, certainly be expected as commercially-available semiconductor sensors have not been identified at the present time. Attempts at costing the device are made in Paragraph 4.0.

3.8 Semi-Infinite Model, Thermistor

Two model designs have been selected for a semi-infinite model using a thermistor; a model with its surface nickel plated to form an electrical resistance heater, and a simple all-epoxy model (no nickel plate) that is externally heated by quartz lamps. The nickel-plated model is fabricated in the same manner as outlined for the semi-infinite model using conventional T/C. The quartz lamp model is simply an epoxy model with thermistor beads cast in the surface. Changes in thermistor output are between 3 to 5% per ^{o}C, depending on the thermistor materials. A number of circuits are commercially available for measuring thermistor resistance (DM-85 and -112) which can be related to temperature from vendor-supplied calibration curves. Temperature uncertainties can range from $\pm 0.5^{o}R$ using relatively simple circuits to less than $\pm 0.001^{o}R$ using complex and expensive circuits which are normally restricted to a narrow temperature range.

Although the thermistor, relative to the conventional T/C, offers greater measurement sensitivity, the large volume of the thermistor produces another error. Since the semi-infinite model operates on the theory of transient heat conduction (Equation 15 or 16), the finite volume of the thermistor causes the temperature to be measured somewhere below the surface of the model. The error will depend on surface temperature gradient, bead diameter and the bead's thermal diffusivity ($K/\rho c$) relative to the thermal diffusivity of the surrounding material. The thermistor bead is largely ceramic with a diffusivity close to the epoxy model. Computer calculations were performed to determine the thermistor's measured temperature and the actual surface temperature of the model. The results are shown in Figure 10. For comparison, the temperature measured

by a conventional T/C embedded in a 0.003-inch nickel plate is also presented. For the conditions analyzed, the thermistor temperature is approximately 2°R below the actual surface temperature, compared to 2.5°R for the T/C. This error can be minimized if, during model calibration, the model thermal response is close to the response that occurs in the tunnel. This is difficult to accomplish and therefore the thermistor error must be considered as -2°R for the condition analyzed.

Error analyses have been performed on the thermistor model for the conditions of Figure 10. The error sources are as follows:

(1) Laboratory calibration error in measuring $\rho C\delta$ = 3% (Reference DM-35).

(2) Temperature measurement error = $\pm$0.5°R using a relatively simple recording circuit (Reference DM-85). This applies to both the recovery and instantaneous surface temperature. The resulting error in convective coefficient $\varepsilon h/h$ is 0.089 for both temperatures.

(3) The error induced in the convective coefficient because the thermistor occupies finite volume is $\varepsilon h/h$ = 0.357 for a temperature that is 2°R below the actual "undisturbed" surface temperature.

(4) Error induced by thermistor lead wire conduction is 4.3% per Table 4.

(5) The calibration of electrical dissipation constants, C_1 and C_2 of Equation 4 is 3% in measured heat flux (Reference DM-35) and heat losses that occur during calibration are estimated to be 4%.

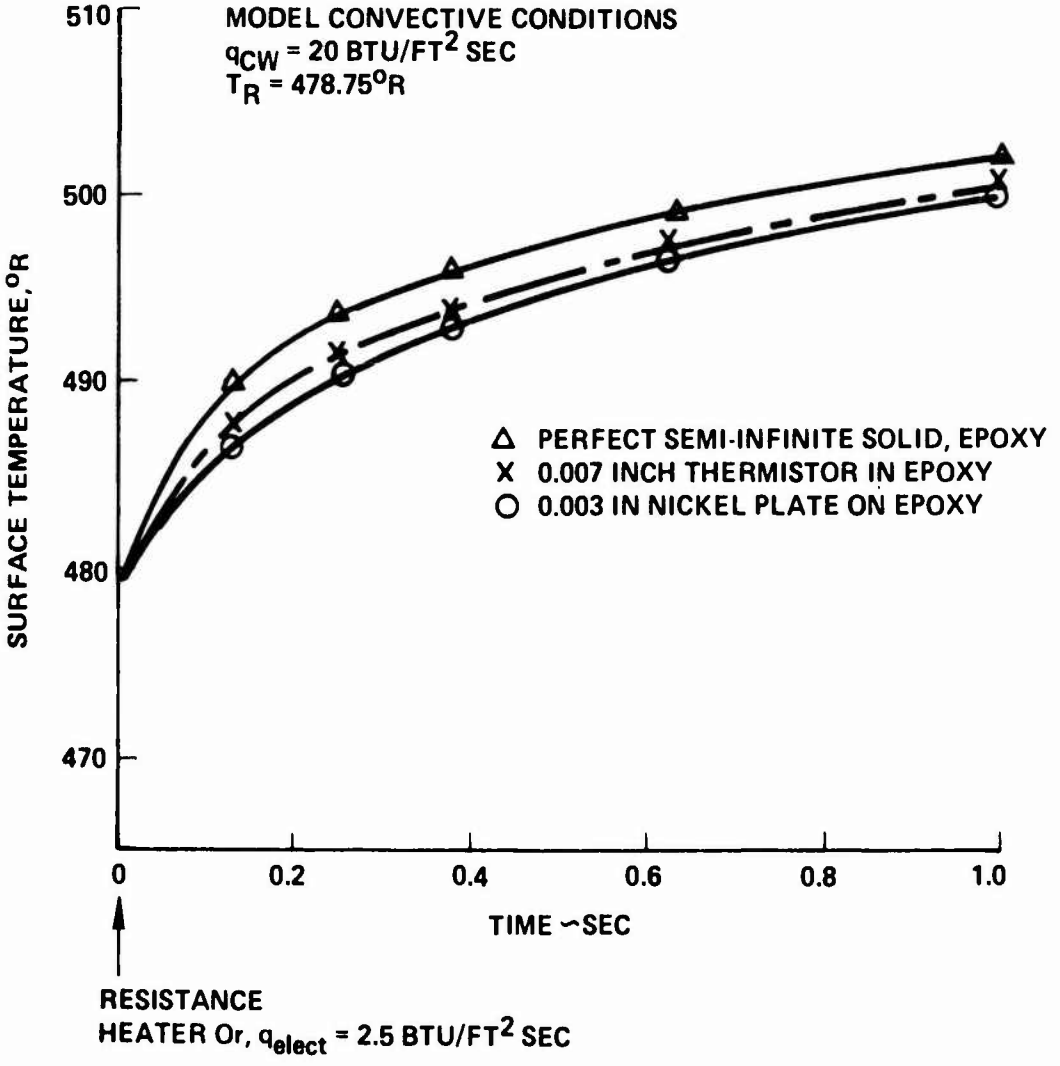

Figure 10. Semi-Infinite Model Surface Temperature Measurement

The above error sources result in a convective coefficient RSS error of 38.5%. This is considerably higher than other candidate sensors. Although the error can be reduced by using a smaller thermistor diameter or increasing electrical heater power, the resultant improvement in measurement accuracy is not expected to be competitve with the 1-D thin skin, 2-D foil or wafer thermopile.

3.9 Pyroelectric

Pyroelectric sensors operate on the principle that the electrical polarization of the sensor material is dependent on the rate of temperature change (DM-48). This feature can be used to measure heat flux by using the sensor as a 'slug' calorimeter. In this form, the sensor is a thin slab of pyroelectric material (e.g., barium titanate) with electrodes attached to both sides. A change in temperature causes a change in polarization which, in turn, produces a change in electrical current. This change can be related to the incident heat transfer if both the thermal gradient in the sensor and the sensor conduction heat losses are small.

The sensor, as constructed and tested in Reference DM-48, was a barium titanate disk, 0.10 inch in diameter and 0.007 inch thick. A schematic of the sensor is presented in Figure 11. Of the pyroelectric materials examined, barium titanate was found to have maximum signal output per unit heat transfer. The disk was mounted on a nylon plug with epoxy so that the disk was insulated from the adjacent structure. The sensor sensitivity in this configuration was approximately 150 mv/w with a response time of between 3 and 5 milliseconds. Calibration tests

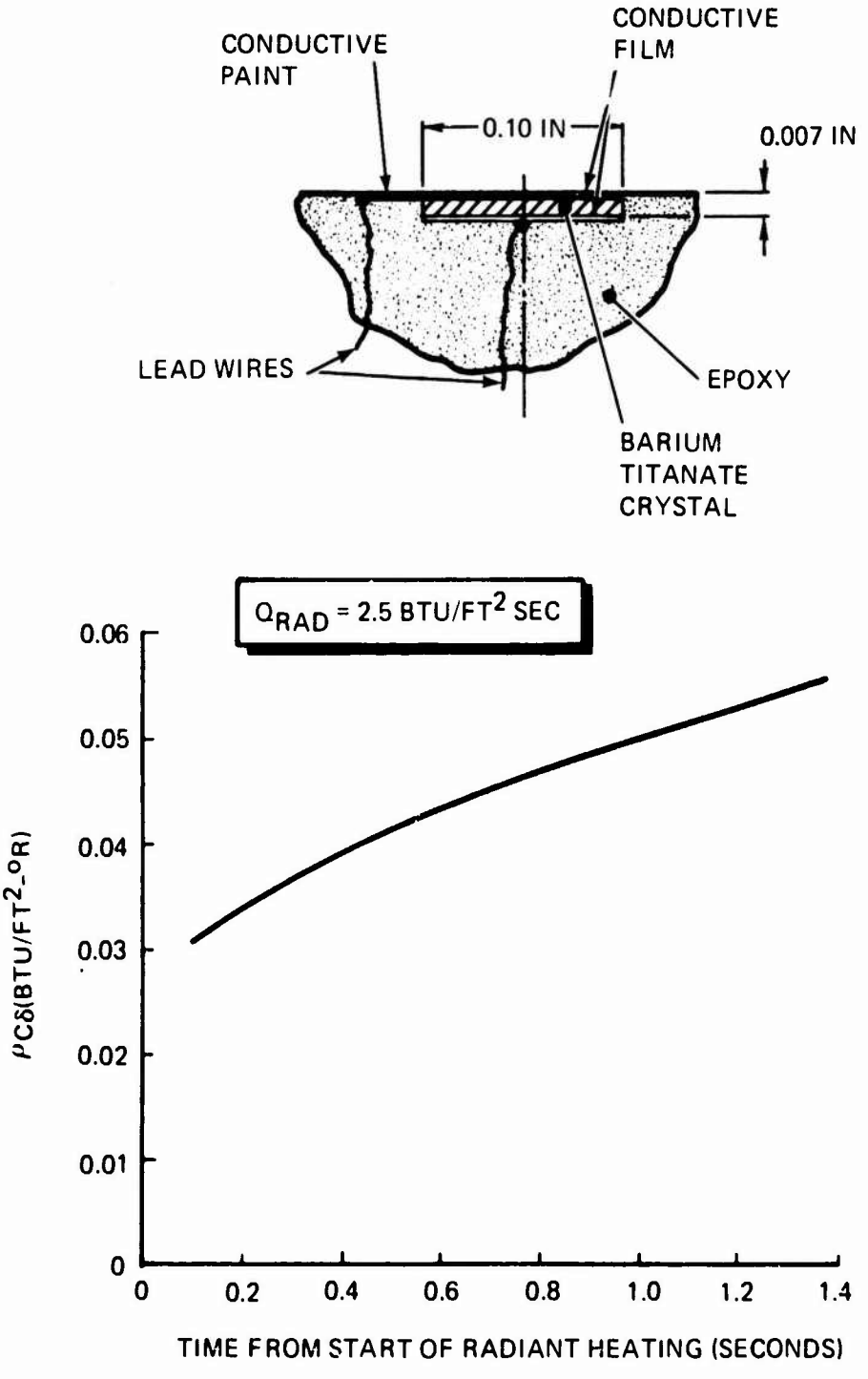

Figure 11. Sensor Constant Calculated from Laboratory Test

performed on the sensor resulted in nearly a linear sensor output with incident heat flux. Data acquired in tunnel tests showed no evidence of piezoelectric effects. Reasonable agreement between T/C and ferroelectric inferred heat transfer rates were achieved.

As noted, the measurement accuracy of the sensor developed in Reference DM-48, depends on the sensor temperature gradient, conduction losses and the incident surface heat flux. In their application, the measurement times were short and the incident heat flux was essentially independent of surface temperature. For cold wind tunnels, these conditions are not entirely true. That is, the incident heat flux is dependent on surface temperature because the recovery temperture is relatively close to the ambient temperature. To use a pyroelectric sensor plug, similar to that developed in Reference DM-48, in cold wind tunnels, the model must be heated with external quartz lamps (i.e., resistive heating of the surface cannot be accomplished because of the sensor plugs). External lamp heating is limited to lamp and optical collimation ($\sim$5.0 Btu/ft^{2}sec on the model) and therefore the test duration must be longer than that encountered in impulse tunnels. To evaluate the sensor errors in cold wind tunnels, the computer code in Appendix B was applied to the Reference DM-48 design.

In the pyroelectric sensor analyses, the material properties presented in Appendix B were used. The barium titanate wafer was assumed to be epoxied to the nylon plug using a low thermal conductivity cement in order to minimize conduction losses (Epoxy 1095 of Appendix B). To use the sensor data in defining the convective coefficient, Equation 2 must be satisfied where the constant, $\rho C\delta$, is determined from laboratory

calibration tests using Equation 1. Computer simulation of the laboratory tests were performed using a radiant heat source. The computer results confirmed the calibration test data of Reference DM-48 in that the sensor output was very nearly a linear function of the heat source intensity. The constant, $\rho C\delta$, as measured in the laboratory is, however, a function of the time from which the model is exposed to the radiant heat source. This is a consequence of conduction heat losses to adjacent sensor structure. The constant is presented in Figure 11 as a function of the time from the start of model heating. Because the constant is time-dependent, a problem arises as to what value should be used in reducing the cold wind tunnel data. To minimize this problem, Equation 1 was modified to include a lumped conduction term. The modified equation is:

$$q_{rad} = \rho C\delta \frac{dT}{dt} + C_3 (T - T_o) \qquad (20)$$

where the constant, $\rho C\delta$, is evaluated at an early time from the start of model heating so that heat conduction losses are a minimum. Constant C_3 is evaluated at a radiation heat load that produces approximately the same dT/dt at the same time as those measured in the actual tunnel test. This ensures that heat conduction rates (i.e., temperature gradients) are similar.

The computer code was then applied to a tunnel condition with q_{cw} = 20 Btu/ft^{2}sec, recover and initial temperature were both equal to 478.8 R°and q_{rad} = 5.0 Btu/ft^{2}sec. The convective coefficient was inferred from

$$h(T_r - T) + q_{rad} = \rho C\delta \frac{dT}{dt} + C_3 (T - T_o) \qquad (21)$$

using the sensor constants, $\rho C\delta$ and C_3, that were evaluated from laboratory calibration. The error was found to be a function of the time at which both the constants of Equation 20 and the convective coefficient are evaluated. The error in convective coefficient is presented in Figure 12 as a function of time from the start of lamp heating. Also included in the figure is the sensor temperature rate of change error which was assumed to be $\pm 1^{\circ}R$/sec. The resulting error is a function of time. It should be noted that due to the nonlinearity of conduction losses and the change in temperature rate of change, the sensor measurement error could possibly be reduced if a computer simulation of the sensor is used to reduce the data. This simulation will require sensor dimensions and material properties to model the laboratory calibrations and tunnel tests. The accuracy and cost to perform this type of data reduction will require laboratory evaluation.

Since surface temperature cannot be measured with the pyroelectric sensor, a thermistor, T/C or thin film gage will be required. This gage should not be placed over the pyroelectric device because of possible thermal isolation resulting from the gage and electrical insulation required between the gage and the conductive surface of the pyroelectric sensor. Therefore, the temperature gage should be placed adjacent to the sensors, either laterally displaced on the surface or on the sensor's backface. Both locations will induce an error. From the computer simulation of the above tunnel conditions, the temperature gradient across the pyroelectric sensor is between 2 and $5^{\circ}R$, depending on the time from the start of model irradiation. This gradient and the error in backface temperature measurement can be estimated in the actual

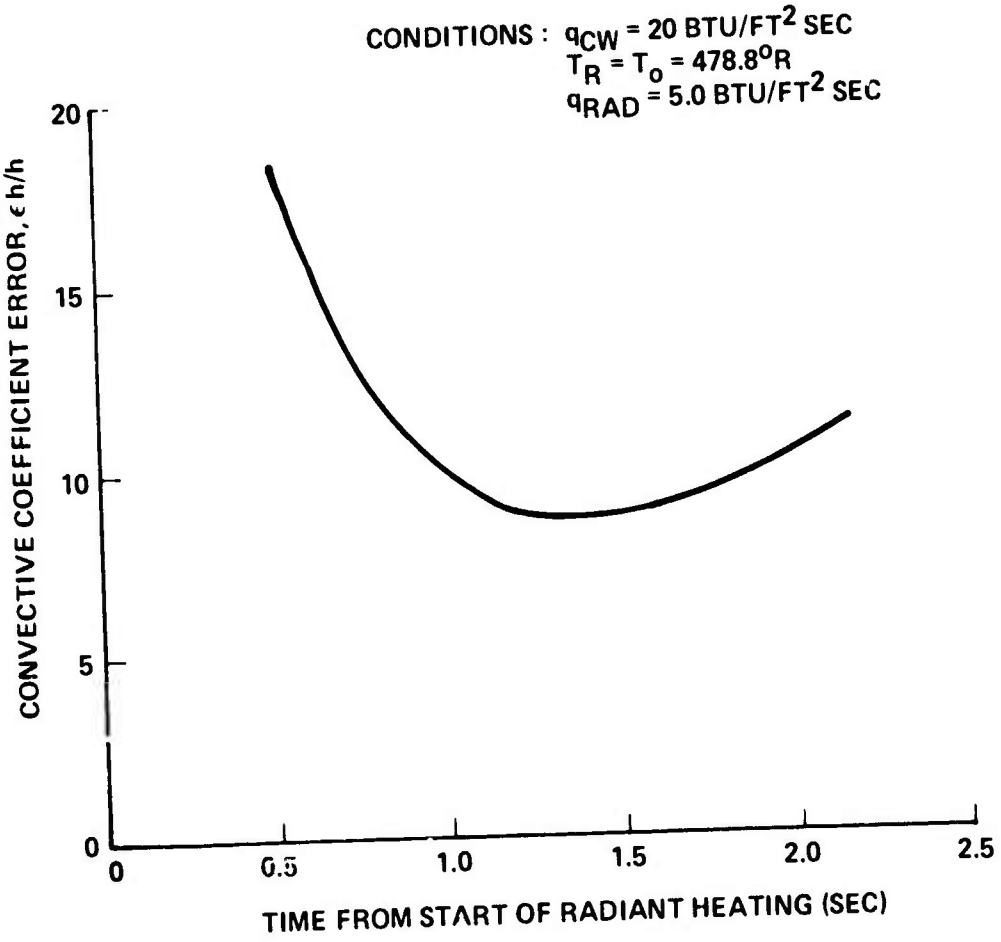

811130

Figure 12. Dependence of Convective Error on Time of Data Reduction

application by computer simulation with the resulting error estimated to be 0.5 to 1°R due to uncertainties in material properties and thickness. Placing the gage on the surface will produce errors resulting from (1) spatial variations in convective heating, (2) variations in radiation heating resulting from emissivity differences, and (3) internal conduction. These errors can be significant because, for example, the surface temperature of the epoxy model and pyroelectric device at the above tunnel conditions is predicted to differ by 10 to 20°R, depending on the time from model heating. Therefore, a backface temperature sensor is recommended. A thin film resistor similar to those commercially available from BLH is recommended.

The error analysis that was applied to the pyroelectric sensor is summarized below.

(1) Errors due to sensor temperature gradients, sensor conduction losses and temperature rate of change produce a convective coefficient error of 8.7% based on the results of Figure 12. It should be noted that the actual error will be larger than this because of uncertainties in the computer simulations that are used to generate data similar to that presented in Figure 12.

(2) Laboratory calibration error of sensor constants is $\pm$3% (Reference DM-35), plus a 1% error resulting from the $\pm$1°R/sec measurement error.

(3) Uncertainty in the incident radiation from the quartz lamps is 5% (Oriel Optics), and heat losses during tunnel calibrtaion (e.g., free convection) are approximately 2%.

(4) Uncertainty in surface temperature was assumed to be $\pm 0.5^{\circ}R$ due to the error in estimating temperature gradient (does not apply to recovery temperature because of steady-state) across the pyroelectric sensor and $\pm 0.7^{\circ}R$ for the thin film measurement uncertainty (Reference DM-95). These error sources produce an RSS uncertainty in convective coefficient of 1.5% for the instantaneous surface temperature and 1.2% for recovery temperature. These errors apply to the condition of minimum error as presented in Figure 12.

The above error sources result in a convective coefficient RSS error of 10.9%.

The sensor plug as constructed in Reference DM-48 is also recommended for the cold wind tunnel model. The sensor design is presented in Figure 11. Electrical connections to the conductive surfaces of the pyroelectric sensor are made with conductive paint. Experience with similar contacts on similar crystals (e.g., the piezoelectric crystals of Reference DM-113) have shown that these connections are extremely fragile. Also, as pointed out in Reference DM-48, fabrication of the pyroelectric wafer was difficult because of the brittleness of the pyroelectric crystal. The sensor can therefore be expected to be susceptible to structure loading.

Operation of the pyroelectric sensor should involve the following procedures.

(1) Determination of wafer thickness and diameter during fabrication for use in computer data reduction.

(2) Laboratory calibration of each sensor to determine the constants in Equation 20.

(3) With the tunnel nonoperating, calibrate the incident model heat flux at each sensor location as produced by the quartz lamps.

(4) With the tunnel operating and stabilized, measure recovery temperature with the backface temperature gages. Turn on the quartz lamps and monitor the outputs from both the temperature gages (T_w) and pyroelectric devices (dT/dt).

(5) Use the above data in a computer simulation of the gage to evaluate the convective coefficient.

3.10 Liquid Crystals

Liquid crystals are crystals in an anisotropic fluid solution that are capable of reflecting light selectively. The wave band of the reflected light is temperature-dependent. This property has been used to measure surface temperature and has the unique characteristic of not requiring direct contact with the surface. Liquid crystals have been used in wind tunnel applications (References DM-53, TS-1, -11, -18, -19, and M-69a) and in RF fields (References TS-38 and OS-33) where metallic lead wires cannot be used. In wind tunnel applications, the liquid crystals are encapsulated to prevent smearing by the interaction of the gas shear stress. The encapsulated liquid crystals (ELC) are commercially available (e.g., NCR and BDH Chemicals, Ltd.) to measure temperatures over a particular temperature range. Outside the temperature range, they are colorless. The active temperature range can be as small as 1°R or can be

made as wide as 90°R by mixing a number of different crystals together. The crystals are completely reversible, however a small amount of hyptersis has been reported (Reference TS-38).

Cholesteric encapsulated liquid crystals, when irradiated with white light, reflect light with a wavelength that is temperature-dependent. The reflected light is, however, only a small part of the total light. Therefore, to observe the reflected light, the model must absorb the remaining light. This is done by giving the model surface a diffuse black color to which the ELC are applied.

An important feature of the ELC is that only the wavelength of the reflected light needs to be measured to infer temperature. The reflected wavelength can be measured directly by using a monochromator or recorded on photographic film. The film can then be processed at a later time and reviewed visually or optically using a monochromator to infer temperature. Since the reflected wavelength is independent of the intensity or brightness of both the incident and reflected light, the measurement is not influenced by the illumination conditions, properties of the film or the conditions in which the film is developed (factors that can be important for the thermal phosphors, Sensor 11). The physical relationship between the light source, model surface and the recorder (monochromator or color film) must satisfy the law of specular reflection. Thus, model curvature must be considered in placing the light source and recorder. Multiple light sources can be used with one recorder to encompass large areas of a curved model. Model curvature, however, does not produce an error in the inferred temperature, like it can for the thermal phosphors (Sensor 11) and the IR scanner (Sensor 12).

Temperature measurement resolutions between 0.2 to 1.0°R are reported in wind tunnel applications (References OS-33, M-69a and TS-38) which depend largely on the procedures used to reduce the photographic film. The time required for the crystals to respond to a change in temperature is dependent on the crystal thermal mass and the time required for the crystals to realign themselves molecularly. Crystal realignment is quoted to be less than 0.1 second (References M-69a and TS-29). For the 10 to 15 μm paint thickness used in Reference TS-18, the ELC was found to follow temperature steps greater than 36°R/second. This is well within the 10 to 20°R/second temperature changes that are predicted for the tunnel models operating for times greater than 1.0 second after model heating.

ELC has been applied to wind tunnel models using both the 1-D thin skin and semi-infinite solid calorimeter approaches (References M-69a and TS-18, respectively). Reference TS-18 instrumented the thin skin model with thermocouples to evaluate the accuracy of the ELC to infer convective coefficients. The results are reproduced in Figure 13, where it can be seen that the ELC and thermocouple results are in excellent agreement.

ELC can be used to measure temperature over a large area of a model. The area is dependent on the recorders's field of view and the ability of the model's surface to reflect light to the recorder (i.e., model curvature effects). Spatial resolution of the temperature field will depend on recorder optics, the size of the photograph to be used in data reduction, and the procedures used to measure the wave band of the reflected light. For cold wind tunnel applications, it is recommended

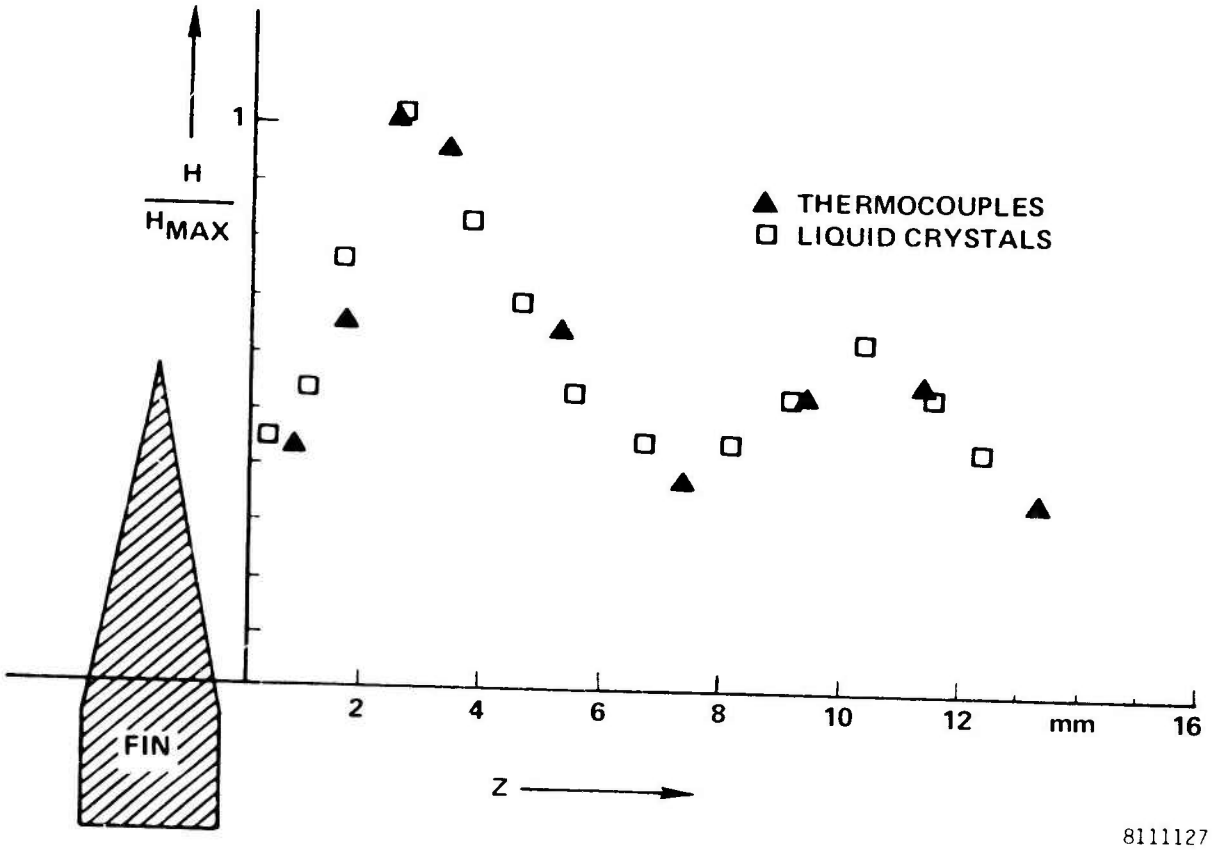

Figure 13. Comparison of Liquid Crystal and T/C on Thin Skin Inferred Convective Coefficients

that the calibration and data reduction techniques of Reference TS-18 be used. These techniques include laboratory calibration of the ELC model to determine wavelength vs. temperature. A monochromator is used to compare the calibration photographs with the tunnel test photographs to infer model temperature. This is accomplished by passing white light through the calibration photograph that was produced at temperature, T_1. The monochromator wavelength is varied until maximum output is achieved. With the monochromator at this fixed setting, the tunnel test photograph is scanned with the white light source. The locations where transmission is measured correspond to T_1. Thus, by scanning the photograph, the T_1 isotherms can be defined.

Use of the ELC in cold wind tunnels to measure convective coefficients can involve the transient semi-infinite solid (Equation 16) transient thin skin (Equation 2), or quasi-steady thin skin (Equation 3). These concepts are described below.

Since it is desirable to measure the coefficients over a large part of the model using a single photograph, temperature variations due to indepth conduction are undesirable. Thus, the thin skin model should be a thin shell thermally isolated from the internal structure. The thin skin model design of Paragraph 3.1 would result in temperature gradients, and is therefore not recommended. The electroforming techniques of Reference OS-46 have been successfully used to make thin nickel shells very similar to the ogive-cylinder shape of the current program (Reference TS-18). The shell is supported by an internal structure using insulator pads. This approach is also recommended for cold wind tunnel applications. Chromel wires can be welded to the inside surface to provide T/C verification of

the ELC data. A model design for the thin skin model could not be devised wherein the thin shell is resistively heated. Therefore, the thin skin model must be heated with external quartz lamps. The quartz lamps will also serve as the white light source for ELC reflection. The lamps and corresponding movie camera(s) are placed outside the tunnel and physically located to ensure specular reflection off the model surface and to minimize direct radiation from the lamps to the camera. As pointed out in References TS-11 and M-69a, problems can arise from the small amount of reflection that is scattered and reflected off the tunnel windows and other tunnel hardware. This can be solved by proper lamp-camera placement and window design modifications. In Reference M-69a, a special window had to be designed to minimize the "light curtain" produced by the light source.

Applying the ELC on the model surface can be performed using the procedures of Reference TS-18. This involved electrically plating black chrome on the nickel surface to absorb the light that is not reflected by the ELC. Before application of the crystals, the ELC slurry was filtered through an 8 μm filter and lowered in concentration by adding 50% water heated to 590°R. The ELC mixture is applied to the surface using a standard air brush. An ELC thickness of 15 μm was found to be satisfactory.

Calibration of the model involves determination of the temperature vs. wavelength relationship for the ELC coating. This can be achieved by using the actual model or painted copper disk, instrumented with, for example, a thermistor. A heat load is then applied to the sample in incremental steps. After a given heat load is applied, the

model is allowed to equilibrate. The model is photographed at the noted temperature. Data reduction of the tunnel test films (taken by a still camera or a movie camera) involves the procedures of Reference TS-18 as outlined above.

As noted in Reference TS-18, data reduction could be simplified if a color TV-camera and the appropriate color processing electronics were used instead of the photographic film and monochromator. This would eliminate the monochromator data reduction procedure at the sacrifice of time response. Investigations using the TV-camera were not performed in the present program, however, they are recommended for further investigation should ELC be selected as a candidate system.

The operation procedures of the ELC applied to a thin skin model should involve the following:

(1) Calibrate the ELC to determine the wavelength vs. temperature relationship. This can be performed in the laboratory or test tunnel (with the flow off) and is accomplished by heating the model to different steady-state temperature levels, recording the T/C output and taking a photograph of the model.

(2) Determine the constant ρCK in the laboratory by using a radiant heat source and Equation 1.

(3) Determine the incident radiation heat flux on the model in the tunnel with no flow. This is performed by irradiating the model with the quartz lamp and photographing the model with high-speed cameras (temperature can also be measured with thermistors or thin film).

(4) After calibration, the tunnel is started and allowed to equilibrate. The model is photographed to determine recovery temperature. The lamps are turned on and the model is photographed (high-speed movie cameras) until quasi-steady-state is reached.

(5) Data reduction involves using the Step 1 calibration film in conjunction with the measured ρCK, the lamp calibration and tunnel test data to determine model surface temperature distributions. Equation 1 is used to determine model radiant heating. Equation 2 or 3 is used to determine convective coefficient.

An unknown in the quartz lamp heating approach is the ability to sufficiently eliminate light energy that is not selectively reflected by the ELC to the camera. The radiation energy required to heat the model during tunnel test (approximately 2.5 Btu/ft^2 sec) is significant and reflections off the model (black but with an emissivity less than 1.0), tunnel walls and tunnel window can obscure the reflected energy. Quartz lamp heating is not recommended without experimental evaluation.

The ELC applied to a thermally semi-infinite model can be heated electrically. Model fabrication can follow the procedures outlined in Paragraph 3.3 for the semi-infinite model with conventional T/C. Like the thin skin models, thermistors or thin film sensors in the nickel plate are recommended to provide backup or verification to the ELC method. The nickel is plated with black chrome and painted with ELC using procedures described above for the thin skin. Operation procedures for the sensor are the same as for Sensor 3 (see Paragraph 3.3) except calibration of the liquid crystal is required as described in Step 1 above. The procedures

are as follows:

(1) Laboratory calibration using a radiant heat source to determine $K\rho C$ from Equation 17.

(2) For the resistance heater, determine the constant in Equation 4 using the procedures outlined for the 1-D thin film resistance heater (Paragraph 3.1).

(3) Same as Step 1 above for the thin skin design.

(4) With no model heating, the tunnel is started and stabilized. After the model has come to near thermal equilibrium, the model is photographed to determine recovery temperature. At time, t_o, the resistance heater is turned on. The model is photographed (high-speed cameras) to determine transient temperature response. After sufficient data has been recorded, the test is terminated.

(5) Equation 16 is used with the above data to determine the convective coefficients.

An error analysis was applied to the ELC. For the resistance heating design, an error is induced by the thin nickel plate that is used to electrically heat the surface. The data reduction procedures use Equation 16 to infer the convective coefficient. This equation was derived assuming 1-D heat transfer in a single material. The nickel plate introduces a second material and, because of its relatively high thermal conductivity, can "smear" the surface tempertaure distribution produced by a convective coefficient gradient over the surface. These errors were

evaluated using the computer code of Appendix B. The geometries that were analyzed were an epoxy model with a nickel plate thickness of 0.003 and 0.0015 inches. The tunnel conditions were the convective heating gradients presented in Figure 2. The region analyzed is indicated in the figure. The recovery temperature and initial temperature were both 478.8°R. The results of the analyses are presented in Table 6 for 1) an all-epoxy model with 1-D and 2-D conduction, and 2) an epoxy model with 0.003 inch of nickel with 1-D and 2-D conduction. The temperature at a node with q_{cw} = 24.6 Btu/ft^2 sec is presented in the table.

Table 6. Effect of 2-0 Condition on Semi-Infinite Solid Surface Temperature Response

Time (sec)	Surface Temperature (°R)			
	All-Epoxy Model, 1-D	All-Epoxy Model, 2-D	Epoxy Model 0.003 Nickel, 1-0	Epoxy Model 0.003 Nickel, 2-0
0.0	478.75	478.75	478.75	478.75
0.254	492.96	493.01	490.32	490.22
0.502	496.69	496.67	494.49	494.47
1.005	500.67	500.68	499.16	499.15
2.003	504.69	504.68	503.78	503.77

As can be seen from the 1-D and 2-D nickel/epoxy results, the temperature "smearing" produced by the nickel plate is negligible. The nickel/epoxy produces a surface temperature that is lower than the all-epoxy model because of its higher $K\rho C$ constant. The error induced in the convective coefficient was evaluated by computer simulations of the laboratory calibration test, Step 1 and the tunnel test, Step 4, in the above operational procedures. The temperatures predicted by the computer were used in Equation 17 to determine ρCK and Equation 16 to calculate the convective coefficient. The conditions were the same as those used to generate the data of Table 6. The results are presented in Table 7 for an

all-epoxy model, and nickel/epoxy models with 0.0015 and 0.003 inch of nickel plate on the surface.

Table 7. Convective Coefficient Error Induced by Nickel Plate on Semi-Infinite Solid

Model Design	T_w at 1.00 sec in Lab Calibration (°R)	ρCK from Equation 17	T_w at 1.00 sec in Tunnel Test (°R)	Convective Coefficient Error ϵ_h/h
All-Epoxy	567.66	0.00561	500.68	0.0
0.003" Nickel on Epoxy	562.56	0.00752	499.15	0.117
0.0015" Nickel on Epoxy	566.01	0.00615	500.04	0.047

The error sources for the ELC and their resulting uncertainty on the convective coefficient are presented below for both lamp and electrical heating methods. The temperature measurement error was assumed to be $\pm 0.2^{\circ}$. This is the resolution stated for the ELC of References 4-69a and TS-13 when a monochromator is used in the data reduction effort.

(1) For the resistance heating method (semi-infinite solid), the temperature measurement resolution in $\pm 0.2^{\circ}R$ produces an error in the convective coefficient of 3.6%. This applies to both recovery temperature and instantaneous surface temperature.

(2) For the lamp heating method (1-D thin skin) operating in quasi-steady-state, the temperature measurement resolution of $\pm 0.2^{\circ}R$ produces an error of 0.4% on the convective coefficient. Operating in the transient condition, the error is 3.0%.

(3) Calibration of ρCK for the resistance heater and $\rho c\delta$ for the thin skin are both 3.0% (Reference DM-55).

(4) Calibration of the ELC wavelength vs. temperature will be greater than the 0.2°R ELC measurement resolution because temperature must be measured by another device (e.g., T/C, thermistor, etc.). Under laboratory conditions, temperatures using a thermistor can be easily measured to within ±0.2°R. Therefore, assume overall calibration error is ±0.4°R. For resistance heating, the error in convective coefficient is 7.1% for both the recovery and instantaneous surface temperature. This error for lamp heating is 0.8% and 6.0% for steady-state and transient measurements, respectively.

(5) For electrical heating, calibration of the heat dissipation is 3.0% for the measurement of heat flux and 4% for heat losses that occur during calibration.

(6) For lamp heating, the tunnel calibration for a temperature uncertainty of ±0.2°R produces an error of 1.0% in convective coefficient. Intensity variation in the lamp is 5% (Oriel Optics).

(7) For resistance heating, the nickel surface plate produces an error of 4.7% (Table 7).

The RSS errors for the candidate heating and data reduction methods are presented in Table 8. Quartz lamp heating with the steady-state, thin skin data reduction method produces a very low measurement error. As has been pointed out, the large amount of radiant energy needed to heat the model with lamps may interact with the photographic process, so the reflected energy off the ELC cannot be identified (e.g., similar to overexposure of the film). This will depend

on the degree to which the model can optically be isolated from the quartz lamps. The degree of isolation can only be answered experimentally because scattering and/or reflection of the energy is a complex function of model geometry, lamp-model-tunnel window-camera orientation and auxilliary tunnel hardware.

Table 8. ELC Convective Coefficient Measurement Error

Heating Method	Data Reduction Method	Error, ε_h/h (%)
Resistance, Semi-Infinite Solid	Transient	13.5
Lamp, Thin Skin	Transient	11.2
Lamp, Thin Skin	Steady-State	5.3

Although resistance heating results in larger measurement error, it will be simpler to implement and use in the tunnel. Isolation of the camera from the light source for resistance heating is not as important, thus simplifying installation of model and instrumentation hardware. At the present time, resistance heating is recommended.

3.11 Thermal Phosphors

Thermal phosphors are a class of material that emit visual energy while being activated by a different waveband of energy. Typically, the activating energy is lower in wavelength than the emitted energy. At a constant level of incident energy, the emitted energy level is a function of the phosphor temperature. This property has been used to measure temperature fields over a model's surface by the application of a thermal phosphor paint (Reference TS-6, -7, -29, OS-33 and M-88). In these applications, the thermal phosphor was irradiated with an ultra-violet source and the resulting brightness of emitting radiation recorded on photographic film.

Important parameters that can influence the measurement accuracy of the thermal phosphor technique include the following:

(1) Sensitivity and calibration of the phosphor,

(2) Absolute intensity of activating energy,

(3) Nonuniform activation energy over the model,

(4) Model curvature effects, and

(5) Variations in film optical density resulting from either film quality, photographic recording and/or film processing.

The errors resulting from these parameters will depend on the thermal phosphor and method used to process and reduce the data. One method that was developed by Reference TS-6 and further improved on by

Reference TS-29 involved taking a pretest photograph of the illuminated model. The photograph is then used in conjunction with the test photographs to determine relative intensity changes. The relative changes are related to local heat transfer by the correlation of intensity to the heat transfer rate measured by discrete sensors on the model surface. The effects of film variablity, nonuniform illumination, and model curvature are nearly eliminated. This requires, however, that the activation energy, film quality and film processing for the pretest and during test conditions are the same.

The thermal phosphors that were used in References TS-6 and TS-29 were supplied by U.S. Radium Corporation under the trade name of Radelin. There are a number of Radelin phosphors that are available, each differing in the temperature range over which they are active. Radelin 1807 and 3215 have an active temperature range of 470 to 570°R and 500 to 770°R, respectively. Data reduction was performed by scanning the pretest and test photographics with an isodensitometer. Time responses of less than 1 millisecond are reported (Reference TS-29). Temperature uncertainty was within 4°R (References TS-6 and TS-29).

A second, and apparently more accurate method of using thermal phosphors, was developed by Reference OS-33. The method involves the use of two thermal phosphors that differ in the spectral distribution of their emitted energy (two-color phosphor). If the emitted radiation from the two phosphors are spectrally separated and individually detected, the ratio of the two intensities can be related to temperature. If the activating energy does not saturate the phosphors, then temperature measurement is independent of the activating energy, recording film and

model curvature. The thermal phosphors of Reference OS-33 were rare-earth types and were selected for a particular temperature range. Gd_2O_2S:Eu, for example, is active between 480 and 670 °R. Data analysis of the two phosphors can be accomplished using a data recorder similar to that developed by Reference OS-33. This recorder divides the emitted energy with a beam splitter into two beams that are then passed through interference filters to isolate the wavelengths of interest. The filtered beams are focussed on silicon photodiode detectors. The ratio of the two signals can then be related to temperature by prior calibration. A measurement accuracy of $\pm 0.2^{\circ}R$ is reported for a one-second measurement time (Reference OS-33). This recorder is, in essence, a two-color monochromator which can scan either (1) the model during actual tests, or (2) color photographs taken of the model during test. Because of the long measurement interval, a scan of photographs taken during model testing is recommended for cold wind tunnel applications.

The application of the thermal phosphor technique to cold wind tunnels is very similar to the liquid crystal technique (Paragraph 3.10) except that model heating by external lamps is most likely to be impossible. Because the intensity of radiation emitted by the phosphor is to be measured, irradiating the model with quartz lamps will make the detection of emitted radiation difficult. Prior experience has found that satisfactory temperature resolution is achieved if the activating energy is filtered so that only UV energy is incident on the model (References TS-6, -29 and M-88). Lamps are not available commercially that, when filtered, produce the UV energy needed in cold wind tunnels to result in a significant temperature change. Therefore, model heating must be

accomplished by resistively heating a metallic film plated on the surface.

The semi-infinite model design, operational techniques and the data reduction equations presented in Paragraph 3.10 also apply to thermal phosphors. The lamp used to illuminate the liquid crystal model is filtered so that only UV energy is incident upon the model surface. The two-color phosphor approach, described above, is recommended in order to eliminate errors induced by variations in UV energy, recording film and model curvature. The camera used to measure the wavelength of energy reflected by the liquid crystals is used to measure the intensity of energy emitted by the phosphors. A monochromator or a recorder similar to that of Reference OS-33 is used to scan the test photographs to determine the relative intensities of the two phosphors. Laboratory calibration tests are performed to relate the relative intensity to temperature.

The temperture measurement accuracy, $\pm 0.2\ R^{\circ}$ quoted by Reference OS-33. is the same as that reported for liquid crystals. Since calibration of the two techniques are similar and the model design and data reduction equations are the same, the measurement error of the thermal phosphor should be similar to the error presented in Table 8. Therefore, an error in the convective coefficient of approximately 13.5% is to be expected for the thermal phosphor technique. It should be noted that relative to liquid crystals, the thermal phosphor technique can induce an error associated with photographic coverage. For the liquid crystal, the reflected wavelength is related to temperature and variations in film quality or film processing are not likely to influence this measurement. For the thermal phosphor, however, the ratio of intensities for the two phosphors is related to temperature. If the photographic

films used in calibration and/or test cause differences in the relative intensity because of, for example, optical density, then an error will result. It cannot be determined with the data available if this error is important. Also, the calibration tests that are used to determine the relatively intensity versus temperature must use the tunnel viewing windows. These windows are a source of attenuation which is most likely wavelength-dependent.

3.12 IR Scanner

The spatial temperature distribution over a surface may be determined by scanning the emitted infrared (IR) radiation (References OS-23, -32, -39, -40, -43, -44, and M-116). A wide variety of systems based on this principle have been developed and used to measure convective coefficients in aerodynamic tunnels (References OS-40, -44 and M-116). Such thermal imaging systems have been in operation for many years and their development has continued at a steady pace because of their military and industrial applications. When these IR imaging sytems are linked with analog-to-digital converters and to advanced computer hardware and software, a powerful instrument is created that is capable of quantitatively computing, evaluating, and displaying temperature and heat transfer data. Pioneering work in the application of such a system has been underway at AEDC by the Von Karmen Facilities (VKF) staff since 1974. A comprehensive description of their system is presented in Reference OS-40. This type of system combines the obvious advantages of thermal mapping with the quantitative ability and automated data reduction of discrete gages.

The IR systems that have been used in aerodynamic tunnels are IR scanners. The scanner is an IR radiometer that focuses a small area of the tunnel model on to, typically, one detector. The detector scans the model by the use of mirrors that are mechanically varied so as to produce a point-by-point, line-by-line image of the object viewed. The AGA 680 IR scanner used by AEDC (Reference OS-40) produces an image composed of 70 lines with 110 points per line. The 7700-point matrix is scanned 16 times a second.

The IR detector elements are designed to be sensitive in the 3 to 5 micron wavelength range, a "window" in which the atmosphere has low absorptance. In general, detectors must be cooled to cryogenic temperatures to achieve high sensitivity. Detectors can be made capable of resolving temperature differences as small as 0.01°C, although 0.2°C is a value quoted for faster scanners. Infrared detectors of thermal radiation do not have an absolute DC response because they are affected by their own temperature and radiation from within the radiometer. The solution to the problem involves the use of a reference temperature source of known temperature and emissivity. Uncertainties in these values add to the uncertainties in the measured temperatures.

There are two basic areas of uncertainty in an IR heat transfer measurement system: uncertainties in the surface temperature measurement itself and uncertainties in converting the surface temperature measurement into a heat transfer coefficient. The primary parameters in the temperature measurement system are the following:

- Scanner calibration constants

- Scanner measurement repeatability
- Reference temperature
- Reference target emissivity
- Model emissivity
- Tunnel window transmittance factor

For the AEDC scanner, the above system parameters result in uncertainties in local surface temperature of from 1% to 2.5% of the absolute value as shown in Figure 14. Figure 14 was reproduced from Reference OS-40. As can be seen, at the recovery temperatures expected in the cold wind tunnel (480 to 530 deg R), a measurement error of up to 12 degrees R can be expected with the IR scanner. To minimize the effect of this error on convective coefficient, it is recommended that discrete surface temperature measurements be made using thermistors (or T/C) embedded in the model. The thermistor temperatures are used to measure model temperatures when the model is in an isothermal condition, thus minimizing the error induced by the thermistor bead, Paragraph 3.8.

Once the surface temperature history has been determined, the second problem is to convert this into a heat transfer coefficient distribution. This requires a knowledge of the thermophysical properties of the model surface material, and an analysis method to account for heat conduction away from the surface. The simplest and best analytical model is a one-dimensional, semi-infinite solid. If the surface material has a sufficiently low thermal diffusivity (i.e., is a good insulator) and is thick enough, the backface temperature will remain constant during the

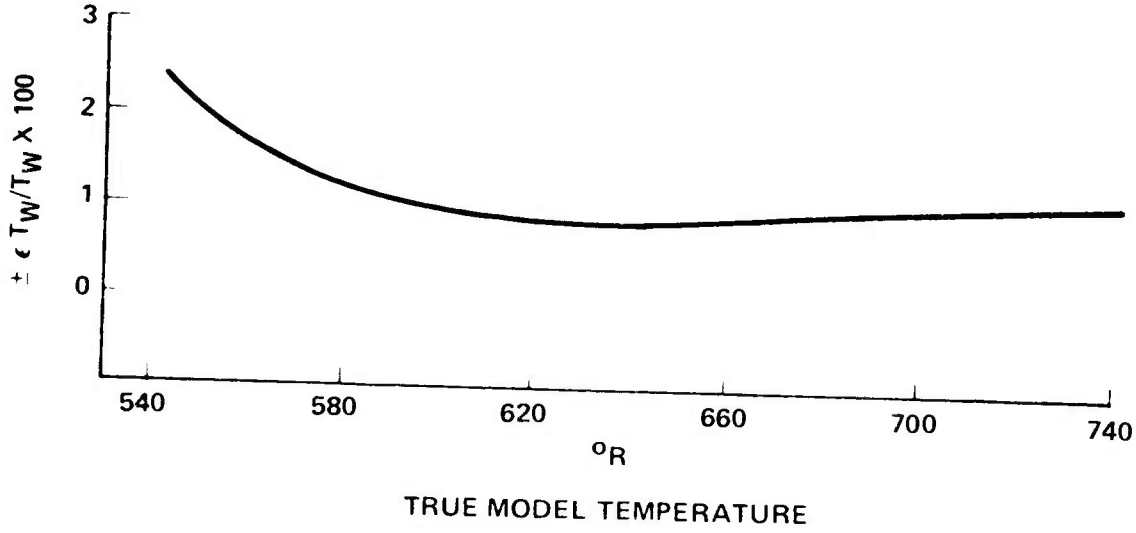

Figure 14. Effect of Random Errors on Model Surface Temperature Calculation

test. The importance of two-dimensional, or lateral, heat conduction will depend on the heat transfer distribution over the model surface and the thermal properties of the model material. The semi-infinite solid with a resistively-heated metallic plate on the surface is recommended. This model design is the same as the design described for the liquid crystal. Quartz lamps could possibly be used, but filtering will be required so that energy in the IR scanner waveband is not reflected off the model causing a background in the energy emitted by the model itself. The lamps and filters appear to be more complex than the resistance heater design and therefore are not recommended for further study.

Other major areas of concern with IR scanning systems are the spatial resolution of large temperature gradients, correlation of the temperature matrix data to specific locations on the model and the tunnel window. Experimentation with the AEDC system has shown that a steep temperature change gets "smeared" over a 0.3- to 0.6-inch wide band, and that a hot spot must be about 3/8 inch in diameter before the measured temperature resonse approaches the hot spot temperature. The temperature resolution limitations arise from the fact that although the scan identifies "points" that are close together (30 to 50 mils apart), each point is assigned the average temperature of a spot approximately 0.3 inch in diameter. The other problem of relating matrix locations with actual model locations usually is approached by providing physical "markers" at known locations on the model which are visible on the thermal image. In this way, the "geometric coordinates" of each matrix point can be estimated.

It should be noted that the above spatial resolution of 3/8-inch is applicable to the AEDC system and is dependent on the data averaging technique, scanner spot size, and the physical size of the facility and model under investigation.

The tunnel window separates the scanner from the flow environment. It must withstand the internal tunnel pressures and transmit IR energy in the appropriate wavelengths. Typical window materials include germanium, magnesium fluoride, and magnesium oxide. AEDC has reported (Reference OS-40) difficulties with their IRTRAN-2 material involving changes in transmittance due to surface contamination and/or moisture absorption. This has required in-tunnel calibration with black-body sources just prior to testing.

A block diagram of the AEDC system is shown in Figure 15. Once the tunnel data and thermal data reside in the main computer (a DEC-10, in this case), it can be processed in any number of ways to apply corrections and to prepare it for display in printed or plotted formats. A ten-color video monitor photograph from the system is presented in Figure 16. The pictures show the temperature contours on a 6-degree sharp cone in AEDC Tunnel B. The silicone rubber model has a cylindrical rod protruding from the surface, and is shown with both laminar and turbulent approach flow.

The material constant, $K\rho C$ of Equation 16, can be evaluated by laboratory calibration from Equation 17 or by the selection of materials and fabrication procedures that result in a $K\rho C$ constant that can be determined from handbook material property data. The design selected for the IR scanner and other instrumentation concepts using the semi-infinite approach uses resistance heating of thin metallic strips plated over the epoxy model. As

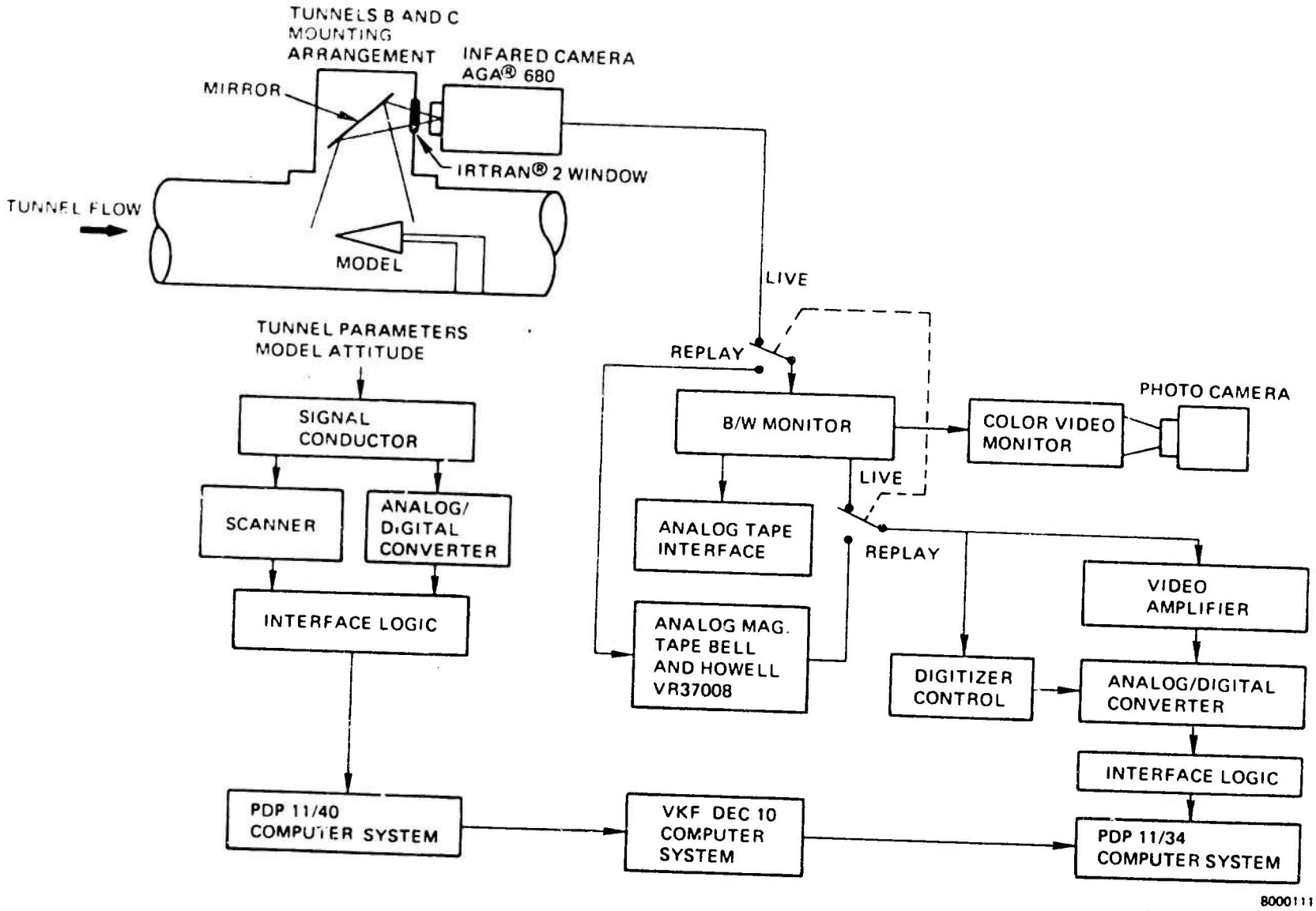

Figure 15. Block Diagram of AEDC IR Sensor System

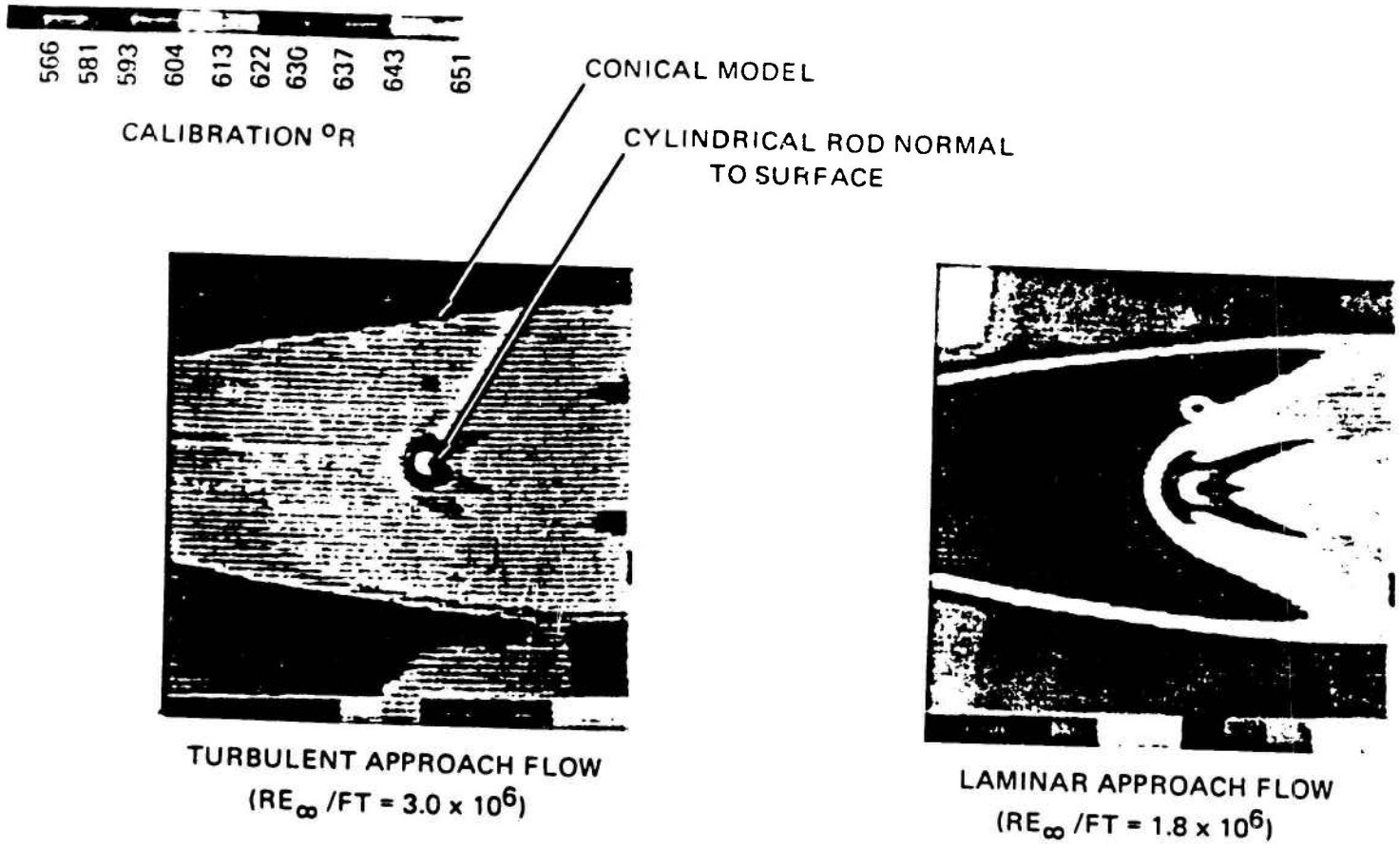

- 6° SHARP CONE IN AEDC/VKF TUNNEL A

Figure 16. Typical Infrared Thermal Image

noted, this approach requires some laboratory investigation to determine cost effectiveness and accurate fabrication procedures. Also, the resulting model should at least initially undergo laboratory calibration to determine the constant $K\rho C$ which is an effective value for the composite model.

The operational procedures of the IR scanner in cold wind tunnels are similar to those presented in Paragraph 3.10 for liquid crystals and are as follows.

(1) Laboratory calibration using a radiant heat source to determine the material constant, $K\rho C$, from Equation 17.

(2) Laboratory calibration of the resistance heater to determine the constants of Equation 4 using the procedure outlined in Paragraph 2.1.

(3) Pretest tunnel calibration with a black body source to determine window transmittance.

(4) The following temperatures inferred by the scanner are defined as "apparent temperature" because corrections have not been made for surface emissivity, model curvature, and transmittance of the tunnel window. With the tunnel nonoperating, scan the model to determine the apparent initial temperature, T_0. Measure the model temperature with a discrete device (i.e., thermistor). Turn the heater power on and scan the model to determine the apparent temperature, T_0, at time = t_1.

(5) With the tunnel operating and stabilized, allow the model to reach a thermal equilibrium (approximately 30 seconds). Scan the model to determine the apparent recovery temperature, T_R. At the same time, record the thermistor measurements of the actual recovery temperature

at discrete points. Turn the heater on and scan the model after approximately 3 seconds to measure the apparent temperature, T_W, at the time, t_1. Terminate the test.

(6) Post-test tunnel calibration with a black body source to determine window transmittance.

The IR scanner data using the computer techniques of, for example, Reference OS-40, can then be used to determine the apparent temperature as a function of model position for the above four model scans (two scans each in Steps 5 and 6). The thermistor temperatures are used to denote local recovery temperature. Recovery temperature distributions over the model are determined by using the IR scanner temperature field to extrapolate between thermistors. The apparent temperatures, T_R and T_W, measured in Step 5 and the constants measured in Steps 1 and 2 are used in Equation 16 to determine the area over the model surface that apparent temperature can be used to infer convective coefficient. That is, those areas of the model in which nonlinear effects occur due to optical properties of the model and tunnel window. The apparent temperatures measured in Step 5 are then used in Equation 16 to infer the convective coefficients.

The recommended data reduction technique "normalizes" some of the major variables in the tunnel test out of the problem. The model surface emissivity, model curvature, window transmittance and some of the scanner optical properties are of secondary importance. What is important is that they are constant in the pretest and during test scans. The convective coefficient is determined as the "difference" in response to identical optic conditions and heat dissipation with the tunnel flow on and off.

The error sources for the IR scanner and their uncertainty on the convective coefficient are as follows. Recovery temperature measurement error is $\pm 0.5^{\circ}R$ using the thermistor data and a relatively simple recording circuit. If the IR scanner is used to infer temperature without benefit of the thermistor, the resulting error would be $\pm 12^{\circ}R$, which is unreasonable. The $\pm 0.5^{\circ}R$ thermistor error produces a convective coefficient error of 8.9%.

The scanner temperature measurement error or transient wall temperature, T_W of Equation 16, is $\pm 6^{\circ}R$ (1% of absolute value per Figure 14). The corresponding error on convective coefficient is greater than 36% (see Paragraph 3.3). This error is not competitive with the errors of other sensor candidates and, therefore, the IR scanner is not recommended for cold wind tunnels. It should be noted that IR scanners provide very good measurement accuracies in hot wind tunnels where the surface temperature is relatively high compared to ambient or initial model conditions.

3.13 Phase Change Paints

Phase change paints have been extensively used in ground test facilities to infer convective heating (References TS-41 and M-88). In its usual form, a thin coating of the paint is applied to a thermally-thick model (i.e., semi-infinite). The coating undergoes a visible phase change at a known temperture. The precise time at which the change occurs is determined as a function of model surface location from an examination of movie film. The convective coefficient is then determined from the 1-D semi-infinite conduction equations (Equation 15 for radiation heating and Equation 16 for resistance heating).

Reference M-88 reports that, relative to thermal phosphors, discrete 2-D foil gages and IR scanning, the phase change paint technique provided the most definitive convective coefficient distribution. They attributed this to higher resolution provided by the paint technique in their application. The interpretation of the surface temperature is approximately +0.5 percent of the paint rated value (Reference M-88). Since the phase change paint is not reversible, the model must be stripped and repainted between tests.

Reference M-125 indicates that the quality and usefulness of paint inferred convective coefficients is inferior to the IR scanner. It is noted that the phase change paints suffer from problems associated with selecting the proper paint change temperture. That is, the change must not occur too early in the test to cause large time measurement errors, nor too late when the temperature change is relatively small. Also, acquiring data in low heating gradient situations induces large errors because the change is not distinct. In large heating gradient situations, as were evidently inherent in Reference M-88, problems arise with centering the phase change at a time that results in acceptable error, thus indicating multiple paints. Multiple paints are undesirable because the surface temperature response can be effected and data reduction/correlation become difficult.

In cold wind tunnel applications, phase change paints can be used to infer convective heating, provided the recovery temperature is determined by other means (e.g., surface thermistors and T/C). That is, phase change paints cannot be used for measuring temperatures below ambient which can be the case in cold wind tunnels. Therefore, the semi-infinite model design of Paragraph 3.3 or 3.8 can be used, which employs surface T/C or thermistors, respectively. The model can be heated either resistively or radiatively. Phase change paints are commercially-available (e.g., TEMPILAQ) with a wide selection of the temperature-sensitive value. Aerosol paints can be used to apply a thin coating to the model's surface.

The operational procedures of the phase change paint are as follows:

(1) Laboratory calibration using a radiant heat source to determine the material constant, $K\rho C$, from Equation 17.

(2) For the resistively heated model, laboratory calibration of the resistance heater to determine the constants of Equation 4 using the procedure outlined in Paragraph 3.1.

(3) For the radiatively-heated model, tunnel calibration of the incident radiant heat flux using the time of phase change as determined by movie coverage in Equation 17.

(4) With tunnel flow, the model is allowed to reach thermal equilibrium. Record thermistor (or T/C) measurements of the recovery temperature at discrete points. Heating by the resistor or lamps is initiated and

the model is photographed with high-speed film.

Data reduction involves determination of the time at which phase change occurs at specific locations on the model. This time, the temperature rating of the paint, the measured recovery temperature and the heating constants are used in Equation 15 or 16 to determine the convective coefficient.

The error sources for the phase change paint and their resulting uncertainty on the convective coefficient are presented below. The parameters that were used in the error analysis include q_{cw} = 20 Btu/ft^{2}sec, T_R = 478.8°R, nominal q_{elect} = 2.5 Btu/ft^2 sec, and nickel plate thickness = 0.002 inch.

(1) The temperature measurement error of the paint is $\pm$3°R (0.5% of absolute per Reference M-88) and produces a convective coefficient error of 30.5%.

(2) The temperature measurement error of the thermistor is $\pm$0.5% which measures the recovery temperature T_R (also equal to initial temperature T_o). The corresponding error in convective coefficient is 8.9%.

(3) Calibration of ρCK and its implication on convective coefficient is 3.0% (Reference DM-35).

(4) For electrical heating, calibration of the heat dissipation is 3.0% for the measurement of heat flux and 4% for heat losses that occur during calibration.

(5) For lamp heating, the $\pm 3^{\circ}R$ uncertainty in paint temperature measurement causes a 4.3% error in incident heating and a similar error in convective coefficient.

(6) For resistance heating, the nickel surface plate produces an error of 4.7% (Paragraph 3.10).

(7) Uncertainty in time at which phase change is noted is assumed to be 0.1 second (Reference M-88). The corresponding errors in radiation heating and convective coefficient are 1.6 and 4.6%, respectively.

The RSS errors for resistance and radiation heating methods are 33.0 and 32.9%, respectively. These errors are large relative to other candidate sensor techniques and, therefore, quantitative convective coefficients are not recommended. Because of the relative low cost of phase change paints, the model coated with the paint and tested to determine critical areas for discrete sensor placement is, however, recommended. Reference M-109 indicates that the use of paints in research blowdown facilities may be acceptable, but their use in production facilities is not encouraged.

4.0 SENSOR COMPARISON

Sensor comparisons are made using the sensor descriptions presented in Paragraph 3.0 as a basis. The sensors are compared on technical merit and costs in the following paragraphs.

4.1 Technical Comparison

The technical aspects of each candidate sensor are compared and rated in Table 9. The comparison parameters basically follow those derived from Reference DM-89. A weighting factor based on the objectives in the cold wind tunnel application was applied to each parameter. These objectives were to measure with sufficient accuracy the recovery temperature and convective heat transfer coefficients on an ogive cylinder at variable angle-of-attack and, at the same time, minimize (1) the complexity of model/sensor fabrication, (2) the complexity of data acquisition/data reduction and (3) facility requirements. As can be noted in the table, the parameters are weighted from 1 to 5, with the convective coefficient measurement error given the highest weight factor.

The rating in Table 9 was based largely on conjecture using library reviews, computer simulations and general experience in the areas of instrumentation design, model/sensor fabrication and data acquisition. The rating criteria was based from 1 to 10, with 10 being excellent or simple and 1 being poor or very difficult. The grading value vs. convective coefficient error that was used in the table is presented in Figure 17.

Table 9. Technical Rating of Candidate Heat Transfer Measurement Concepts

Comparison Parameter	Weighting Factor	① 1-D Thin Skin: Lamp	① 1-D Thin Skin: Resistance	② 2-D Foil: Fluid	② 2-D Foil: Element	③ Semiconductor: Lamp	③ Semiconductor: Resistance	④ Wafer Thermopile: Fluid	④ Wafer Thermopile: Element	⑤ Thin Film: Self	⑤ Thin Film: Lamp	⑤ Thin Film: Resistance	⑥ Semi-ss Semiconductor Lamp	⑦ Semiconductor Thermopile Fluid	⑧ Semi-ss Thermistor: Lamp	⑧ Semi-ss Thermistor: Resistance	⑨ Pyroelectric Lamp	⑩ Liquid Crystals: Lamp	⑩ Liquid Crystals: Resistance	⑪ Thermal Phosphors Resistance	⑫ IR Scanner Resistance	⑬ Phase Change Paints: Lamp	⑬ Phase Change Paints: Resistance
Accuracy																							
1) Data Reduction Theory	2	10	10	10	10	8	8	10	10	10	8	8	8	10	5	8	4	8	8	8	8	8	8
2) Calibration	2	9	9	9	9	6	7	10	10	9	6	7	8	4	6	7	5	5	6	6	8	8	8
3) Spatial Resolution	2	9	9	8	8	9	9	8	8	8	8	8	8	9	9	9	9	10	10	10	9	10	10
4) Effect of Model Temp	2	8	8	8	8	9	9	9	9	9	8	9	8	9	9	9	9	10	10	10	10	10	10
5) Effect of Model Roughness	2	8	8	8	8	9	9	8	8	8	8	9	8	9	9	9	5	10	9	9	9	10	9
6) Customize Sensitivity	1	7	7	7	7	7	7	10	10	7	8	8	10	10	9	9	7	9	8	7	5	7	7
7) Accuracy of Calibration	1	8	8	8	8	8	8	7	7	8	8	8	9	7	8	8	8	6	6	6	6	6	6
8) Recovery Temp Error, °R	8	4.0	4.0	4.0	4.0	4.0	4.0	4.0	4.0	0.7	0.7	0.7	0.1	0.1	0.5	0.5	0.7	0.2	0.2	0.2	6.0	3.0	3.0
9) Convection Coef (error), %	5	6.0	12.0	14.3	14.3	36.0	36.0	10.0	10.0	20.0	19.1	18.5	5.0	5.0	40.0	38.5	10.9	5.3	13.5	13.5	40.0	32.9	33.0
10) Major Error Source	-	Temp	Temp	Temp	Temp	Temp	Temp	Temp	Temp	Cor	Temp	Temp	Cal	Cal	Sd Dia	Bd Dia	Cond Losses	Cal	Cal	Cal	Temp	Temp	Temp
Model Fabrication																							
1) Model Fabrication	2	7	5	7	6	8	6	5	5	7	7	5	4	3	8	5	7	8	8	8	8	8	8
2) Sensor Fabrication	2	7	7	7	7	8	8	8	8	7	7	7	3	3	9	8	7	5	7	7	2	10	10
3) Instrument Placement	1	6	6	6	6	8	8	6	6	7	7	7	5	5	5	5	5	10	10	10	10	-	10
4) Applicability to Other Models	1	6	6	7	7	8	8	7	7	8	8	7	5	5	7	7	8	8	8	9	9	10	10
5) Prior Experience	2	8	8	9	9	8	8	8	8	8	8	9	4	4	4	4	5	8	8	8	8	10	10
6) Use with Other Sensor Concepts	1	8	8	9	9	9	9	9	9	9	9	9	9	9	9	9	8	10	10	10	10	10	10
Model Durability																							
1) High-Pressure & Vibrations	1	7	7	8	8	9	9	9	9	9	9	9	8	9	8	8	3	9	9	9	9	9	9
2) Impingement	1	5	5	5	5	9	9	9	9	7	7	7	7	7	9	8	3	10	10	10	10	10	10
3) Temperature	1	6	5	10	10	6	5	10	8	8	6	5	7	9	4	5	5	8	5	5	5	8	5
Facility Requirements																							
1) Data Recording	2	9	9	9	9	9	9	9	9	8	8	8	9	9	8	9	8	8	9	9	2	10	10
2) Tunnel Alterations	2	5	9	8	9	6	9	8	9	9	4	9	4	8	4	9	4	3	5	8	7	4	10
3) Operating Procedures	1	6	8	9	9	8	8	10	10	7	8	9	7	10	8	8	7	5	7	7	7	7	9
4) Data Reduction Procedure	2	10	10	10	10	8	8	10	10	1	8	9	9	10	8	8	8	8	5	5	2	8	5
Overall Rating, Average	37	7.3	7.3	8.0	8.0	6.8	6.9	8.5	8.5	5.6	7.5	7.7	7.2	7.7	5.5	5.8	8.9	8.0	7.7	8.0	5.8	7.6	7.9

93/94

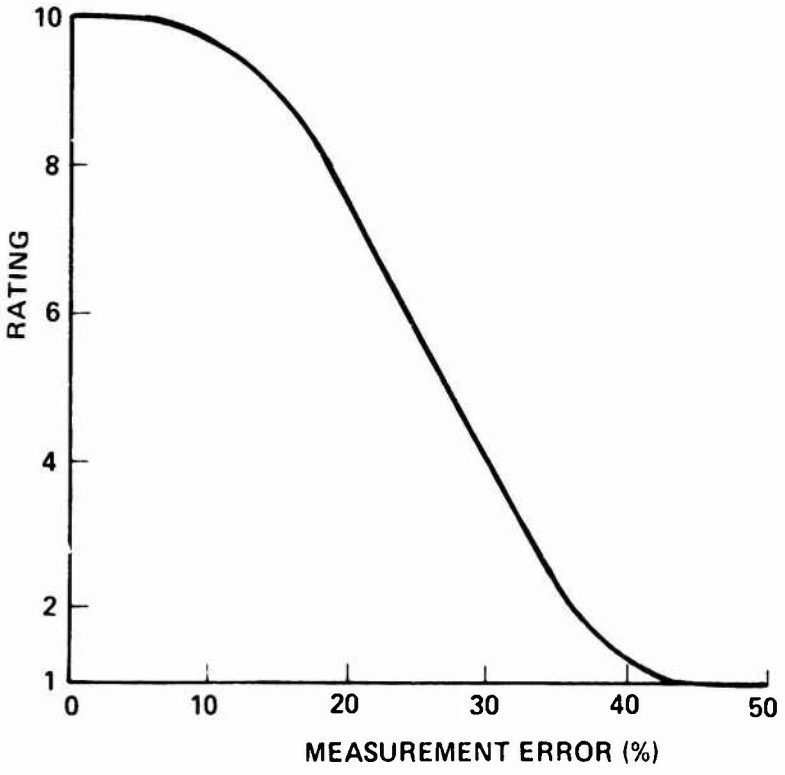

Figure 17. Technical Rating of Convective Coefficient Measurement Error

The wafer thermopile (Sensor 4) has the highest rating (8.5). The 2-D foil (Sensor 2), liquid crystals (Sensor 10), thermal phosphor (Sensor 11) and phase change paint (Sensor 13) are all rated very close to 8.0. In comparison, the baseline sensor, 1-D thin skin, has a rating of 7.3. The key features of each sensor and their comparison to other competing sensors are summarized below.

The thin skin, Sensor 1, has the advantage over most other sensors of being capable of operating at steady-state conditions. This eliminates the requirement for measuring transient temperature responses and, provided conduction losses are tolerable, the convective coefficient and recovery temperatures are independent of material properties and model design. The model does require external heating, either with external quartz lamps or by the resistance heating of a thin metallic film plated on the model's surface.

The 2-D foil, Sensor 2, has the advantage of being capable of operating at steady-state conditions, but relative to the thin skin, has the added advantage of being heated internally by a fluid or an electrical heater element. These heating methods minimize the requirements on tunnel operation (e.g., placement of quartz lamps) or model fabrication (e.g., plating a resistance metallic film). The measured convective coefficient is a function of material thermal conductivity and sensor design.

The semi-infinite solid with conventional T/C, Sensor 3, offers the advantage of not requiring holes in the model, as do the thin skin and 2-D foil. Therefore, more measurement locations are possible over the model's surface. Convective coefficient is calculated from the measured

transient surface temperature and, therefore, convective coefficient is critically dependent on the uncertainty in the temperature measurement. The temperature uncertainty ($\pm 4^{\circ}R$) induces a relatively large error on the convective coefficient. The semi-infinite solid is heated externally in the same manner as the thin skin.

The wafer thermopile, Sensor 4, is similar to the 2-D foil in that it can operate under steady-state conditions and can be heated internally by a fluid or an electrical heater element. The thermopile can be calibrated by the vendor prior to model fabrication. The thermopile measures heat flux and a resistance thin film or thermistor can be used to measure surface temperature.

The thin film, Sensor 5, infers the convective coefficient by measuring the transient surface temperature response of a semi-infinite solid. Relative to the conventional T/C, the thin film offers greater accuracy in the measurement of temperature. External heating of the model is required.

The semi-infinite solid with a semiconductor T/C, Sensor 6, offers excellent measurement accuracy. The T/C's are, however, not commercially available and specially fabricated and calibrated sensor plugs will be required for model applicatons. These installation and model fabrication requirements necessitate the use of external quartz lamps for model heating.

The semi-conductor thermopile, Sensor 7, is similar to the wafer thermopile (which uses conventional T/C) except the semi-conductor T/C's are not commercially available. Thus, specially fabricated and calibrated sensor units are required for model applications.

The semi-infinite solid with a thermistor, Sensor 8, offers good temperature measurement accuracy, but the relatively large volume of the sensor bead results in a temperature measurement averaged over its indepth thickness. In the transient temperature measurements required by the semi-infinite solid, a relatively large error in convective coefficient results.

The pyroelectrical, Sensor 9, has the advantage over other transient sensors of measuring directly the temperature rate of change and, therefore, lower measurement error can be expected. The sensor is not available commercially, thus requiring the insertion of sensor plugs in the model. These installation requirements necessitate the use of external quartz lamps for model heating. The sensor has the disadvantage over other sensor concepts of being fragile because of crystal brittleness and weak electrical contacts.

The liquid crystal, Sensor 10, measures the surface temperature of a semi-infinite solid by the selective reflection of light at different wavelengths. This "non-contact" sensor allows the measurement of recovery temperature and convective coefficient distributions over a relatively large area of the model's surface. An external white light source is required that is located so that specular reflection occurs from the lamp to model to recording camera. Temperature measurement is independent of

lamp instensity, model curvature, model optical properties, film quality and film processing. Data reduction involves scanning the photographs with a monochromator. Data reduction can possibly be simplified and made more cost-effective by using a color TV camera and color processing electronics.

The thermal phosphor, Sensor 11, measures the surface temperature of a semi-infinite solid by the emission intensity of the phosphor. This "non-contact" sensor, like the liquid crystal, allows the measurement of recovery temperature and convective coefficient distributions over a relatively large area of the model's surface. An external UV lamp is used to activate the thermal phosphor. The emitted intensity, which is temperature-dependent, is recorded on photographic film. Conventional data reduction involves measuring the relative intensity profiles of pretest and during-test photographs using an isodensometer to infer temperature distributions. This, to some extent, minimizes the effect of model curvature, UV light intensity and photographic processing on the measurement error. To completely eliminate any random fluctuations in these error sources, a mixture of two phosphors with two different emission spectras is recommended. The relative intensities of the two phosphors can be measured by a monochromator and related to tempertaure.

The IR scanner, Sensor 12, is "non-contact" like the liquid crystal and thermal phosphor, with temperature inferred by measuring the energy emitted by the surface. The model's surface is resistively heated. The IR scanner, at cold tunnel conditions, results in a relatively large temperature measurement error. Also, the IR scanner is a very complex

instrument with data recording and data reduction requiring complex computer techniques.

The phase change paint, Sensor 13, is a "non-contact" device that measures surface temperature by denoting the time of phase change from test movies. Because the tunnel supply temperatures can be below ambient, phase change paint cannot be used to measure recovery temperature, thus requiring auxilliary sensor concepts, e.g., thermistors. The phase change paint is relatively simple in both model designs, data recording and data reduction. Fairly large errors in the convective coefficient are produced by the uncertainty in phase change temperature ($\pm 3^{\circ}R$).

4.2 Cost Comparison

Cost estimates were made for each candidate sensor and the results are presented in Table 10. Each sensor is costed separately. Nonrecurring costs are presented to identify the capital equipment costs and/or development effort that is required to experimentally evaluate unknowns in sensor operation or sensor fabrication. Unit costs are presented based on using proven fabrication and operation techniques with one model being tested one time.

The costs were estimated assuming that an instrumentation firm performs or assists the government in the following efforts:

(1) Procures the hardware noted in Table 10.

(2) Fabricates the model per government-furnished design drawings.

Table 10. Cost Estimates of Candidate Heat Transfer Measurement Concepts

[illegible]	[illegible]	[illegible]	[illegible]	[illegible]	[illegible]	[illegible]	[illegible]	[illegible]	[illegible]	[illegible]	[illegible]	[illegible]	[illegible]
[illegible]	[illegible]	[illegible]	[illegible]	[illegible]	[illegible]	[illegible]	[illegible]	[illegible]	[illegible]	[illegible]	[illegible]	[illegible]	[illegible]
[illegible]	[illegible]	[illegible]	[illegible]	[illegible]	[illegible]	[illegible]	[illegible]	[illegible]	[illegible]	[illegible]	[illegible]	[illegible]	[illegible]
[illegible]	[illegible]	[illegible]	[illegible]	[illegible]	[illegible]	[illegible]	[illegible]	[illegible]	[illegible]	[illegible]	[illegible]	[illegible]	[illegible]
[illegible]	[illegible]	[illegible]	[illegible]	[illegible]	[illegible]	[illegible]	[illegible]	[illegible]	[illegible]	[illegible]	[illegible]	[illegible]	[illegible]
[illegible]	[illegible]	[illegible]	[illegible]	[illegible]	[illegible]	[illegible]	[illegible]	[illegible]	[illegible]	[illegible]	[illegible]	[illegible]	[illegible]
[illegible]	[illegible]	[illegible]	[illegible]	[illegible]	[illegible]	[illegible]	[illegible]	[illegible]	[illegible]	[illegible]	[illegible]	[illegible]	[illegible]
[illegible]	[illegible]	[illegible]	[illegible]	[illegible]	[illegible]	[illegible]	[illegible]	[illegible]	[illegible]	[illegible]	[illegible]	[illegible]	[illegible]
[illegible]	[illegible]	[illegible]	[illegible]	[illegible]	[illegible]	[illegible]	[illegible]	[illegible]	[illegible]	[illegible]	[illegible]	[illegible]	[illegible]

*X/Y is X = nonrecurring costs, Y = per model + 1 test cost.
**Costs are $ x 10-3.
***Hardware assumed already available at tunnel.
†Ratio of sensor cost to cost of Sensor (1).

101/102

(3) Performs or subcontracts sensor calibration as noted in Table 10.

(4) Assists wind tunnel personnel in tunnel modifications, data acquisition and model installation.

(5) Performs data reduction on tunnel-supplied data.

The labor hours and other direct costs presented in Table 10 were converted into total sensor costs by using PDA labor, overhead and G&A rates. The total costs were then normalized using the 1-D thin skin cost as a basis. The normalized costs are presented in the table.

Where applicable, cost estimtates were made for resistance model heating, rather than the external lamp method because of the former's lower cost. As noted in Paragraph 3.1, a laboratory effort is required to evaluate resistance heater fabrication and implications on model performance (i.e., surface roughness and plate structural integrity). This task was included in the nonrecurring model fabrication estimates.

As can be seen in Table 10, the 2-D foil, Sensor 2, is the most cost-effective of all sensors, in both nonrecurring and unit costs. This is largely attributable to its metal construction and internal fluid heating method. The phase change paint method, Sensor 13, has the same nonrecurring cost as the 2-D foil, but higher unit costs attributed largely to the resistance surface heater and photographic data reduction procedure.

5.0 SENSOR RECOMMENDATIONS

Paragraph 3.0 has described the design, fabrication, tunnel operation and errors of candidate sensors in cold wind tunnel applications. Paragraph 4.0 has compared each sensor on a technical and cost basis. The sensor designs and comparisons were based on instrumenting an ogive/cylinder model that is to be tested in the AFWAL Mach 3 tunnel. The model and tunnel features and conditions were presented in Paragraph 2.0. It should be noted that a particular tunnel condition and model heating value were used in the error analysis. The error magnitudes can therefore be expected to change for other tunnel-model conditions or combinations. The dependence of sensor errors on tunnel condition and model geometry were not analyzed; however, for the condition selected, it is not expected that the relative error between sensors will change appreciably for other AFWAL tunnel conditions. Also, the comparisons of Paragraph 4.0 were based on conjecture which is, of course, dependent on the literature at hand and experience in instrumentation, model fabrication and wind tunnel testing. Thus, the comparisons of Paragraph 4.0 can be expected to change depending on the personnel performing the task and their relative experience in each technical aspect/cost item presented in Tables 9 and 10, respectively. Additional features that can influence sensor ratings are the relative objectives of the particular test. That is, for example, the relative ranking of measurement resolution, measurement error and cost will influence sensor selection.

To minimize the subjectiveness that could be involved in final sensor selection, it is recommended that a limited fabrication and test effort be performed to investigate critical features of the sensor sytems that are concluded in this study to be prime candidates for cold wind tunnel applications. These efforts should then be integrated into the investigations of this program to identify changes or revisions to the results presented in Paragraphs 3.0 and 4.0.

An overall summary of each sensor is presented in Table 11. The measurement error and technical rating of Table 9 and the cost rating of Table 10 are presented in the table. Also in the table, the sensors are ranked as to overall utility for making cost-effective, accurate convective heat transfer measurements in cold wind tunnels. The key reasons for sensor ranking are presented below in the order of the overall sensor utility.

(1) The wafer thermopile, Sensor 4, was ranked first because of its high technical rating, low measurement error and cost effectiveness. The sensor is capable of steady-state operation with internal heating. Calibrated thermopiles are commercially available. The convective coefficient is, however, measured discretely requiring multiple sensors to define heat transfer distributions.

(2) The 2-D foil, Sensor 2, has many of the advantages of the wafer thermopile and was rated second. Relative to the wafer, the 2-D foil is not quite as accurate and a little more complex to fabricate.

(3) The liquid crystal, Sensor 10, was rated third because, relative to the wafer and 2-D foil, it offers the ability to measure heat transfer

Table 11. Sensor Comparison Summary

Sensor	Measurement Error		Technical Rating	Cost Rating		Overall* Utility
	Temperature (°R)	Convective Coefficient (%)		Nonrecurring	Per Model + 1 Test	
(1) 1-D Thin Skin, Resistance Heating	4.0	15.0	7.3	1.0	1.0	7
(2) 2-D Foil, Fluid Heating	4.0	14.3	8.0	0.91	0.84	2
(3) Semi-∞ T/C, Resistance Heating	4.0	36.0	6.9	1.33	1.44	11
(4) Wafer Thermopile, Fluid Heating	4.0	10.0	8.5	1.11	1.59	1
(5) Thin Film, Resistance Heating	0.7	18.6	7.7	1.59	1.89	5
(6) Semi-∞, Semiconductor T/C, Lamp Heating	0.1	~5.0	7.2	2.47	2.77	9
(7) Semiconductor Thermopile, Fluid Heating	0.1	~5.0	7.7	1.73	1.99	8
(8) Semi-∞ Thermistor, Resistance Heating	0.5	38.5	6.8	1.45	1.47	12
(9) Pyroelectric, Lamp Heating	0.7	10.9	6.8	2.22	2.33	10
(10) Liquid Crystal, Resistance Heating	0.2	13.5	8.0	1.98	1.93	3
(11) Thermal Phosphor, Resistance Heating	0.2	13.5	8.0	2.55	2.47	4
(12) IR Scanner, Resistance Heating	6.0	>40.0	5.8	9.80	1.67	13
(13) Phase Change Paint, Resistance Heating	3.0	33.0	7.9	0.91	1.20	6

*1 is the most desirable; 13 is the least desirable.

distributions over a large portion of the model. It is slightly inferior to the above two sensors in measurement error, technical rating and cost. The liquid crystal was selected over other "non-contact" sensors because it (a) is essentially insensitive to model curvature, illuminating light intensity and photographic properties, and (b) has the capability of being cost-competitve by using color TV camera hardware to record and reduce data. By using, for example, discrete, thin film resistance thermometers on the surface, a hybrid sensor concept can be used to simultaneously compare one measurement concept with another.

(4) The thermal phosphor, Sensor 11, has many of the advantages of the liquid crystal and was ranked fourth. A design feature (i.e., two phosphors with different spectral emission) that has been used on discrete thermal phosphor sensors to cancel out the effects of activating light intensity, model curvature and photographic properties has not been applied to large area photographs of wind tunnel models. This feature is the reason the phosphor is rated below the liquid crystal. The phosphor has the advantage over the crystal of not requiring that the light-model-camera placement follow the law of spectral reflection. This feature may limit the area over the model surface which the liquid crystal can take measurements. The use of the thermal phosphor with another sensor also offers the advantage associated with a hybrid sensor system.

(5) The thin film resistance thermometer, Sensor 5, is selected fifth because of its relative low measurement error in surface temperature. Compared to the above four sensors, however, it is inferior in both

the convective coefficient measurement error and technical rating. It does offer cost advantages over the liquid crystal and thermal phosphor. Because of its temperature measurement ability, it is recommended to be used in conjunction with the liquid crystal and thermal phosphor as a hybrid design method.

(6) The phase change paint, Sensor 13, apparently offers good measurement resolution and low cost in some applications, but has large measurement error. Also, the sensor requires the use of a second temperature measurement device because recovery temperature can be below ambient. the use of phase change paint with the thin film sensor is recommended as a hybrid system. The thin film provided data at discrete points with which the paint data can be used for extrapolation to define heat transfer distributions over the model's surface.

(7) The 1-D thin skin, Sensor 1, is rated seventh, below the wafer thermopile and 2-D foil because it cannot be heated internally and has a slightly larger measurement error. The thin skin is rated below the thin film resistor because of temperature measurement resolution. Use of a thermistor instead of a conventional T/C as the temperature sensor would result in the thin skin being slightly superior to the thin film, however, the structural integrity of the nickel plate with a thermistor must be experimentally evaluated. The thin skin is rated below the liquid crystal, thermal phosphor and phase change paint because of the former's inability to measure convective heating over a large area of the model.

(8) The semiconductor thermopile, Sensor 7, offers excellent measurement

resolution and can be operated at steady-state conditions with internal heating. The sensor is not commercially available and, therefore, sensor costs are high. The resolution provided by commercial thermopiles using conventional T/C's is more than adequate because the convective coefficient error is dictated by the ability to measure surface temperature. The more-sensitive semiconductor thermopiles are concluded, therefore, to be an over-design for cold wind tunnel applications.

(9) The semiconductor T/C in a semi-infinite solid, Sensor 6, is placed ninth because of technical rating and cost. The device is not commercially available and fabrication features require that the device be installed on a plug which is then inserted in the model. This feature has the disadvantage of requiring external light sources for heating which, relative to resistance heating, is expensive.

(10) The pyroelectric crystal, Sensor 9, is rated low because of technical rating and cost. The device is not commercially available and fabrication methods require that the sensor be installed on a plug which is then inserted in the model. This feature, like Sensor 6, requires expensive external light sources for model heating. The pyroelectric sensor is technically rated lower than the other discrete sensors listed above because it is structurally fragile and data reduction should be supported by computer simulations to minimize error.

(11) The semi-infinite solid using conventional T/C, Sensor 3, is rated low because of measurement error. The temperature measurement sensitivity

of the T/C under transient conditions, induces an unacceptable error on the convective coefficient.

(12) The semi-infinite solid using a thermistor, Sensor 8, produces an unacceptable error in the convective coefficient because of bead sizes. If bead sizes lower than 0.007 inch are commercially available, then the conduction error may be lowered so the device can become competitve with the thin film resistor, Sensor 5, which is rated fifth.

(13) The IR scanner, Sensor 12, is rated last because of measurement error and cost. The IR scanner is desirable when the temperature rise of the model is high enough so that the uncertainty in temperature measurement is close to other sensor errors. Also, the nonrecurring cost is approximately 10 times that of the baseline sensor.

Based on the investigations that have been performed and documented in the preceeding paragraphs, the wafer thermopile, 2-D foil, liquid crystal and thermal phosphor sensors (Sensors 4, 2, 10 and 11, respectively) are the prime candidates for cold wind tunnels. Hybrid versions of liquid crystal and thermal phosphor sensors are recommended using thin film resistance thermometers (or thermistors, if bead size less than approximately 0.003 inch are commercially available). Design drawings for the recommended sensors are presented in Appendix C. It should be noted, as mentioned above, that the ranking could be interpreted as subjective. Laboratory investigations are therefore recommended in order to minimize any possible oversights that are inherent in these recommendations.

APPENDIX A. LITERATURE SEARCH

A.1 INTRODUCTION AND SUMMARY

A literature search was performed for the purpose of identifying candidate instrumentation techniques that can effectively measure heat transfer to models operating in wind tunnels with a total temperature close to ambient. The objectives of the search were to identify the following:

1. New, innovative measurement techniques.
2. Advances in conventional techniques.
3. Details on sensor operation (i.e., sensor physics of operation, error, and data reduction).
4. Details on sensor application (i.e., model fabrication, sensor installation).

The search identified approximately 300 candidate references. The articles and/or abstracts of over 80 percent of these references were reviewed to determine their respective applicability to cold wind tunnels. The remaining articles could not be located by the techniques used in the search.

From the literature review, twelve (12) candidate instrumentation techniques were identified that are recommended for further evaluation. These techniques include the following:

1. 1-D thin skin T/C (baseline)
2. 2-D foil T/C
3. Metalized surface T/C
4. Thermopile, wafer
5. Thin film resistor
6. P-N semiconductor, surface
7. P-N semiconductor, wafer
8. Thermistor
9. Ferroelectric sensor, surface
10. Thermal phosphor
11. Liquid crystal
12. IR scanner

In the following paragraphs, the procedures that were involved in the literature search are described together with a list and summary of all identified references. Also presented are the reasons for selecting the above candidates together with a description of each sensor.

A.2 LITERATURE SEARCH

The literature search was performed using the library facilities at PDA Engineering, University of California at Irvine (UCI) and The Aerospace Corporation. The sources that were reviewed in the search included the following:

- Engineering Index (EI), 1965- June 1981
- International Aerospace Abstracts (IAA), 1963-1975
- NASA Scientific and Technical Aerospace Reports (STAR), 1965-1980
- Applied Science and Technology Index (ASTI), 1965-1978
- NASA Aeronautical Engineering Cumulative Index, 1976-1979
- Cumulative Index to NASA Technical Briefs, 1970-1979
- NASA Technical Memoranda, 1972-1976
- NASA Technical Translations, 1965-1975
- NASA Contractor Reports, 1973-1977
- NASA Technical Reports, 1961-1975
- NASA Technical Notes, 1973-1976
- The Aerospace Corporation Library Literature Search, 1965-1980
- Technical Information Center (formerly DDC) Search, 1953-1980

The key words that were used in the search included the following:

- Heat Transfer Measurement
- Convective Heating
- Aerodynamic Heating
- Heat Flux Gage/Sensor
- Heat Transfer Gage/Sensor
- Calorimeter
- Temperature Measurement
- Thin Film
- Thin Foil
- Thin Skin
- Liquid Crystals
- Phosphors, Thermal
- Infrared Cameras/Scanning

The candidate references that were identified in the search are presented in Tables A-1, -2, -3 and -4. The references are divided into four categories based on sensor type; Direct Measurement, Temperature Sensitive Coatings, Optical and Miscellaneous. The direct measurement category involves the physical attachment of a sensor on a model for measuring temperature. Temperature sensitive coatings and optical methods are self-descriptive. Miscellaneous involves references with more than one sensor category or requires review for category definition.

A.3 LITERATURE REVIEW

The libraries at PDA, the Aerospace Corporation and UCI were used to locate the references identified in Paragraph A.2. The references that were found and reviewed are noted in the tables to this appendix. A brief summary of each reference that was reviewed is also given in the tables. Those references that could not be located and appear to be very useful to the program will be ordered through the proper agency.

The measurement techniques were evaluated based on the following criteria:

1. Measurement sensitivity, accuracy and repeatability of data.
2. The requirement for changing model surface temperature from ambient conditions.
3. Equipment requirements and applicability to model type and facility.
4. Calibration and data reduction.
5. Cost of equipment, fabrication and operation.

The measurement techniques that were identified in the literature review are described in the following paragraphs by category.

A.3.1 Direct Measurement Techniques

The direct measurement techniques and sensor elements that have been identified are summarized in Table A-5. The calorimeter design(s) that appears to be most suitable for each particular sensor are noted. The calorimeter types are particular designs that place the sensor in a situation wherein the response can be used to infer heat flux.

The 1-D thin skin calorimeter operates on the principle that the model material in the vicinity of the sensor is isothermal so that the response of a sensor on the skin's backface can be used to infer heat flux. The 2-D foil calorimeter (Gardon gage) is a thin disk that is heatsunk around its circumference. Heat incident on the disk causes a temperature gradient between the disk's center and circumference that is related to heat flux by prior calibration. The semi-infinite solid is simply the direct measurement of surface temperature. The wafer calorimeter is the measurement of the temperature difference between the two surfaces of the wafer. The null point calorimeter is a particular version of the semi-infinite solid except the surface temperature is inferred by drilling a particular size hole to a given depth from the surface. The hole depth and diameter are sized to cause a "hot spot" wherein the temperature at the bottom of the hole (next to the surface) is at the surface temperature of the undistributed material. The slug calorimeter is similar in principle to the 1-D thin skin except lateral conduction losses are generally reduced by using an insulator.

Discussions of sensor designs as applied in the above calorimeter types follow.

Thermocouple (T/C)

Thermocouples can be used in all the above mentioned calorimeters. The measurement sersitivity for single junction T/C are nearly 1/30 of the sensitivity that can be acquired by thermopiles and p-n semiconductors. The Chromel-Constantan junction has the highest T/C emf output with 0.061 mv/°C. In comparison, a p-n germanium junction has an output of 2.0 mv/C(DM-22)*.

The T/C is, however, cost effective because of its simplicity in fabrication, calibration and data reduction. The calorimeters using T/C that have been selected for further evaluation include 1-D thin skin, 2-D foil and semi-infinite solid. Schematics of these calorimeters are presented in figure A-1. The 1-D thin skin was selected because the concept has had extensive experience in hot and cold tunnel heat transfer measurements. This device will be the basis for comparing the other selected sensors. The measurement sensitivity and response time depends largely on wall thickness and material type. The wall thickness must be minimized to enhance responsitivity and yet thick enough to survive structurally. Also, the diameter of the thin wall section and the T/C wire diameter must be sized to minimize conduction errors. Thin skin calorimeters have been sized to measure heat fluxes of less than 1 Btu/ft^{2}sec with response times of approximately 10 millisconds (DM-21). Calorimeter construction methods depend largely on measurement space, model design, responsivity, structural loads and cost. Typical construction methods are as follows:

1. Milling, chemically etching or electro-discharge machining thin-walled sections in the model and welding T/C on the backface.
2. Plating a metal layer over a model with pre-drilled holes. T/C are positioned in the holes with temporary filler material. After plating, which forms a T/C on the surface, the filler is removed chemically or by heating.
3. Bonding a thin-metal foil over a model with pre-drilled holes and welding T/C to the backface.

The 2-D foil calorimeter was selected because it provides an instantaneous-direct measurement of heat flux with lateral conduction heat losses inducing little or no error. The device is also easily calibrated (M-40). The nonuniform surface temperature can, however, induce error if the difference in recovery and surface temperature is of the same order as the temperature gradient across the foil. A rugged foil calorimeter has a practical measurement range of approximately 5 Btu/ft^{2}sec with a response time of approximately 50 milliseconds.

The semi-infinite solid was selected because the approach offers two alternate designs. The design variations involve:

1. Metalized surface with one lead extending into the epoxy model with the other lead being the metalized surface. The metalized surface can be continuous or striplined to form a series of resistance heaters over the surface.

---

* References in Tables A-1 to -4. DM = Direct Measure, TS = Temperature Sensitive Coatings, OS = Optical Systems and M - Miscellaneous.

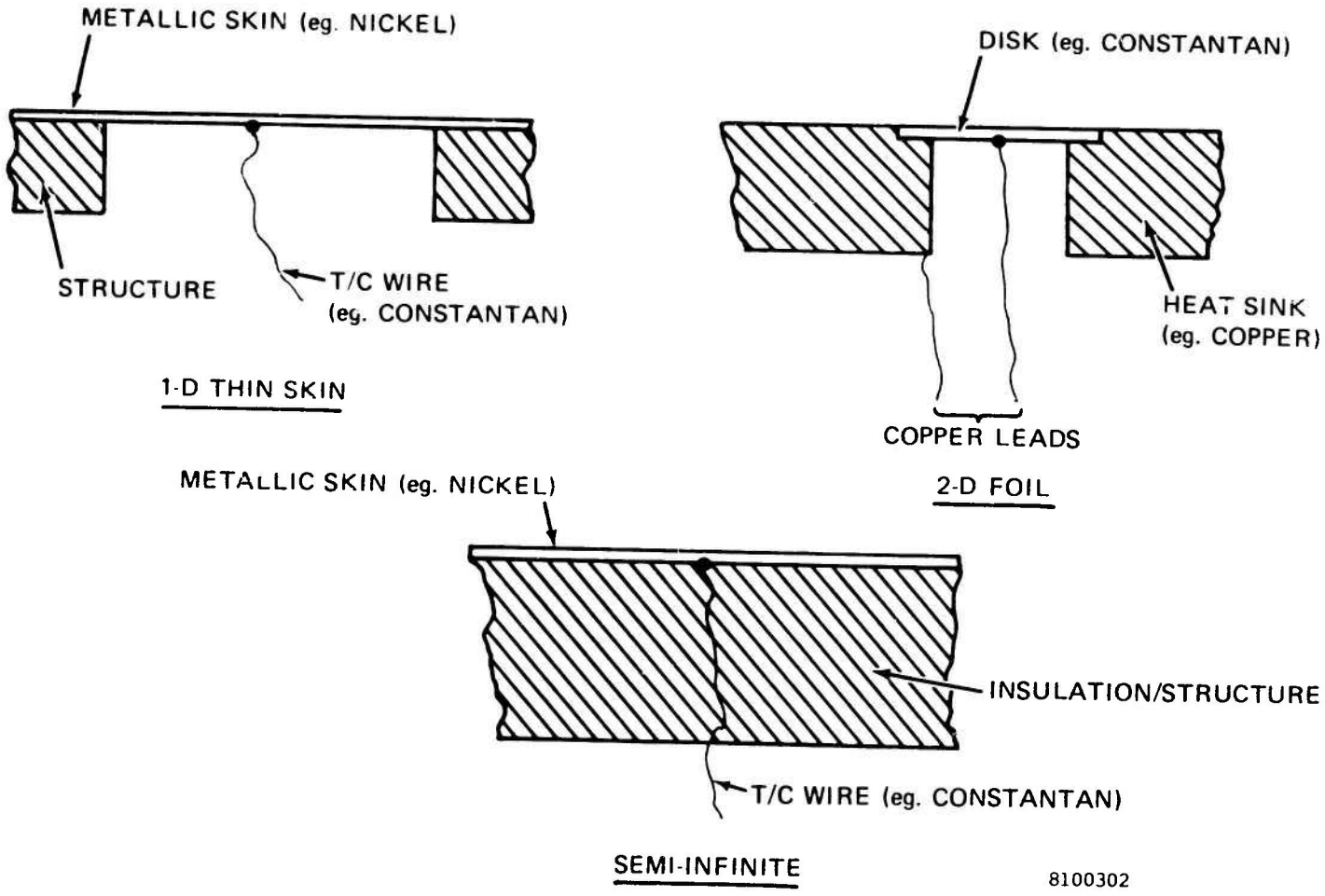

Figure A-1. Examples of T/C Type Calorimeters

2. Coax T/C with an insulated T/C wire penetrating the model and folded over at the surface to form a junction.

The use of a T/C on a wafer calorimeter was not selected because the thermopile, which is a candidate, is far superior in this application. The null-point calorimeter was not selected because this is a version of the above semi-infinite solid approach for applications that have high heating rates. The slug was not selected because it is similar in concept to the 1-D thin skin and more complex because of insulation requirements.

Thermopile

The thermopile consists of a number of differential thermocouples electrically connected in series so that their outputs are additive. To achieve a temperature difference between the two sets of junctions, one set of junctions is typically grouped in a common location that receives heat directly. The other set is attached to a heat sink. The thermopile in this orientation is commonly used in one of two calorimeters: wafer or suspended as shown in Figure A-2.

The wafer type has one set of junctions on the exposed surface of an insulating wafer and the other set between the wafer and model body. Heat flow causes a temperature gradient across the wafer which is proportional to the incident heat flux. The measurement sensitivity and therefore the measureable heat transfer rate is limited by the space available to mount the wafer. Response times are limited by the wafer thickness and thermal properties. Accurate low heat flux measurements are typically achieved with a response time of approximately 250 milliseconds (DM-35). The wafer is structurally rugged when properly attached to the model. The wafer thermopile is a candidate for use in cold wind tunnel tests because of measurement sensitivity and ruggedness.

The suspended thermopile is very fragile and it is therefore not recommended as a candidate for cold wind tunnel applications. This type of thermopile involves the attachment of one set of junctions on a receiver disk that is suspended by lead wires that attach the other set of junctions to a hollow-cylinderical heat sink (DM-21). The suspended thermopile is typically used in environments with very low aerodynamic loads (e.g. radiometers).

Thin Film

The thin film sensor was selected as a candidate because of its extensive use in wind tunnel applications (DM-4, -35, -41, -53, -55, -56, -60, -63). The thin film sensor is a very thin temperature-sensitive resistance film deposited on an insulating substrate. Application of the resistive film can range from simple painting, epoxying, flame spraying, electroless deposition and electroplating to the methods used in the manufacture of microelectronic circuits: vacuum evaporation and sputtering (DM-63). The recent advances in microelectronic circuit manufacturing have made it possible to produce a thin film sensor that is cost competitive with the simple methods and at the same time offer increased reliability, ruggedness and sensitivity. Materials that are most commonly used as the resistance element are platinum, nickel, aluminum, gold and iridium. The substrate is typically glass or quartz. The sensor is ruggedized by the deposition of an SiO_2 coating. The resistance element and protective coating thickness are typically 400 and 8000 A, respectively. Time constants are less than 10 milliseconds (DM-4).

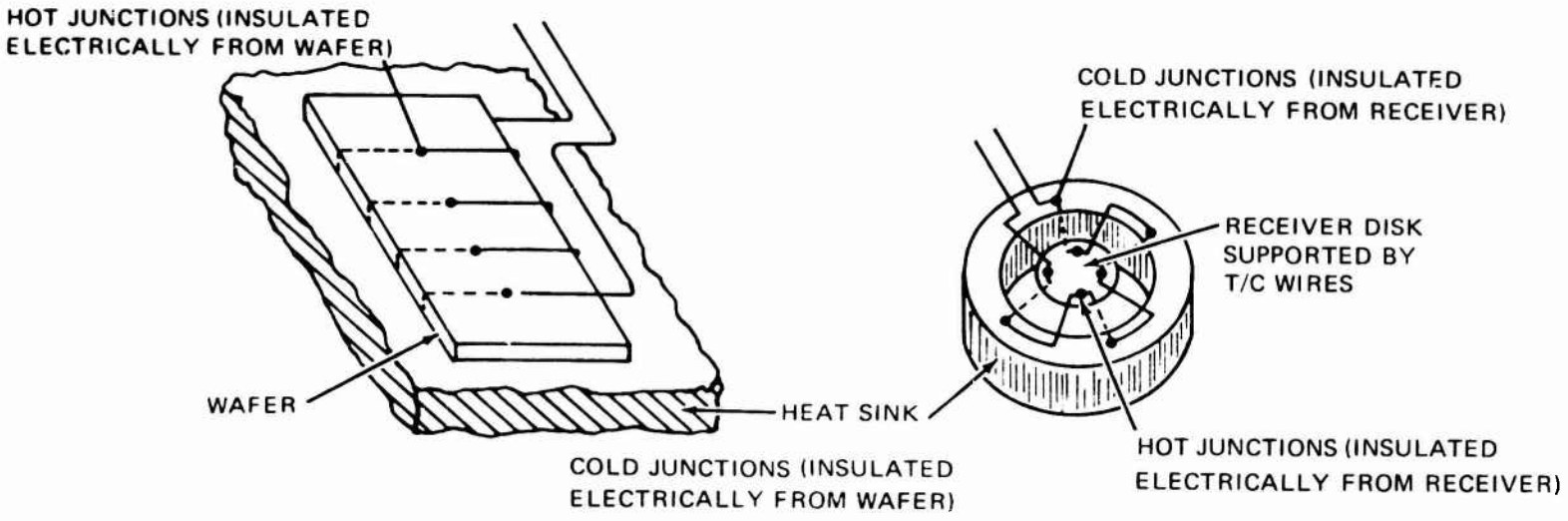

Figure A-2. Thermopile Configuration

Semiconductors

Semiconductor thermocouples are similar to conventional thermoelectric thermocouples except the Seebeck coefficient for the former is between 30 and 100 times that of the latter. Semiconductors have been successfully used in measuring surface temperatures for the semi-infinite type calorimeter (DM-22) and temperature gradients for the wafer-type calorimeter (DM-50). The semiconductor elements are usually very small and the formation of the junction requires another material. This material effects the temperature-EMF relationship and unlike the conventional T/C, each individual semiconductor T/C requires individual calibration.

The semiconductor T/C in the semi-infinite solid configuration is reported to measure heat transfer rates as low as 0.1 Btu/ft^{2}sec with a resolution of ± 10 percent (DM-22). In this application the T/C had a sensitivity of 2 mv/°C with a response time of approximately 10 milliseconds The T/C elements were p-n germanium packaged in a 4 mm dia x 5 mm threaded plug. The instrument in this configuration appears to be very useful in cold wind tunnel applications and is therefore a candidate for further evaluation.

The semiconductor T/C in the wafer configuration appears also to be very useful in cold wind tunnels. The sensor described in DM-50, although designed for cryogenic purposes, appears in principle to be applicable. The sensor had good resolution 0.2 mv/°C but was configured so the response time was 5 seconds. The semiconductor was $AgSbTe_2$.

Thermistor

Thermistors are resistance thermometers using a semi-conductor as the sensor element. The sensors can be made as small as 0.010 inches in diameter with 0.001-inch lead wires. The sensing element is encased in ceramic to provide electrical insulation of the sensing element and lead wires. Thermistor resistance change between 300 and 1200°R is 10^6 times the resistance charge of metallic elements used in thin film gages (DM-85). Thermistor resistance is, however, extremely nonlinear with temperature. The thermal contact problem induced by the ceramic insulation causes the thermistor to be inferior to conventional T/C in the 1-D thin skin application. However, because of its high measurement sensitivity and ruggedness, it appears attractive for use in the semi-infinite solid-type calorimeter.

Ferroelectric

Ferroelectric sensors operate on the principle that the electrical polarization of the sensor material is dependent on the rate of temperature change (DM-48). Thus the sensor output can be related directly to incident heat flux. The sensor is a thin slab of ferroelectric material (e.g. barium titanate) with electrodes attached to both sides. A change in temperature causes a change in polarization which in turn produces a change in electrical current. This current change can be related to heat flux by prior calibration.

The sensor constructed and tested in DM-48 was a barium titanate disk, .10 inches in diameter and 0.007 inches thick. The disk was mounted on a nylon plug. The sensor sensitivity in this configuration was approximately 150 mv/w with a response time of between 3 and 5 milliseconds. Excellent data was acquired in tunnel tests with no evidence of spurious output.

A.3.2. Temperature-Sensitive Coatings

There are four categories of temperature-sensitive coatings: liquid crystals, thermal phosphors, color (or phase) change paints, and low-temperature ablators (LTA). Quantitative heat transfer data has been acquired on liquid cyrstals (TS-1, TS-11, TS-17) and thermal phosphors (TS-6, M-88). Color change paints provide more qualitative data and appear to have no advantage over liquid crystals or thermal phosphors. LTA materials have been used to infer surface heating by the analogy between mass transfer and heat transfer (TS-27).

Liquid crystals indicate colors as a function of temperature within the temperature range for which they were prepared. When illuminated by white light within their active temperature range, they selectively reflect light of discrete wavelengths and thus indicate discrete colors in the spectrum. This occurs by changes in their molecular structure that occur with changes in temperature. This change is reversible. Their active temperature range can be as narrow as 0.5°C or as wide as 50°C. They possess high resolution of up to 20 lines/mm with a response time of less than 0.2 seconds (TS-1). There are three methods of applying cholesteric liquid crystals to a test surface (TS-1). In the first method, the crystals are coated directly on to the surface; in the second, the surface is primed with a black paint before application of the crystals; and in the third, the crystals are coated on to a thin plastic film which is then attached to the test surface with the coated face exposed. Care is required in their application and use because contamination can change their temperature response. In wind tunnel application, an external light source will be required for illumination with uniform model illumination being impossible for the coated nosetip configurations of interest. A pre-run calibration technique may be devised that can minimize errors due to nonuniform illumination.

Thermal phosphors can be made wherein emission is temperature dependent and reversible. The dependence of phosphor brightness results from differences in electron energy levels that is produced by specific trace impurities in the crystal lattices of the pure phosphor (TS-6). The active temperature range and also the temperature resolution can be varied by changing the impurities. The minimum temperature change that phosphors can resolve with the photographic techniques available in TS-6 is quoted to be 0.2°C. The response time of the phosphor by itself is reported to be approximately 1 millisecond causing the response time of the phosphor coated model, in most cases, to be dependent on the thermal diffusivity of the model material. As with liquid crystals, phosphors require external light for activation, e.g., UV light source. Errors can be generated by nonuniform-nonrepeatable lighting. Errors are also introduced by random variation in the optical film density and nonuniformities in film development.

Liquid crystals and thermal phosphors both appear attractive for getting heat transfer data over a large area of the model with no disturbance to the flow field or alteration to the model. The concepts are therefore recommended for further investigation.

The use of LTA materials to infer heat transfer in cold wind tunnels is questionable. Calculations were performed on a sphere-cone with a 7° cone half angle, 0.5-inch nose radius and a 1.5-inch base radius. The

flow was Mach 3 with a total temperature of 530°R and model stagnation pressures of 70 and 570 psia. The results show cold wall heat fluxes of 40 and 400 Btu/ft^2-sec on the hemisphere, down to 15 and 75 But/ft^2 sec on the afterbody. From the LTA studies of TS-28, camphor or napthalene appear to be most applicable for cold wind tunnel applications because of their structural stability and relatively high ablation rate. On the hemisphere nose, the camphor ablation rate will be 2.8 x 10^{-5} in/sec and 5.3 x 10^{-5} in/sec. Measurement errors and ablation of the model prior to and after the test indicate that ablation depths of at least 0.020 inch are required in the model to result in reasonable inferred heat transfer rates. This indicates that test durations of approximately 2000 seconds are required at the 70 psia condition.

A.3.3 Optical Systems

Optical systems that have some potential for measuring surface heat transfer rates include the following:

1. IR Scanner
2. Laser Holograms
3. Wollasten-Schlieren
4. Moch Zehnder Schlieren
5. Semi-focusing Color Schlieren

The Schlierens and laser holograms are used extensively for flow visualization with some attempt to infer surface convective heating (OS-1, OS-2, OS-11). Surface heating is deduced by extropolation of gas density profile down to the surface and has been accomplished in hot gas tunnels and shock tubes with 2-dimensional models. Application of these techniques to cold wind tunnels with axisymmetric models at angle of attack do not appear to be feasible. These approaches are not recommended for further evaluation.

The IR scanner has been used successfully to measure model heat transfer in hot tunnels (OS-30, OS-33, OS-38, M-88). Relative to the other candidate sensors identified in the above paragraphs, the capital equipment costs for the IR scanner are large. The IR scanner and data processing equipment involve a large initial investment; however, once installed and working the systems offer great capability in acquiring heating data over a large area of the model.

The IR scanner is an IR radiometer that is scanned over the test area. A point-by-point and line-by-line IR image of the model is produced that is translated into discrete emission values for each point. If the surface emissivity (directional emission characteristics for other than normal viewing) is known, the temperature can be calculated. The large number of discrete data points that are generated requires the use of a high speed computer for data interpretation.

Measurement resolution of the scanner is reported to be 0.2°C for fast response scanners. The use of the IR scanner in hot wind tunnels have shown the heat transfer rate inferred by the IR method to be very close to

those inferred by both thermal phosphors and direct foil calorimetery (M-88). In this case, however, the measurement region was normal to the angle of incidence thereby eliminating off normal emission errors. Based on these data correlations, the IR scanner is recommended for further evaluation for use in cold wind tunnels.

A.4.0 RESOLUTION ENHANCEMENT

The measurement resolution of convective heat transfer can be enhanced by either increasing sensor sensitivity and/or increasing the temperature potential between model and gas recovery temperature. Three sensors have been identified that, relative to conventional T/C and resistance thermometers, offer high measurement sensitivity. These are the thermopile, semi-conductor T/C and ferroelectric devices and in cold wind tunnel applications, they may or may not need active methods for increasing the temperature potential. The other candidates identified in Paragraph A.3, all appear to require some type of active method for enhancing resolution. Active methods include external quartz lamps, self heating of resistance thermometers, metalized resistance surface heaters, microwave and hot fluid. These methods are summarized in Table 5. The particular sensor application in which further investigation is recommended is also identified in the table.

Quartz lamps involves heating the model's surface with external lamps properly positioned so a uniform radiation heat flux is obtained in the region of interest. Quartz lamps are available that can produce model heat fluxes as high as 10 Btu/ft^{2}sec. The temperature response of a Teflon model irradiated with an external heat flux of 2.5 Btu/ft^{2}sec is presented in Figure A.3. The steady state temperature shifts that are caused by external heating are between 10 and 100°F for convective transfer rates of between 20 and 100 Btu/ft^{2}sec, respectively. These temperature shifts are inversely proportioned to the local convective heat flux and eliminate the need for fast response time sensors. If the incident radiation heat flux is known, the convective heat flux can be simply calculated from the measured temperature shift. The incident radiation heat flux can be measured by calibrating the model and quartz lamps in a near vacuum where convective heat transfer is neglible.

Self heating is an attractive approach for resistance-type sensors. The voltage applied to measure resistance can also be used for self heating to produce the desired temperature shift. A metalized surface layer can be used as a heater to increase the resolution of conventional thermocouples. Microwave or induction heating is attractive because direct contact between the heating element and model is not required. The use of a fluid to heat the model requires flow channels and seals causing complexities in the model design. However, internal fluid heating may have advantages over the external quartz lamp for 3-D models.

A.5.0 CONCLUSIONS

The literature search and review has identified thirteen (13) candidate instrumentation techniques that are recommended for further evaluation for use in cold wind tunnels. The techniques are summarized in Paragraph A.1. Also, five (5) methods for increasing measurement sensitivity are recommended for further review. These methods and the instrumentation techniques for which they appear applicable are presented in Table A-5.

● AFFDL MACH 3 FACILITY

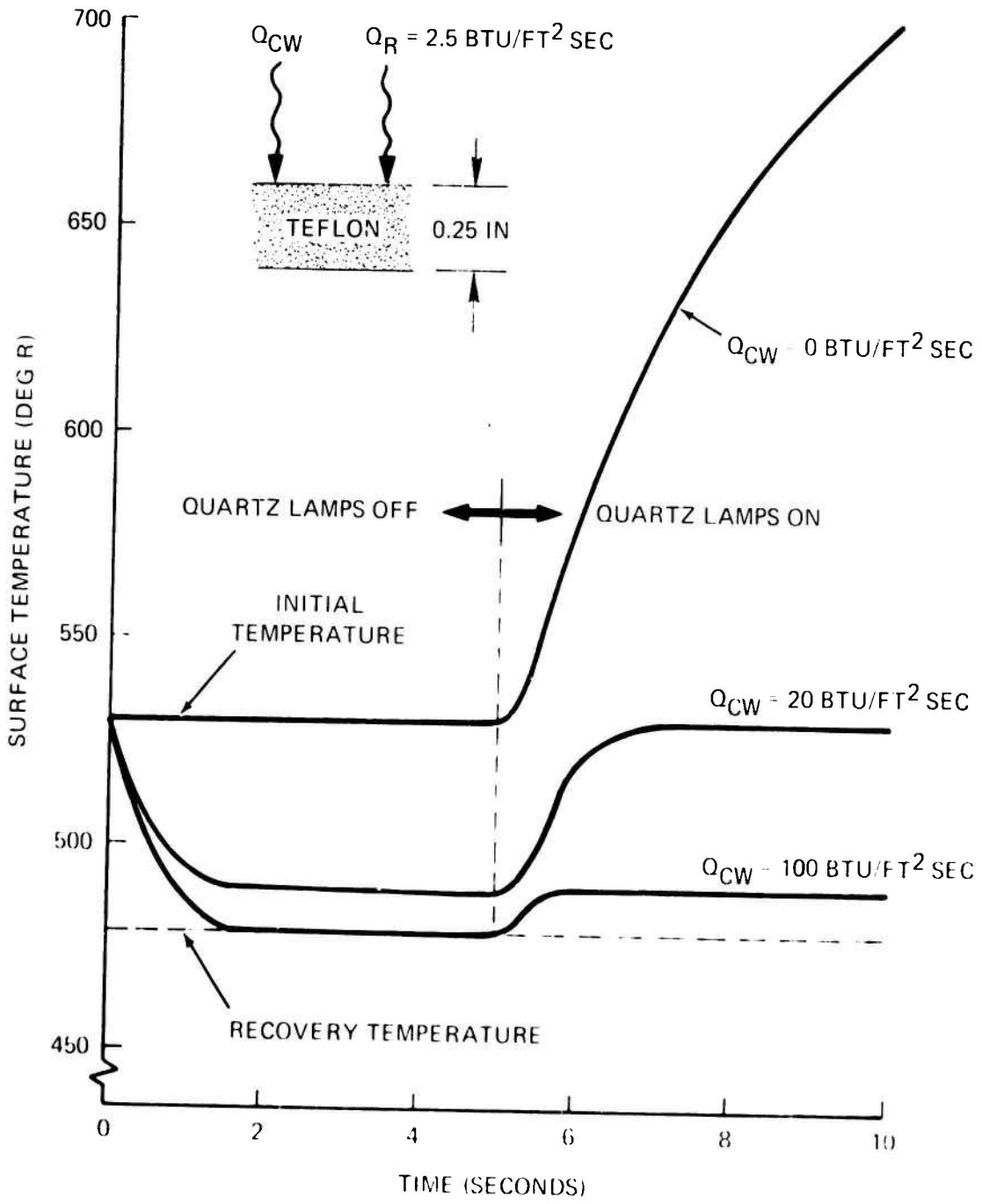

Figure A-3. Computed Model Temperature Response Histories

TABLE A-1. DIRECT MEASUREMENT TECHNIQUES

REFERENCE	SOURCE	APPLICABLE	REVIEWED	SENSOR	SUMMARY
1. Hager, N.E., Making and Applying a Thin-Foil Heat Flux Sensor (ASTI), Inst. Tech., 14:54-8, October 1967.	ASTI	Yes	Reviewed * Article	Wafer T/C	Measures ΔT across wafer to get heat flux
2. Ash, R.L. Response Characteristics of Thin Foil Heat Flux Sensors (ASTI), AIAA Journal, Vol. 7, No. 12, p. 2332, December 1969.	ASTI	No	Reviewed * Article	Thin Foil (Gardon)	Thermal analysis only on thin foil calorimeter
3. Kirk, W.P., Technique for Attaching Fine Wires to Provide a Large Surface Area for Low Temperature Heat Transfer (ASTI). Rev. Sci. Inst., 42:1087-9, July 1971.	ASTI	No	Reviewed Abstract	Thermopile	Application to dillution refrigerators
4. Willeke, K. and Bershare, D., Improved Thin-Film Gauge for Shock-Tube Thermal Studies (ASTI), Rev. Sci. Inst., 44:22-5, January 1973.	ASTI	Yes	Reviewed * Article	Thin Film	Deposited Pt. film with SiO_2 protective coating
5. Ebeling, K., et al, Microcalorimeter for Measuring Heat of Straining or Destraining of Sheetlike Materials (ASTI), Rev. Sci. Inst., 45:419-26, March 1974.	ASTI	No	Reviewed Article	T/C	Water bath calorimeter
6. Frauenfelder, R., New Automatic Heat Flow Calorimeter (ASTI), Rev. Sci. Inst. 49:452-5, April 1978.	ASTI	No	Reviewed Article	Thermopile	Bomb calorimeter measuring heats of reaction
7. Direct Heat Transfer Measurements - Watch your Step (EI), ISA 19th Conference (2) Physical and Mechanical Measurement Instrumentation-Proceedings Preprint 16.7-2 for Meeting 12-15 October 1964, 8p.	EI	No	Reviewed Abstract	Gardon Gage	General overview
8. Bachmann, R.C., et al, Investigation of Surface Heat-Flux Measurements with Calorimeters(EI), ISA Trans. Vol. 4, No. 2, Apr. 1965, pp. 143-151.	EI	No	Reviewed Article	Slug Cal.	Conventional slug calorimeter, nothing new
9. Springer, B.S. and Ulbrich, R.H., Modified Hot-Wire Thermal Conductivity Cell (EI), Rev. Sci. Inst., Vol. 38, No. 7, July 1967, p. 938-941.	EI	No	Reviewed Article	Gas Cell	Measures k and accommodation coefficient of gases
10. Mamnitskii, V.M., Automatic Regulation of Adiabatic Region for Low-Temperature Calorimeter Instruments and Experimental Techniques (EI), No. 2, March-April 1967, p. 415-419.	EI	No	Reviewed * Article	Thermopile	Heater Control System for Cryo-calorimeter
11. Bocharov, V.V., et al, Calorimeters for Measuring Short Low-Energy Pulses (EI), Intstruments & Exp. Techniques, No. 1, Jan-Feb 1967, p. 180-81.	EI	No	Reviewed Article	Quantum Generator	Measures energy from light pulses

*Have copy.

TABLE A-1. DIRECT MEASUREMENT TECHNIQUES (Continued)

REFERENCE	SOURCE	APPLICABLE	REVIEWED	SENSOR	SUMMARY
12. Gardner, J.E., et al, Crystal Thermometer Calorimeter (EI), Rev. Sci. Inst., Vol. 38, No. 5, May 1967, p. 652-654.	EI	No	Reviewed Article	Quartz Crystal	Crystal controlled oscillator with temp. dependent freq.
13. Firth, J.M. and VanMal, H.H., Heater Circuits for Calorimetery (EI), Rev. Sci. Inst. Vol. 38, No. 5, May 1967, p. 652-654.	EI	No	Reviewed* Article		Simple heater circuit for calorimeter
14. Christensen, E.M., Application of Foil Calorimeters to Measurement of Space Vehicle Environment and Exhaust Plume Heating (EI), ISA 20th Conference (2) Phys & Mech. Meas. Inst. - Proceedings Preprint 17.9-4 for Meeting 4-7 October 1965, 19p.	EI	No	Reviewed Article	2-D Foil Cal.	Commercial foil calorimeter used on orbital craft.
15. Wool, M.R., Calorimeter Measurement of Heat Transfer at Hypersonic Conditions (EI), J. Spacecraft & Rockets, Vol. 11, No. 6, June 1974, p. 363-7.	EI	No	Reviewed Abstract	Melt cal.	Melting calorimeters in ballistic range
16. Calibration Technique for Calorimeter Heat Transfer Gages (IAA), A63-13763,08-05.	IAA	No	Reviewed Abstract	Coolant ΔT	Skin coolants to measure aero-heating
17. Effect of Near Discontinuity in Surface Temperature on the Aerodynamic Heating Rate which is Measured by a Calorimeter Heat Transfer Gage (IAA), A63-13780, 08-15.	IAA				
18. Kapinos, V.M. and Nikitenko, N.I., Determination of Heat Transfer in a Rectangular Duct by Means of Embedded Alpha-Calorimeters (IAA), A63-15395, 11-13, Int. J. Heat Mass Transfer, Vol. 6, 1963, p. 271-276.	IAA	Not useful	Reviewed* Article	Slug Cal.	Slug Cal design and analysis. Elementary
19. Calorimeters for Measuring Radiation and Convective Heating on Airborne Vehicles (IAA) SAE Paper 750 G, A63-23889, 22-15	IAA				
20. Makarov, B.I., Temperature Measurement on Solid Surfaces using Thermocouple, Determining Errors due to Heat Transfer along Thermocouple Electrode (IAA), A65-15219, 06-0823.	IAA	No	Reviewed Abstract	T/C	Computes T/C measurement errors (in Russian)
21. Ledford, R.L. and Smotherman, W.E., Pressure and Heat Transfer Measurements in Hypervelocity Wind Tunnels Using Miniature Transducers (IAA), A65-29224, 18-2648, ISA Transactions, Vol. 4, April 1965, p. 133-142.	IAA	Yes	Reviewed* Article	Thin Skin	Thin skin disk calorimeter
22. Kendal, D.N., Dixon, W.P. and Schulte, E.H., Semiconductor Surface Thermocouples, Determining Heat-Transfer Rates Associated Wind Tunnel Testing (IAA), 18 p. 3048, A67-34103.	IAA	Yes	Reviewed* Article	p-n Ger.	p-n Germanium semiconductor with sensivitity 3 times Cr/Con T/C

*Have copy

TABLE A-1. DIRECT MEASUREMENT TECHNIQUES (Continued)

REFERENCE	SOURCE	APPLICABLE	REVIEWED	SENSOR	SUMMARY
23. Kucherov, N.V., Temperature and Temperature Difference Measurements by Resistance Thermometers (IAA), 04, p. D660, A68-14923.	IAA	Uncertain	Reviewed Abstract	Resistance	Error analysis, (in Russian)
24. Sabodash, V.P., Unsteady Calorimetric Sensor for Measurement of Heat Transfer between Gas Jets and Solid Targets (IAA), 06, p. 1064, A70-17557.	IAA	Uncertain	Reviewed Abstract	Uncertain	Sensor not described. (In Russian)
25. Hill, J.C., et al., External Convective Heat Transfer Coefficients from Quartz-Coated Cylindrical Hot Film Anemometer Probes in Mercury (IAA), 30, p.1599, A70-21582, Int. J. of Heat & Mass Trans., Vol. 12, December 1969, p. 1595.	IAA	No	Reviewed Abstract	Hot Wire Anemometer	Boundary layer probe
26. Nowak, H.D., Hot Wire Anemometers Design and Operation in Fluidics, Discussing Temperature Gradient Due to Heat Transfer Effects (IAA), 14, p. 2579, A71-33435.	IAA	No	Reviewed Abstract	Hot Wire Anemometer	Theory of operation, in German
27. Aerospace Heat Transfer Measurements Using Calorimeters (IAA), A64-17503, 11-15.	IAA	No	Reviewed Abstract	General	Summary of conventiona calorimeters, nothing
28. Johnston, W.V., A Heat Flow Calorimeter, NASA Tech. Brief, GSFC-11434, B73-10221, 03, August 1973.	NASA Tech Brief	No	Reviewed Abstract	Nickel-Cad Cell	Reaction of Ni-Cad Cell proportional to heating
29. Stalmach, C.J., One Wire Thermocouple (NASA Tech. Brief), MSC-220 Winter 1976, also NASA-CR-144364, (N75-29356).	NASA Tech Brief	Yes	Reviewed* Article	T/C Film	Model plated with nickel. Con. Wire intersects surface for junction.
30. vanFossen, G.J., Design of Experiments for Measuring Heat Transfer Coefficients with a Lumped Parameter Calorimeter, NASA Tech. Note 0-7857, January 1975.	NASA TN	No	Reviewed Abstract	Slug Cal.	Analytical review of slug cal with experimental applications.
31. Holanda, R., et al, Miniature Sheathed Thermocouples for Turbine Blade Temperature Measurement, NASA Tech. Note 0-7671, May 1974.	NASA TN	No	Reviewed Article	T/C	Installation technique for T/C in turbine blades.
32. Wagner, R.O. and Weinstein, L.M., Hot-Wire Anemometry in Hypersonic Helium Flow, NASA Tech. Note D-7465, June 1974.	NASA TN	No	Reviewed Article	Hot Wire	Short run time hot wire anemometry
33. Harvey, W.O., Instrumenting Models for Aerodynamic Heat-Transfer Studies Involving Transient Heating Rates, ISA Trans., 6:42-8, January 1967.	ASTI	Yes	Reviewed* Article	Type of Thin Skin	Thin metal sheet over hole in body
34. Anson, D. abd Godridge, A.M., Simple Method for Measuring Heat Flux, J. Sci. Inst., 44:541-4, July 1967.	ASTI	No	Reviewed Article	T/C	Con. water-coated calorimeter using T/C

*Have copy.

TABLE A-1. DIRECT MEASUREMENT TECHNIQUES (Continued)

REFERENCE	SOURCE	APPLICABLE	REVIEWED	SENSOR	SUMMARY
35. Hornbaker, D.R. and Hall, D.L., Heat Flux Measurements; a Practical Guide (ASTI), Inst. Tech. 15:51-6, February 1968.	ASTI	Yes	Reviewed* Article	Thin film, foil and Thermopile	Good review of thin film, foil and thermopile colorimeter
36. Tanner, R.I., Theory of a Thermal Fluxmeter in a Shear Flow (ASTI), J. App. Mech., 34:801-4, December 1967, (EI) ASME Paper 67-WA/APM-7 for meeting 12-17 November 1967.	EI	Uncertain	Reviewed* Article	Thin Foil	Physics and theory of thin foil calorimeter
37. Haring, H.G. and Kroun, J., Homemade Heat Flux Meter (ASTI), Chem. & Ind., p. 1623, 19 December 1970.	ASTI	Yes	Reviewed* Article	Thermopile	Thermopile with wafer to measure heat flux in chemically reacting situations
38. Ash, R.L., et al, Sources of Error in Vacuum Calibration of Heat Flux Sensors, (ASTI), Sci. Inst., 41:1112-14, July 1970.	ASTI	No	Reviewed* Article	Thin foil gage	Errors due to mismatch in gage and adjacent surface emissivities
39. Some Heat Transfer Measurements in Compressible Turbulent Boundary Layers, (ASTI), Aeronautical Journal, 77:94-8, February 1973.	ASTI	Uncertain	Reviewed Abstract	T/C	Surface T/C
40. Yap, D., et al, Calibration and Tests of a Yaw Sphere Thermometer System for Sensible Heat Flux Measurements (ASTI), J. App Meteorology 13:40-5, February 1974.	ASTI	No	Reviewed Article	Hot Wire Anemometer	Use of hot wire anemometer to define boundary layer profiles
41. Nerem, R.M., Laminar Boundary Layer Heat Transfer Measurements on Flat Plate in Dissociated and Partially Ionized Air (EI), Heat Transfer & Fluid Mechanics Inst., 19th Proceedings, 22-24 June 1966, P. 409-427.	EI	Yes	Reviewed* Article	Thin film	Pt. resistance gage on pyrex
42. Gerashchenko, O.A., Boundary Properties of Oblique-Layer Heat-Flux Detectors (EI), Measurement Tech., No. 12, December 1969, p. 1703-1705.	EI	No	Reviewed* Article	T/C	Oblique T/C. English translation not meaningful
43. Pamashville, M.S., Investigation of the Zonal Sensitivity of Gang Thermoelectric Pickups (EI), Heat Transfer Sov. Res., Vol. 7, No. 1, January - February 1975, p. 122-214.	EI	No	Reviewed Abstract	Yanishovsky Pyrometer	Thermoelectric pickup
44. Wong, H.Y., Measurement of Convective Heat Loss from a Solid Surface to an Airstream (EI), J. Phys. E: Sci. Inst., Wol. 12, No. 4, Aprin 1979, p. 270-271.	EI	No	Reviewed* Article	Thin foil	Conventional thin foil colorimeter

*Have copy.

TABLE A-1. DIRECT MEASUREMENT TECHNIQUES (Continued)

REFERENCE	SOURCE	APPLICABLE	REVIEWED	SENSOR	SUMMARY
45. Use of Transient Thin-Wall Technique in Measuring Heat Transfer Rates in Hypersonic Separated Flows, (IAA), A63-15960, 12-13.	IAA	Yes	Reviewed Abstract	Thin skin	Theory of thin skin
46. George. A.R. and Reinecke, W.G., Conduction Errors Using Thin-Skinned Method of Measuring Convective Heat Transfer Rates and Recovery Temperatures (IAA), A63-20522, 19-13, AIAAJ, Vol. 1, p. 1950, August 1963.	IAA	Yes	Reviewed* Article	Thin skin	Normal and tangential conduction error analyses
47. Lee, R.E., et al, Velocity Profile, Skin Friction Balance and Heat Transfer Measurements of Two-Dimensional Turbulent Boundary Layer of Freestream Mach No. 5, 17, p. 3144, A68-34127, Heat Trans. and Fluid Mech. Inst., June 17, 1963, Proceedings, University of Washington.	IAA	No	Reviewed Abstract	Slug Cal.	Conventional slug calorimeter
48. Hickman, T.G., and Burdick, G.A., Pyroelectric Transducers of Barium Titanate for Heat Transfer Measurement under Hypersonic Flow, Discussing Calibration (IAA), 18 p. 3370, A68-35538	IAA	Yes	Reviewed* Article	Ferroelectric	Electrical polarization is temp dependent
49. Covert, E.E. and Gollnick, A.F., Ceramic Heat Transfer Gage for Supersonic Wind Turnel Investigation of Blunt Swept Wing Leading Edges Aerodynamic Heating, 15, p. 2613, A69-31272, ISA Advances in Test Measurements Proceedings, Vol. 5, p. 535, 1968.	IAA	Uncertain	Reviewed Abstract	Aluminum Silicate with Teflon	
50. Schulte, E.H. and Kohl, R.F., Low-Temperature High-Sensitivity Temperature-Compensated Heat Flux Transducers to Measure Conductive and Radiative Heat Transfer, (IAA), 02, p. 0303, A70-12740, Rev. Sci. Inst., Vol. 40, -. 1420, November 1969.	IAA	Yes	Reviewed* Article	p-n semiconductor	$AgSbTe_2$ semiconductor is put in a thermopile arrangement to measure ΔT across two plates.
51. Vas, I.E. and Oskom, B., Heat Transfer Measurements Using the Quasi-Transient Technique, Princeton University, 1976.	AFWAL	Yes	Reviewed* Article	Slug	Slug calorimeter heated by hot air
52. Davenport, N.C., Heat Transfer in a Region of Glancing Shock Wave/Boundary Layer Interaction, Cranfield College of Aeronautics, AFOS R-76-3006B, June 1978.	AFWAL	Yes	Reviewed* Article	Slug	Slug calorimeter in cold wind tunnel
53. Kubota, H., Investigation of Three-Dimensional Shock Wave Boundary Layer Interactions, Cranfield College of Aeronautics, AFOSR-76-3006, January 1980.	AFWAL	Yes	Reviewed* Article	Thin Film and Liquid Crystal	Thin film with self heating. Describes use of liquid crystals

*Have copy.

TABLE A-1 DIRECT MEASUREMENT TECHNIQUES (Continued)

REFERENCE	SOURCE	APPLICABLE	REVIEWED	SENSDR	SUMMARY
54. Ainsworth, R.W., The Measurement of Heat Transfer Rates to Film-Cooled External Surfaces and the Internal Passages of Turbomachine Components Using Thin Film Gages, 24, p. 3130, N76-33445, OUEL-115276.	STAR	Uncertain	Reviewed Abstract	Thin Film	
55. Miller, H.R., Heat Transfer Techniques and Measurements in Douglas Aerophysics Lab: Hypervelocity Impulse Tunnel:, N65-26578, Douglas Aircraft, Santa Monica SM-43066, December 1964.	STAR	Uncertain	Reviewed Abstract	Thin Film	Thin film theory, calibration and data reduction
56. Geller, V.M. and Zelikovisky, Z.I., An Experimental Investigation of the Errors of Measurement of Surface Temperature, N66-26112, 14, p. 2550, Joint Publications Research Service, Washington, DC, Izvestiya Vuzov: Instrument Building, No. 6, 1965, 12 May 1966, 233p, Trans. into English of Izv. Uchebn Zavedenii Priborostr (Lenningrad) V. 8, No. 6, 1965, JPRS-35741, TT-66-31907.	STAR	No	Reviewed Abstract	Thin Film	Errors in thin film sensors
57. Frye, J.W., Jr., Thin Film Heat Transfer Gages, N66-30552, 17p 3341, Air Force Institute of Technology, Wright-Patterson AFB, March 1966, GAM/ME/66A-3; AD-632394.	STAR	Uncertain	Reviewed Abstract	Thin Film	Literature survey and application to shock tube (in German)
58. Lipowski, K., Temperature Measurements in a Small Tube Wind Tunnel, N67-13459, 04p0547, DLR-FB-66-56, AVA-FB-66-10, August 1966.	STAR	Uncertain	Reviewed Abstract	Thermal Probe	Probe for short duration temperature measurement. In German.
59. Jet Propulsion Laboratory, Hypervelocity Laboratory, N67-15701, 06p0860, NASA-CR-81201, JPL-SPS-37-41, Vol IV.	STAR	Uncertain	Reviewed Abstract	Thin Film	Data report on facility with some description of thin film gage uses
60. Pickard, R.F. and Loyd, J.R., Development of a Pressure and Force Transducer Calibration Procedure for the Hypersonic Shock Tunnel Vol. III, N67-18004, 07p1087, NASA-CR-81716; ER67-2, Vol. III.	STAR	Uncertain	Reviewed Article	Thin Film	Describes fabrication, calibration and cost reduction of thin film gages
61. Advisory Group for Aerospace Research, High-Temperature Turbines, N71-17372, 07p1099, AGARO-CP-73-71.	STAR	Uncertain	Reviewed Abstract	T/C	Use of T/C in gas turbines, describes installation and errors
62. Kapinos, V.M., et al. Determining Mean Heat Transfer Coefficients with Built-in Alpha-Calorimeters, N72-31960, 22p3031, AD-741525, FSTC-HT-735-72, 1970.	STAR	No	Reviewed Abstract	Slug	Uses "alpha calorimeter" which is a slug calorimeter. Nothing new

TABLE A-1 DIRECT MEASUREMENT TECHNIQUES (Continued)

REFERENCE	SOURCE	APPLICABLE	REVIEWED	SENSOR	SUMMARY
63. Christensen, Orla, "New Trends in Hot-Film Probe Manufacturing," DISA Information, No. 9, February 1970.	DISA	Yes	Reviewed* Article	Thin Film	Describes fabrication of thin film with protective coatings
64. Wade, W.H. and Slutsky, L.J., Quartz Crystal Thermometer, Rev. Sci. Instr., 33, 212, 1962.	Referenced in DM #12	No	Reviewed Article	Quartz Crystal	Crystal enclosed in He. filled glass tube
65. Thibault, J. and Hoffman, T.W., A Heat Flux Meter to Determine the Local Boiling Heat Flux Denisty during a Quenching Experiment, Int. J. Heat and Mass Transfer, Vol. 22, p. 177, February 1979.	J. Heat & Mass Transfer	No	Reviewed* Article	Thin Foil	Conduction analyses and use of conventional foil calorimeter
66. Kochenschnieder, E.L. & Pallas, S.G., Sensor for Heat Transfer Measurements, Sci. Inst., 45:1164-5, September 1974, (IAA), 23 p 3365, A74-24788.	ASTI	No	Reviewed Article	Thermopile	Uses thermopile to measure gas temperature.
67. Ginoux, J.J., Steady-State Technique for Local Heat-Transfer Measurement and Its Application to a Flat Plate, (EI), J. Fluid Mechanics, Vol. 19, Part 1, p. 21-29, May 1964.	EI	Yes	Reviewed* Article	Thin Resis. Film with T/C	silver film plated over insulator that is resistively heated. T/C molded in model in contact with film measures surface temp.
68. Jolls, K.R. and Sforza, P.M., Ferroelectric Transducer for Heat Transfer Rates and Flow Measurement in Gaseous Systems with Autostabilized Temperature, Noting Film Coefficient, 19 p. 3307, A69-35749, Institute of Electrical and Electronics Engineers Publication 69C 19AES, p. 278, 1969.	IAA	Uncertain	Reviewed Abstract	Ferro-electric	Detector uses ferro-electric properties of triglycine sulphate to measure temperature
69. Nestler, D. C., et al, "Heat Transfer to Steps and Cavities in Hypersonic Turbulent Flow", AIAA J., Vol. 7, No. 7, 1970.	AIAA	No	Reviewed* Article	Thin Skin	Use of thin skin approach to measure convective heating, nothing new or useful
70. Vital, R. J. and Bartz, J. A., "Surface Measurements on Sharp Flat Plates and Wedges in Low-Density Hypersonic Flow", AIAA J., Vol. 7, No. 6, June 1969.	AIAA	Yes	Reviewed* Article	Thin film	Thin film pt therometer over pyrex glass
71. Hager, N.A., Thin Foil Heat Meter, Rev. Sci. Instr., 36, 1564, 1965.	DM-50	No	Reviewed* Article	T/C	Ca-Co wafer calorimeter
72. Brown, E.A., et al, Steady-State Heat Flux Gage, Rev. Sci. Instr., 32, 934, 1961.	DM-50		Reviewed Article	Thin film	Pt. resistance film
73. Kinzie, P.A. and Sosa, E.N., Voltage Output Characteristics of Axial Gradient Heat Flux Transducers, Rev. Sci. Instr., 37, p. 599.	DM-50	No	Reviewed Article	Wafer T/C	

*Have copy.

TABLE A-1 DIRECT MEASUREMENT TECHNIQUES (Continued)

REFERENCE	SOURCE	APPLICABLE	REVIEWED	SENSOR	SUMMARY
74. Nerem, R. M. & Stickford, "A thin-film Radiative Heat Transfer Gage", AIAA J. 2, 1647, 1964.	DM-50	Yes	Reviewed* Article	Thin Film	Pt. thin film on pyrex with black coating
75. Vidal, R. J., Cornell Aero. Lab., Rep. No. Ad-917-A-1, WADC TN-56-315, AD-97238, 1956.	DM-50			Thin Film	
76. Woodruf, L.W., et al, "Interpretation of Asymptotic Calormieter Measurements, AIAA J., Vol. 5, No. 4, p. 795, April 1967.		Yes	Reviewed* Article	2-D Foil	Theory of operation
77. Oruma, Y., "Thermocouple Consisting of Ger Thin Film Deposited in Vacuum", J. Applied Phys (Japan) p. 814, Oct. 1965.					
78. Pyroelectric Detection Techniques and Methods, NASA-CR-44, N64-24825, April 1964.	STAR	Yes	Reviewed Abstract	Pyroelectric	$BaTiO_3$ & $PbTiO_3$ detector noise & resp. time at optical freq.
79. Martins, W. D. & Ripperger, E.A., "The Development of a Probe-Type Thin Film Microthermocouple for Biomedical Use", Univ. of Texas, TR N. 120, February 1972.					
80. Knonpka, W. Heat Transfer Instrumentation for the Grumann Hypersonic Shock Tunnel, Preort RM-287, July 1965, Ad-469-667.	DDC	Uncertain	Reviewed Abstract	Thin Film	Fast response thin film Pt. sensor
81. Weker, P.J., Thin-Film Gages for Heat Flux Measurements in Shock Tunnels, DLR-Mitt-67-15, June 1967, AD-835-427.	DDC	Uncertain	Reviewed Abstract	Thin Film	Theory, preparation and application of thin film, in German
82. Woodley, J.G., and Cox, S.G., Heat Transfer Measurements on a Flat Plate in the RAE 15-Inch Shock Tunnel, RAE-TR-69014, Feb. 1969, AD-857-7196	DDC	Uncertain	Reviewed Abstract	Thin Film	Particular application of thin film
83. Sykes, D.M. and Winter, D.F., The Design of Thin Skin Heat Transfer Models, AD-264-096, September 1961.	DDC	No	Reviewed* Abstract	Thin Skin	Obsolete thin skin
84. Brown, D.L. and Token, K.H., Instrumentation and Recording Equipment Used in Conjunction with the ARL Twenty-Inch Hypersonic Wind Tunnel, AD-419-046, September 1963.	DDC	Uncertain	Reviewed Abstract	T/C	Conventional T/C
85. Fenival Electronics, Catalog L-1B, 63 Fountain St., Framington, Mass.	Vendor	Yes	Reviewed Article	Thermistor	Thermistor Catalog
86. Winkelmann, R.E., "Experimental Investigations of a Fin Protuberance Partially Immersed in a Turbulent Boundary Layer at Mach 5," Naval Ordnance Lab, NOL TR 72-33, January 1972.	AFWAL	Yes	Reviewed* Article	Thermopile	Wafer Thermopile bonded on heating element

*Have copy.

TABLE A-1 DIRECT MEASUREMENT TECHNIQUES (Continued)

REFERENCE	SOURCE	APPLICABLE	REVIEWED	SENSOR	SUMMARY
87. Coleman, H. W. and Lemmon, E.C., "Turbulent Heat Transfer and Pressure in the Interference Region of Fins Mounted on a Cone", Sandia Lab. Livermore, SCL-RR-720309, Feb 1973	AFWL	Yes	Reviewed* Article	Thin Skin	Thin skin calorimeter with model cooling to enhance resolution
88. Page, R. J., "Shock-Induced Separation of a Turbulent Boundary Layer:, University of Washington, Thesis,1975	AFWL	Yes	Reviewed* Article	Thin Film	Self heating of thin film
89. Stalmach, C.J., "Development in Convecture Heat Transfer Models Featuring Seamless and Selected-Detail Surfaces Employing Electroless Plating", Vought Sys. Div., Report 2-57110/5R-3227, June 1975	AFWL	Yes	Reviewed* Article	Various	Reviews use of T/C and model fabrication with metallic surface coatings
90. Spitzer, C.R., "A Comparative Performance Analysis of Pyroelectric Heat-Transfer Sensors for Use in Hypersonic Impulse Facilities;, 2nd International Congress on Inst. in Aerospace Simulation, Aug 1966	DM-89				
91. Stempel, F C. And Rall, D L., "Application and Advancements in Field of Direct Heat Transfer Measurements", ISA-J, V. 11, No. 4, p. 68-73, April 1964.	EI	Yes	Reviewed* Article	Slug, 2-D Foil, Wafer	General review of sensors
92. Starner, K.R. and Thompson, W.P., "ARC Tunnel Studies of Nonequilibrium Stagnation Point Heat Transfer," Heat Transfer and Fluid Mechanics Inst., 19th Proceedings, p. 428, June 1966.	EI	No	Reviewed Abstract	Slug and Wafer	High heat flux measurements
93. Koizumi, M. and Ichikwaw, M., "Measurement of Heat Transfer to Furnace Walls Using Thermoelectric Heat Flow Meter," Japan Soc. Mech. Eng., Bul. Vol.8, No. 32, Nov. 1965, p. 695-701.	EI	No	Reviewed Abstract	2-D Foil Cal.	Application of 2-D Foil
94. Semeriou, S., "Linear Temperature and Temperature Difference Sensor," Inst. Exp. Tech. Vol. 20, No. 1, Part 2, January 1977, p. 301-302.	EI	No	Reviewed* Article	Ferroelectric	Accuracy 0.01°C from 0 to 100°C, time constant less than 0.5 sec
95. Thomas, L.R., "Thick Film Platinum Resistance Temperature Detectors," Advanced Instr. Vol. 32, Part 2, 1977.	EI	Yes	Reviewed* Article	Pt. Resistance	Cost reductions using thick film technology
96. Leppavvori, S., "Thick Film Capacitive Temperature Sensor," Proc. Electron Components Conf. V. 28th, 1978, Publ. by IEEE (Cat. No. 78 CH1349-0 CHMT), New York, 1978, p. 47-50.	EI	Uncertain	Reviewed Abstract	Resistance	Barium Stranium Titanate resistance gage

*Have copy.

TABLE A-1. DIRECT MEASUREMENT TECHNIQUES (Continued)

REFERENCE	SOURCE	APPLICABLE	REVIEWED	SENSOR	SUMMARY
97. Johnston, K.H., "Characterization of Platinum Thin Film Resistors as Temperature Sensors," Proc. Int'l. Microelectron Symp., Minneapolis, MN, Sept. 25, 1978, Publ by Int. Soc. Hybrid Microelectronics, Montgomery, AL, p. 93-99, 1978.	EI	Uncertain	Reviewed Abstract	Resistance	High purity pt. film that requires no calibration.
98. Stroik, E.P., "RTD's Are Studier Than You Think," Instrum Control System, Vol. 53, No. 6, June 1980, p. 28.	EI	No	Reviewed Article	Resistance	Probes for rugged thin film resistors.
99. Richards, B.E., "Developments in Heat Transfer Measurements Using Transient Techniques, "Int'l. Congr. on Instrumentation in Aerospace Simulation Facilities, 7th ICIASF, December 1977, R. Mil. Coll. of Sci., Schrivenham, England, Sept. 6-8, 1977, published by IEEE (Cat. No. 77CH1251-8AES), N.Y., 1977, p. 81-88	EI	Uncertain	Reviewed Article	Thin Film	Use and calibration of thin semi-∞ gages.
100. Praul, S.N. and Hmurick, L., "Instantaneous Temperature Measurements, "Rev. Sci. Instr., Vol. 44, No. 9, Sept. 1973, p. 1363-4.	EI	No	Reviewed Abstract	T/C	Circuit for correcting T/C time lag
101. Bickle, L.W., "Measuring Transient Surface Temperatures," Instrum. Control System, Vol. 46, No. 11, November 1973, p. 59-62.	EI	No	Reviewed Article	Various	General and brief review of T/C, resistors, paints, IR.
102. Danilov, N.D., et at, "Sensitivity of Gradient Type Thermal Flux Measuring Transducers," Meas. Technology, Vol. 16, No. 8, August 1973, p. 1186-9.	EI	Uncertain	Reviewed Article	Resistance and T/C	Optimization of T/C and Thermoresistors.
103. **Riezenman, M.J., "Integrated Temperature Transducers,"**, Journal of Electronics, Vol. 47, No. 23, November 1974, p. 130-2.	EI	Uncertain	Reviewed Abstract	T/C	Silicon IC with output of 10 Mv/°C.
104. Wells, G.L., "Case for Resistance Elements," Control Eng., Vol. 21, No. 12, December 1974, p. 80-82.	EI		Reviewed Article	Resistance and T/C	Review of resistance vs. T/C devices Errors: T/C =6.3°C vs. Res. = 4.2°C.
105. Ogata, K., et al, "Thin-Film Platinum Temperature Sensor," Nat'l. Tech. Rep. Matsushita, Elect. Ind., V26n3, June 1980, p. 424-432.	EI	Uncertain	Reviewed Abstract	Thin Film	Pt. resistance thin film accuracy.

TABLE A-1 DIRECT MEASUREMENT TECHNIQUES (Continued)

REFERENCE	SOURCE	APPLICABLE	REVIEWED	SENSOR	SUMMARY
106. Grundlitz, D.W. and Smith, D.H., "Wide Range Heat Flux Measurements Using Surface Temperature Sensors," Inst. Environmental Sciences Proc., 15th Annual Tech. Meeting, Anaheim, CA, April 20-24, 1969, p. 295-300.	EI	No	Reviewed Abstract	"Surflex"	"Surflex" uses computer program to determine fluxes from semi- and finite stab.
107. Willeke, K. and Bershader, D., "Improved Thin-Film Gauge for Shock Tube Thermal Studies," Rev. Sci. Inst., Vol. 44, No. 1, January 1973, p. 22-25.	EI	Yes	Reviewed Article	Resistance	Triple-layered resistance thermometer with SiO_2 coating.
108. Trietley, W L., "A Hybrid Planinum Resistance Thermometer," ISA Proceeding of Conf., Houston, Texas, October 1980, Vol. 32, Part 2, p. 507.	ISA	No	Reviewed Article	Resistance	Pt. wire coiled on sheatned probe.
109. Gauthier, P.A., "Surface Temperature Measurement," ISA Proceedings of Conference, Houston, Texas, October 1980, Vol.32, Part 2, p. 513.	ISA	Yes	Reviewed* Article	T/C and Resistance	Review T/C and Resistance Surface Elements
110. Rogoff, G.L., "Thermocouple Structure for Measurements of Surface Temperature," Rev. Sci. Instrum., Vol. 44, No. 5, May 1973, p. 654-5.	Rev. Sci. Instr.	No	Reviewed Article	T/C	T/C junction in parallel and wrapped around cylinder
111. Progelhof, R.C., et al, "Heat Gage Measures Local Coeffi-cient," December 1970, p. 75 (Don't know source).		No	Reviewed* Article	Slug Cal.	Calorimeter with heaters to reduce conduction losses.
112. Malee, C.S. and Vitale, P., "Thermistors Make Good Thermometers," Electronic Design, No. 8, April 12, 1978, p. 90-92	ASTI	Yes	Reviewed* Article	Thermistor	Circuit to linearize output of thermistor.
113. Kwest Model 329, HTL K-West, Santa Ana, California					
114. Alexander, E.C. and Stetson, J.R., "Heatshield Performance", PDA Report, Contract F04701-77-C-0125, August 1980.					

*Have copy.

TABLE A-2. TEMPERATURE SENSITIVE COATINGS

REFERENCE	SOURCE	APPLICABLE	REVIEWED	SENSOR	SUMMARY
1. Brown, A. and Saluja, C.L., Use of Cholesteric Liquid Crystals for Surface Temperature Visualization of Film-Cooling Processes, (ASTI), J. Physics E: Sci. Inst., 11:1068-72, October 1978.	ASTI	Yes	Reviewed* Article	Liquid Crystals	Cholesteric crystals change color at calibrated temperature increments
2. Grodzka, P.G. and Facemire, B.R., Tracking Transient Temperatures with Liquid Crystals, (EI), Lett. Heat & Mass Transfers, Vol. 2, March-April 1975, p. 169-178.	EI	Yes	Reviewed Abstract	Liquid Crystals	Accuracy is reviewed
3. Lorenz, G.C., Heat Transfer Measurements of Entry Cones with Maneuvering Surface in Simulated Wind Tunnel Testing of Ceramic Cones with Heat-Sensitive Paint, (IAA), A65-21460, 11-1510, AIAA J. Vol. 3, p. 774, April 1965.	IAA	No	Reviewed Article	Paint	Delectotemp Paint
4. Kafka, P.G., et al, Heat Transfer Coefficients for Aerodynamically Heated Wind Tunnel Models Measured by Means of Temperature-Sensitive Paints, (IAA), A65-24454, 14-2008, J. Spacecraft & Rockets, Vol. 2 p. 475, May 1965.	IAA	No	Reviewed Article	Color Change Point	Four color change points to determine model heating distributions
5. Jones, R.A. and Hunt, J.L., Phase Change Photographs Used for Quantitative Aerodynamic Heat Transfer Data with Surface Coating Mate... (...), AIAA Paper 65-131, A65-28865, 18-2719, J. Spacecraft ..., Vol. 2, p. 632, July 1965.	IAA	No	Reviewed Article	Fusible Paint	Fusible paints to determine model heating distributions
6. Czysc, P. and D... ., "Thermographic Heat Transfer Measurement", Instrumen... Control Systems, Vol. 41, p. 71, October 1968.	IAA	Yes	Reviewed* Article	Thermal Phosphor	Describes paint selection, application and data acquisition of phosphors
8. Improved Accuracy with Phase-Change Paints, (NASA AECI), LANGLEY-12025, B77-10212 06.	IAA	Uncertain	Reviewed Abstract	Fusible Paint	Improved processing procedures to enhance accuracy of heating definition
9. Czysz, P. and Dixon, W.P., Quantitative Heat Transfer Measurement Using Thermographic Phosphors, (EI), SPIE-J, Vol. 7, No. 3, March 1969, p. 77-79.	EI	Yes	Reviewed* Article	Thermal Phosphor	Same as #6 above
11. Klien, E.J., Liquid Crystals in Aerodynamic Testing, Aeronautics and Astronics, Vol. 6, No. 7, July 1968.		Yes	Reviewed* Article	Liquid Crystals	Oescribes crystal sensitivity, range and method of application and use

*Have copy

TABLE A-2. TEMPERATURE SENSITIVE COATINGS (Continued)

REFERENCE	SOURCE	APPLICABLE	REVIEWED	SENSOR	SUMMARY
12. Jones, R.A. and Hunt, J.L., Use of Fusible Temperature Indicators for Obtaining Quantitative Heat-Transfer Data, NASA TR-R-230, N66-16162, 66 p. 973., 1966.	NASA TR	No	Reviewed Article	Fusible Paints	Melting paints to obtain heating distribution
13. Romanowski, R.F. and Steinberg, I.H., Development of an Apparatus to Measure Thermophysical Properties of Wind Tunnel Heat Transfer Models, (FI), NASA CR-2434, Sept. 1974.	NASA CR	Yes	Reviewed* Article	Fusible Paints	Heat source/shutter to heat model for measurement of of $\sqrt{\rho ck}$ of model
14. Hefner, J.N., Effect of Geometry Variations on Lee-Surface Vortex-Induced Heating for Flat-Bottom, Three-Dimensional Bodies at Mach 6, NASA Technical Note D7447, November 1973.	NASA TN	No	Reviewed Article	Fusible Paints	Qualitative indication of heating using fusible paints
15. Keyes, J.W., Off Centerline Shock Interference Heating Patterns on Basic Shapes in Hypersonic Flows, NASA Technical Memo X-2866, December 1973.	NASA TM	No	Reviewed Article	Fusible Paints	Qualitative definition of heating using fusible paints
16. Experimental Investigation at Mach 8 of the Effects of Projections and Cavities on Heat Transfer to a Model of the Viking Aeroshell, NASA Technical Memo X-2541.	NASA TM	No	Reviewed Article	Fusible Paints	Qualitative definition of heating using fusible paints
17. Investigation of Three-Dimensional Shock Wave Boundary Layer Interactions. See reference OM-53	AFWAL	Yes	Reviewed* Article	Liquid Crystals	Same as OM-53
18. Scholer, H., "Application of Encapsulated Liquid Crystals on Heat Transfer Measurements in the Fin-Body Interaction Region at Hyperson Speed", AIAA Paper 78-777, 1978.	Referenced in OM-53	Yes			
19. Durao, M.C., "Investigation of Heat Transfer in Straight and Curved Retangular Ducts Using Liquid Crystal Thermography," (STAR), [AD-A)45131], 04P0474, N78-13381, June 1977.	STAR	Yes	Reviewed Atstract	Liquid Crystals	Vortex heating measurements using liquid crystals
20. Vennemann, D., "The Application of Temperature-Sensitive Crystals to Aerodynamic Investigations," [ESRO-TT-77], 14P1599, (STAR), N75-22290, January 1974, P. 28, OFVLR, Porz, West Germany, Report DLR-FB-73-121, August 1973, Orig. German Report avail. from DFVLR, Porz, W. Ger., 10.50DM, (ESTRO-TT-77; OLR-FB-73-121).	STAR	Yes	Reviewed Abstract	Liquid Crystals	Review and application of liquid crystals to thin & thick skin models (In German)

*Have copy

TABLE A-2. TEMPERATURE SENSITIVE COATINGS (Continued)

REFERENCE	SOURCE	APPLICABLE	REVIEWED	SENSOR	SUMMARY
21. Ponteziere, J., "Method of Measuring Thermal Flux of Walls by Thermosensitive Paints," (STAR), N68-13764, 04p0597, ONERA-TP-470, 1967.	STAR	No	Reviewed Abstract	Paints	Nothing useful (In French)
22. Eaves, R.M., et al, "Heat Transfer Investigation of Langley Research Center Wing Configurations at Mach 10.5," (STAR), N72-22894, 13p1808, NASA-CR-120036, DM5-DR-1224-Vol. 1., March 1972.	STAR	Uncertain	Reviewed Abstract	Phosphor Paint	Heat transfer measurements using direct gage & paints
23. Miller, C.S., "Use of the Isodensitracer for Reduction of Pictorial Data," SPIE 11th Annual Tech. Sym., August 1966.					
24. Brown, G.H., et al, "Liquid Crystals," Battelle Memorial Inst. April 1971.					
25. Baker, S.S. and Matthews, R.K., "Demonstration of the Thermographic Phosphor Heat-Transfer Technique as Applied to Aerodynamic Heating of External stores," AEDC-TR-73-128, November 1973.		Yes	Reviewed* Article	Phosphor Paint	Application of use of phosphors
26. Rhudy, R.W., "Flow Visualization Techniques for Use in Hypersonic Wind Tunnels," AEDC TDR-108, AD-448-116, October 1964.	DDC	Yes	Reviewed Abstract	Paint	Heat transfer measurements in low temperature wind tunnels
27. Neal, S.B.H., "Development of the Thin-Film Napthalene Mass-Transfer Analogue Technique for the Direct Measurement of Heat Transfer Coefficients," Int. J. of Heat & Mass Transfer, Vol. 18, p. 559, 1975.	AFWAL	No	Reviewed* Article	Low Temp Ablator	Naphthalene mass transfer to infer heat transfer
28. White, C.O., et al, "Cross Hatch Studies: Data Survey and Data Processing," Aeronutronic-Ford, SAMSO TR 71-300, Vol. I, December 1971.		No	Reviewed Article	Low Temp Ablator	Camphor & Naphthalene mass transfer
29. Rogers, C.E., et al, "A Thermal Mapping Technique for Shock Tunnels and a Practical Data-Reduction Procedure," AIAA Paper 72-1031, AIAA 7th Aerodynamic Testing Conference, Sept. 1972.	AFWAL	Yes	Reviewed* Article	Thermal Phosphor	

*Have copy.

TABLE A-2. TEMPERATURE SENSITIVE COATINGS (Continued)

REFERENCE	SOURCE	APPLICABLE	REVIEWED	SENSOR	SUMMARY
30. Edwards, F.J , "Non-Contact Method of Measuring Surface Temperature," Int. Heat Transfer Conf., 5th Proc., Tokyo, Japan, 3-7 September 1974, V5, papM12.4, p. 289-292.	EI	Uncertain	Reviewed Abstract	Phosphor	Phosphor coatings illuminated with UV, accuracy to 1°C
31. Kubota, H.K., "Heat Transfer Measurement by Use of Temperature Sensitive Paint - Application to a Blunted Elliptical Cone in Hypersonic Flow," Heat Transfer, Jpn Res., V 7, N 4, October 1978, p. 1-13.	EI	Yes	Reviewed Abstract	Paints	Temperature sensitive paints
32. Cesarano, A. and Vincenzo, N., "Surface Temperature Measurements by Liquid Crystals," Termotecnica (Milan), V 31, N 6, June 1977, p. 295-304.	EI	Uncertain	Reviewed Abstract	Liquid Crystals	Calibration and use. (In Italian)
33. Buetefish, K.A., "The Liquid Crystal Method for the Visualization and Measurement of Heat Transfer Distribution," Part of M-69a.	STAR	Yes	Reviewed* Article	Liquid Crystals	Review and use of liquid crystals
34. Durnez, C.H., et al, "Liquid Crystal Fiberoptic Temperature Probe," STAR 08, p. 977, N76-17373, Utah University, AD-AD14655 June 1976, 21 p.	STAR	Uncertain	Reviewed Abstract	Liquid Crystals	Crystals for fiber optics, LED illuminated crystal.
35. Ouden, C. and Hoogendoorn, C.J., "Local Convective Heat Transfer Coefficients for Jets Impinging on a Plate - Experiments Using Liquid-Crystals," Proc. of 5th Int. Confer., Tokyo Japan, 3-7 Sept. 1974, Vol. 5, Society of Heat Transfer Japan, 1974, 293-397.	IAA	Uncertain	Reviewed Abstract	Liquid Crystals	Use of liquid crystals in wind tunnels
36. Cooper, T.E., et al, "Liquid Crystal Thermography and Its Application to the Study of Convective Heat Transfer," J. of Heat Transfer, V97, pp. 442-450, August 1975.	IAA	Uncertain	Reviewed Abstract	Liquid Crystals	Use of liquid crystals in wind tunnels
37. Matthews, R.A., "Aerothermal Mapping and Photographic Data Processing at AEDC," Inter. Congress on Instrumentation in Aerospace Simulation Facilities, 5th, Pasadena, Calif., September 1973, also AEOC-TR-73-90, (A0762928), June 1973.	IAA	Uncertain	Reviewed Abstract	Paint	Phase change paint

TABLE A-2. TEMPERATURE SENSITIVE COATINGS (Continued)

REFERENCE	SOURCE	APPLICABLE	REVIEWED	SENSOR	SUMMARY
38. Giannini, F., et al, "Liquid Crystal Improved Technique for Thermal Field Measurements," Applied Optics, Vol. 18, No. 17, Sept. 1979, p. 3048-52.	ASTI	Yes	Reviewed* Article	Liquid Crystals	Use of liquid crystals to measure temp. over 5°C with resolution of 0.1°C.
39. Trimmer, L.I., et al, "Measurement of Aerodynamic Heat Rates at the AEDC vonKarman Facility," Inter. Congress on Instrum. in Aerospace Simulation Fac., 5th, Pasadena, Calif. Sept. 1973.	OS-40				
40. Carter, L.D., "Supersonic Boundary-Layer Transition Detection Using Thermographic Phospherescent Paint," M.S. Thesis, Univ. of Tennessee, March 1975.	OS-40				
41. Segletes, J.A., "Errors in Aerodynamic Heat Transfer Measurements When Using Phase Change Coating Techniques," J. Spacecraft and Rockets, Vol. 12, No. 2, Feb. 1975.	OS-40	Uncertain	Reviewed* Article	Phase Change Paint	Correction factors for 2-D conduction effects
42. Maise, G. and Rossi, M.J., "Lateral Conduction Effects on Heat Transfer Data Obtained with the Phase-Change Paint Technique," NASA-CR-2435, Grumman, August 1974.	OS-40				
43. Stone, D.R., et al, "Factors Affecting Phase-Change Paint Heat-Transfer Data Reduction with Emphasis on Wall Temperatures Approaching adiabatic Conditions," AIAA Paper No. 72-1030 AIAA 7th Aerodynamic Testing Conf., Palo Alto, Calif, September 1972.	OS-40				

*Have copy.

TABLE A-3. OPTICAL SYSTEMS

REFERENCE	SOURCE	APPLICABLE	REVIEWED	SENSOR	SUMMARY
1. Goldstein, R.J., Interferometer for Aerodynamic and Heat Transfer Measurements (ASTI), R. Sci. Inst., 36:1408, 10 October 1965.	ASTI	No	Reviewed Abstract	M-Z Schlieren and Laser	
2. Sernas, V. and Fletcher, L.S., Schlieren Interferometer Method for Heat Transfer Studies, (ASTI), Journal of Heat Transfer, 92:202-4, February 1970.	ASTI	No	Reviewed Article	Schlieren	Boundary layer characterization. Extrapolate to define surface heating
3. Rotem, Z., et al, Semifocusing Color Schlieren System for Use in Fluid Mechanics and Heat Transfer, (ASTI), Applied Optics, 8:2326-8, November 1969.	ASTI	No	Reviewed Article	Schlieren	Flow visualization
4. Hauf, W. and Grigull, U., Heat Transfer Measurements Based on Optical Methods with Temperature Dependence of Refractive Index Making Temperature Field Visible, (IAA), 21, p. 3826, A70-41373, Advances in Heat Transfer, Vol. 6, p. 133, 1970.	IAA	No	Reviewed Article	Schlieren	Flow visualization
5. Grigull, U., Heat Transfer Visualization, Discussing Shadowgraph, Schlieren and Interference Methods, (IAA), 24, p. 3890, A71-45147, Proceedings of International Heat Transfer Conf., 4th, Versailles, France, Aug-Sept. 1970, Vol. 9 (A71-45146 24-33), Amsterdam, Elsevier Pub. Co., p. 7-21.	IAA	No	Reviewed Abstract	Shadowgraph Schlieren & Interference	Flow visualization
6. Black, W.Z. and Carr, W.W., Application of a Differential Interferometer to the Measurement of Heat Transfer Coefficients, (ASTI), Sci. Inst., 42:337-40, March 1971	ASTI	No	Reviewed Article	Differential Interferometer	Flow visualization
7. Richardson, P.D., Schlieren Methods for Heat Transfer Measurement Using Light Ray Diffraction to Determine Temperature Profile, (IAA), A65-21847, 11-1552, Int. J. of Heat and Mass Transfer, Vol. 8, p. 557, April 1965.	IAA	No	Reviewed Abstract	Schlieren	General description of Schlieren
9. Brooks, R.G., et al, Mach-Zehnder Interferometer Use in Field Study of Heat Transfer without Disturbing Temperature Distributions, (IAA), 09, p 1593, A68-22952, Measurement and Control, Vol. 1, p. T9-T16, January 1968.	IAA	No	Reviewed Abstract	M-Z Schlieren	

*Have ...

TABLE A-3. OPTICAL SYSTEMS (Continued)

REFERENCE	SOURCE	APPLICABLE	REVIEWED	SENSOR	SUMMARY
11. Sernas, V., et al, Interferometric Heat Flux Measuring Device, (ASTI), ISA Trans. 11, No. 4:346-57, 1972.	ASTI	No	Reviewed Article	Interferometer	Flow visualization, very complex for non-axisymmetric models
12. Sandhu, S.S. and Weinberg, F.J., Laser Interferometer for Combustion, Aerodynamics and Heat Transfer Studies, (ASTI), J. Physics E: Sci. Inst., 5:1018-20, October 1972.	ASTI	No	Reviewed Article	Laser Interferometer	Flame temperature field measurements
13. Optical Systems Using Moire Patterns to Obtain Qualitative Data in Boundary Layer, (EI), ASME Paper 67, HT-3 for Meeting of 6-9 August 1967, 8p.	EI				
14. Aung, W. and O'Regan, R., Holographic Interferometer for Heat Transfer Measurement, Studying Free Convection Thermal Boundary Layer on Heated Isothermal Vertical Flat Plate, (IAA), 04 p. 0524, A72-15531, Rev. Sci. Instr., Vol. 42, p. 1755, Dec. 1971.	IAA	No	Reviewed Article	Holographic Interferometer	
15. Black, W.Z. and Norris, J.K., Interferometric Measurement of Fully Turbulent Free Convection Heat Transfer Coefficients (IAA), 10p, 1466, A74-24788, Rev. Sci. Instr., Vol. 45, p. 216, Feb. 1974.	IAA	No	Reviewed Article	Interferometer	Flow visualization
16. Long, S.A., et al, A Simplified Holographic-Interferometry Technique for Real-Time Flow Visualization and Analysis, NASA TN D-7421.	NASA TN	No	Reviewed Article	Interferometer	Flowfield visualization
17. Creel, T.R. and Hunt, J.L., Photographing Flowfields and Heat Transfer Patterns in Color Simultaneously, (ASTI), Astronautics & Aeronautics, 10:54-5, April 1972.	ASTI	No	Reviewed Abstract	Schlieren and Phase-Change Coatings	Flowfield and heating measurements
18. Bernal, G.E., Heat Flow Analysis of Laser Absorption Calorimetry, (ASTI), Applied Optics, 14:314-21, February 1975.	ASTI	No	Reviewed Article	Laser	Calorimeter to measure laser absorption coefficient of gasses
19. Kaufman, Y. and Gersten, A., Simultaneous Heating and Temperature Measurements by an Infrared Laser Beam, (ASTI), Applied Optics, 15:353-7, February 1976.	ASTI	No	Reviewed Article	Laser	Measures temperature of gas absorption cells
20. Laser Holograms Aid in Heat Transfer Studies, (ASTI), Design News, 33:33-7, November 1977.	ASTI				

*Have

TABLE A-3. OPTICAL SYSTEMS (Continued)

REFERENCE	SOURCE	APPLICABLE	REVIEWED	SENSOR	SUMMARY
21. Hopkins, H. and Lacinski, T.M., "Pressure & Heat Transfer Measurements on 1/45th Scale Space Ferry in Grumman Hypersonic Shock Tunnel at Mach 14 & 19," (STAR), N65-24971, 14p2458, Grumman Aircraft RM-249, November 1964.	STAR	No	Reviewed Abstract	Schlieren	Flow visualization
22. Schepers, H.J., "Heat Transfer Investigations of Axisymmetric Bodies at Hypersonic Speeds by Means of Infrared Measurement," (STAR), N72-19319, 10p1325, DRL-Mitt-71-19, October 1971.	STAR	Yes	Reviewed Abstract	IR	Compares IR systems (In German)
23. Hardy, R.G. and Paddock, D.A., New Thermal Radiative Flux Gage, (EI), ISA Trans., Vol. 6, No. 1, January 1967, p. 15-19.	EI	No	Reviewed* Article	IR	Conventional radiometer using thin film resistor
24. Gershchenko, O.A., Dynamic Characteristics of an Absolute Radiometer, (EI), Heat Transfer Sov. Res., Vol. 7, No. 3, May-June 1975, p. 116-118.	EI	Uncertain	Reviewed Abstract	IR	Radiometer
25. Dimeff, J., Self-Calibrating Radiometer, NASA Tech. Brief, ARC-10811, B76-10339 03, Jan 1977.	NASA TB	No	Reviewed Abstract	Differential T/C	Conventional radiometer
26. Bynum, D.S., et al, "Measurement and Mapping of Aerodynamic Heating in VKF Tunnel B with Infrared Camera," AEDC-TR-76-54, (STAR), 16p2079, N77-26116, AD-A033116, November 1976.		Yes	Reviewed Article	IR	IR measurements on hemisphere-cone
27. Boylan, D.E., et al, Measurement and Mapping of Aerodynamic Heating Using a Remote Infrared Scanning Camera in Continuous Flow Wind Tunnels, AIAA 10th Aerodynamic Testing Conference, April 1978.		Yes	Reviewed* Paper	IR	Design details of IR scanner and data reduction
28. Volluz, R.J., Handbook of Supersonic Aerodynamics, Sec. 20, Wind Tunnel Instrumentation and Operation, NOD-261-682, January 1961.	DDC	No	Reviewed Abstract	Schlieren	Flow visualization
29. Grosse-Wilce, H. and Uhlenbusch, J., "Measurement of Local Mass-Transfer Coefficients by Holographic Interferometry," Int. J. Heat and Mass Transfer, Vol. 21, p. 677-82, 1977.	AFWAL	No	Reviewed Article	Interferometry	Camphene model to infer heating by dense vapor.

*Have copy.

TABLE A-3. OPTICAL SYSTEMS (Continued)

REFERENCE	SOURCE	APPLICABLE	REVIEWED	SENSOR	SUMMARY
30. Compton, D.L., "Convective Heating Measurements by Means of an Infrared Camera," NASA TM X-2507, Space Shuttle Aerothermodynamics Tech. Conference, Vol II - Heating, N72-20856, 11p1532, Dec. 1971, N72-20857 to N72-20870.	DM-89	Uncertain	Reviewed Abstract	Various	Describes shuttle heat transfer test. T/C, phosphor, Schlieren, thin film, IR camera, phase-change paint
31. Hsieh, C.K. and Ellingson, W.A., Quantitative Determination of Surface Temperature Using an Infrared Camera," SPIE Proc V124: Mod. Util. Infrared Tech. 3, San Diego, Calif, Aug. 25, 1977, Publ. by SPIE, Bellingham, Wash., p. 228-35.	EI	Uncertain	Reviewed Abstract	IR	Methods for reducing errors due to surface reflections
32. Hsieh, C.K. and Su, K.C., "Design, Construction and Analysis of a Continuous-Temperature Infrared Calibrator for Temperature Measurement Using an IR Scanner," Rev. Sci. Instrum., V50N7, July 1979, p. 888-896.	EI	Yes	Reviewed* Article	IR	Design and Checkout of an IR calibrator. Unique scanner and data reduction equipment.
33. Wickershein, K.A. and Alves, R.B., "Optical Temperature Measurements," Ind. Res. Dev., V21N12, December 1979, p. 82-89.	EI	Yes	Reviewed* Article	Various	Liquid crystal, phosphors and other coatings, excellent article
34. Mangold, R.W., "IR - Yes or No," Instrum. Control System, Vol. 53, No. 6, January 1980, p. 28-29.	EI	No	Reviewed Article	IR	Review of industrial uses of optical pyrometers
35. Mehta, J.M., "Errors Associated with Interferometric Measurement of Convective Heat Transfer Coefficients," Applied Optics, Vol. 16, No. 6, June 1977, p. 1755-59.	EI	No	Reviewed* Article	M-Z and Interferometer	Errors on M-Z and differential interferometer free convection measurements
36. Dung, W., and O'Regan, R., "Precise Measurements of Heat Transfer Using Holographics Interferometry," Rev. Sci. Instrum. Vol. 42, No. 12, December 1971, p. 1755-59.	EI	No	Reviewed Abstract	Holographic Interferometry	Studies of free convection
37. Schepers, H.J., "Optical Measuring Method for Heat Transfer Rates of Models in Hypersonic Wind Tunnels," Dtsch Luft Ranfahrt, Mitt DLR Mitt 73-20, 1973, p 91-117, also ERD-TR-72-9, March 1971.	EI	Uncertain	Reviewed Abstract	Paints	Temperature sensitive paints
38. Greelish, W.T., Non-Contact Temperature Measuring Systems Applied to Industry," ISA Adv. in Instrum., Vol. 31, Part 4, 1976, p. 807.	ISA	No	Reviewed Article	IR	Pyrometer systems

*Have copy.

TABLE A-3. OPTICAL SYSTEMS (Continued)

REFERENCE	SOURCE	APPLICABLE	REVIEWED	SENSOR	SUMMARY
39. Watson, J.L., et al, "A New Scanning Thermometer," J. of Physics E: Sci. Instrum., Vol. 4, 1971, p. 1029-35.		Yes	Reviewed* Article	IR	
40. Boylan, D.E., et al, "Measurement and Mapping of Aerodynamic Heating Using a Remote Infrared Scanning Camera in Continuous Flow Wind Tunnels," AIAA 10th Aerodynamic Testing Conf., San Diego, Calif, April 1978.		Yes	Reviewed* Article	IR	IR errors and sensitivity to low and high temperature wind tunnels
41. Thomann, H. and Frisk, B., "Measurement of Heat Transfer with an Infrared Camera," Inter. J. Heat and Mass Transfer, Vol. 11, 1968, p. 819-26.					
42. Kantsios, A.G., "Infrared Scanners for Temperature Measurement Measurement in Wind Tunnels," Proceedings of 3rd Biennial IR Information Exchange, St. Louis, Missouri, August 1976.					
43. "Update on IR Scanning," Power, October 1977, p. 89-92.		Yes	Reviewed* Article	IR	Reviews various sensors commercially available
44. Martellucci, A., et al, "IR Mapping of Boundary Layer Transition on a Slender Cone," 26th Int'l Instrum. Symposium, Seattle, Wash., May 1980, ISA.		Yes	Reviewed* Article	IR	Use of OS-40 instrument for RV heating studies
45. Asthermer, R.W., "Temperature Measurement by Infrared Thermal Images," Barnes Engineering, Co.		Yes	Reviewed* Article	IR	Summary of different state-of-the-art scanners
46. Rammenzwerg, D. "Techniques of Electroforming and their application in Constructing Models for Hypersonic Experiments," ESRO-TT-9, January 1974.	TS-18	Yes	Review Abstract		

TABLE A-4. MISCELLANEOUS

REFERENCE*	SOURCE	APPLICABLE	REVIEWED	SENSOR	SUMMARY
3. Sensor for Finding Heat Flux, (ASTI), Inst. Tech., 14:53, March 1967.	ASTI	No	Reviewed Abstract		Large 3" dia. sensor
6. "Materials Senser to Measurement Heat Flow," (ASTI), Electronics, 40:228, No. 2, 1967.	ASTI	No	Reviewed Article	Noncontact T/C in Heat Sink	Noncontact thermometer, use convection to equilibrate unit to surface temp.
9 Passive Recording Heat Flux Indicator, (ASTI), Fire Tech., 7:5-16, February 1971.	ASTI				
13. Simple Portable Instrument for Measuring Heat Flux Density 0.1 to 3 watts/cm^2, (ASTI), Eng. Soc. J., 3:70-6, October 1973.	ASTI				
15. Thermal Conductivity Conference (New Measurement Techniques), (EI), J App. Physics, Vol. 15, No. 11, November 1964, p. 1259-1265.	EI				Couldn't find
17. Cookson, R.A., et al, Stagnation Point Heat Flow Meter, (EI), J. Sci. Inst., Vol. 42, No. 4, April 1965, p. 260.	EI	No	Reviewed Article	Water ΔT	Cooling heater temp. rise infers surface heating
20. Design and Calibration of Small Heat Transfer Gage and Its Application, (EI), Advance in Test Meas., Vol. 5, Proceedings of 5th Annual ISA Test Measurement Symposium, 28-31 October 1968, New York ISA Pittsburgh, 1968 Paper 68-636, 10p.	EI				
21. Wide Range Heat Flux Measurements Using Surface Temperature Sensors, (EI), Inst. Environmental Sciences Proceedings 15th Annual Technical Meeting.	EI				
23. Eckert, E.R.G. and Goldstein, R.J., "Measurement Techniques in Heat Transfer, Special Summer Course, June 1968, Univ. Minnesota by the Advisory Group for Aerospace Research and Develop. of NATO, AGARD 130, Technivision Serv. Div. of Engelhard Hanovia Int. Ltd., Slough, England, 1970, 521p.	EI	Uncertain	Reviewed Abstract	Various	Calibration of T/C, resistance thermistors and pyrometers
24. Tuck, E.O., Theory for the Design of Thin Heat Flux Meters, (EI), J. Eng. Math, Vol. 6, No. 4, October 1972, p. 355-368.	EI	No	Reviewed Abstract	2-D Foil	Optimization of 2-D foil gage for particular applications

* Reference numbers not consecutive. After review, references placed in pertinent table.

TABLE A-4. MISCELLANEOUS (Continued)

REFERENCE	SOURCE	APPLICABLE	REVIEWED	SENSOR	SUMMARY
25. Schultz, D.L. and Jones, T.V., "Heat Transfer Measurements in Short Duration Hypersonic Facilities," (EI), University of Oxford, England AGARDograph, No. 165, February 1973, 149p.	EI	Uncertain	Reviewed Abstract	Various	Errors, design and use of semi-oo, pyroelectric and optical gayes.
26. Zhilyaev, I.R. and Omelick, A.I., Thermoelectrical Compensation Instrument for Measuring Thermal Fluxes, (EI), High Temp., Vol. 11, No. 2, March-April 1973, p. 332-335.	EI	NO	Reviewed* Article	Heater	Simple heater design to control calorimeter temperature
29. International Heat Transfer Conference, 5th Proceedings 3-7 September 1974, Tokyo, Japan (EI), Publ. by Japan Society of Mechanical Engineers, Tokyo.	EI				
32. Gortyshov, Y.F., et al, On the Study of Heat Transfer with the Aid of a Local Heat Flux Sensor, Sov. Aeronaut, Vol. 21, No. 3, 1978, p. 25-27.	EI	No	Reviewed Article	2-D Foil	Nothing useful
33. Measurement of Heat Transfer to Hemispherical Cylinders in a Supersonic Rarefied Air Stream, (IAA), A63-14478, 09-13.	IAA				
35. Transducer which Measures Heat Transfer Rates in Hypersonic Wind Tunnels, (IAA), A63-16831, 13-15.	IAA				
37. Wind Tunnel Measurements of the Pressure and Heat Transfer Distribution on Blunt, Axisymmetric Re-entry Type Bodies with Laminar Boundary Layers at Zero and at Large Angles of Yaw in Supersonic and Hypersonic Airstreams, (IAA), A63-25589, 24-02.	IAA				
38. Poliakov, I.A., Meas. Thermal Flux Produced in Reflection of Shock Waves from Plane Heat Cond. Wall, 21, p. 3836, A66-39412, Teplofizika Vøysokikh Temp., Vol. 3, p. 879, Dec. 1965, High Temp., Vol. 3, Nov. 1965, p. 818-26.	IAA	Uncertain	Reviewed Abstract		Method not described in abstract. Article in Russian.
39. Poliakov, I.A., Exponential Point Method Measurement of Heat Fluxes and Surface Temp. in Unsteady Regime, 11, p. 1882, A67-24030, Teplofizika Vysokikh Temp., Vol. 5, Jan. 1967, p. 37.	IAA	No	Reviewed Abstract	Analysis	Analysis to derive heat flux from undefined sensor temp. response
40. Radioactive and Convective Heat Flux Measuring Instruments Calibration for Aerospace Industry, (IAA), 23 p. 4006, A67-41375. 22nd ISA Conference, Vol. 22, Part II, 1967.	IAA	Uncertain	Reviewed Abstract	Calibration	High Cal Engineering Standard Calibrations procedures

*Have copy.

TABLE A-4. MISCELLANEOUS (Continued)

REFERENCE	SOURCE	APPLICABLE	REVIEWED	SENSOR	SUMMARY
41. Pelepeichenko, I.P., et al, Heat Receiver with Correcting Device for Instantaneous Temperature Measurements in Unsteady Gas Flow, Discussing Matching of Time Constants and Heat Transfer Coefficient, (IAA), 13 p. 2118, A67-26352.	IAA	No	Reviewed Abstract		Slow time response gage. Type not identified in abstract
44. Softley, E.F., et al, Transition of Hypersonic Boundary Layers on Concial Body Using Shock Tunnel, Obtaining Surface Transfer Distributions, (IAA), AIAA Paper 68-39, p. 1482, A69-21943, AIAA J., Vol. 7, Feb. 1969, p. 257-263.	IAA	No	Reviewed Article	Unknown	Doesn't describe heat transfer gages, just reviews data
48. Cvetkovic, M., Heat Flow Measurement, Discussing Operation Principles, Heat Conduction, and Stationary and Transient Temperature Conditions, (IAA), 17, p. 3082, A70-34681, Archive for Tech. Messen und Industriell, June 1970.	IAA	No	Reviewed Abstract		Heater circuit (In Yugoslavian)
49. Same as M-23.					
50. Kuchriashev, L.I. and Mel'Shikh, N.L., Heat Transfer Measurement in Shock Tubes, (IAA), 21, p. 3106, A74-41775, Aviatsonnaia Tekhnika, Vol. 17, No. 11, p. 94, 1974.	IAA	No	Reviewed Abstract	Analysis	Analysis of undefined gage (In Russian)
51. Gauge Material Effects on Convective Heat Transfer Measurements in Shock Tubes, (IIAA), A64-16882, 10-13.	IAA				
52. Measurement of Rapidly Changing Temperature in Medium with Unknown Heat Transfer Conditions, (IAA), A64-20223, 16-15.	IAA				
53. Application of a New Test Method and a New Wind Tunnel Data Processing Technique to the Study of Unsteady Heat Conduction Processes, (IAA), p. 0228, A78-27455.	IAA				
54. Lemcke, B., Heat Transfer Measurements on a Delta Wing with Blunted Leading Edges in Hypersonic Flow (NASA AECI), (FFA-TN-AU-648-PT-3), 07, p. 0798, N76-16039, March 1975.	NASA AECI	No	Reviewed Abstract	Schlieren and oil flow	Unsuccessful in measuring heating
55. Johnson, C.B. and Taylor, A.H., Heat Transfer and Pressure Measurement on a Simulated Elevon Deflected 30 Degrees Near Flight Conditions at Mach 7, (STAR), (NASA-TM-X-3563), 22 p 2973, N77-31440, Sept. 1977.	NASA TM	Uncertain	Reviewed Abstract	Doesn't State	

TABLE A-4. MISCELLANEOUS (Continued)

REFERENCE	SOURCE	APPLICABLE	REVIEWED	SENSOR	SUMMARY
56. Aerodynamic Heat Transfer to a Hypersonic Research Aircraft Model/ x-24C at Mach 6, (NASA AECI), p. 0051, A77-14557.	NASA AECI				
57. Measurement of Heat Transfer Rate to a Gas Turbine Stator, (NASA AECI), (ASME Paper 7-GT-119), p. 0039, A79-32935.	NASA AECI				
58. Huff, R.G., A Simplified Method for Determining Convective Heat Transfer Coefficients, NASA Tech. Brief, LEWIS-11156, B70-10575 03, Oct. 1970, NASA-TN-O-5520 and NASA-TM-X1980.	NASA TB	No	Reviewed Abstract	T/C	Measures hot & cold fluid temp separated by wall to infer heat transfer
61. Kilgore, R.A., et al, The Cryogenic Wind Tunnel Concept for High Reynolds Number Testing, NASA Tech. Note D7762, November 1974.	NASA TN	No	Reviewed Article		Wind tunnel design, no instrumentation
63. Stainback, P.C., et al, Experimental Studies of Hypersonic Boundary-Layer Transition and Effects of Wind Tunnel Disturbances, NASA Technical Note D7453, March 1974.	NASA TN	Yes	Reviewed* Article	Thin Film and Thin Skin	Platinum thin-film gages mounted on glass inserts and also thin skin T/C. Data correlation report.
64. Baumeister, K.J. and Papell, S.S., Effect of Gage Size on the Measurement of Local Heat Flux, NASA Tech. Memo X-2943, November 1973.	NASA	No	Reviewed Article	Thin Foil	Predicts local heat flux gradients with sensor of discrete size.
66. Schepers, H.J., Flow and Heat Transfer Measurements in Corner Regions at Hypersonic Speeds, (STAR), [ESA-TT-302], 01P0066, N77-10481, June 1976.	STAR	Uncertain	Reviewed Abstract	Doesn't State	(In German)
67. Mueller, W.J., Development of an Apparatus for Measuring the Influence of Certain Surface Parameters on Aerothermal Heating of High-Speed Missiles, (STAR), 23P3162, N77-33080, Orittes Symposium, 1976, BMVg-FBWT-76-19-Pt-1.	STAR	No	Reviewed Abstract	Doesn't State	Model design & testing in slip flow (In German)
68. Bulmer, R.M., Base Pressure and Heat Transfer Measurements on a Slender Reentry Vehicle at Freestream Mach 18, (STAR), [SAND-74-56], 05P0531, N75-14079, July 1974.	STAR	Uncertain	Reviewed Abstract	Doesn't State	
69. Bachour, F. and Erdtel, O., Experimental Investigations of Heat Transfer in Blunt Cones in Hypersonic Flows at Very Low Densities, (STAR), [DLR-FB-75-28], 24P2996, N75-33008, Feb. 1975.	STAR		Reviewed Abstract	Doesn't	(In German)

*Have copy.

TABLE A-4. MISCELLANEOUS (Continued)

REFERENCE	SOURCE	APPLICABLE	REVIEWED	SENSOR	SUMMARY
69a. Methods for Heat Transfer Measurements, February 1976, 164p., Transl. into English of "Verfahren zur Warmeuebergangsmessung," DGLR, Cologne Report DLR-Mitt-75-11, 1975, 165 p., Proceedings of Meeting of DGLR Sci. Comm. 3.4 on "Testing Tech. in Fluid & Thermo," Gottingen, West Germany, 11 March 1975, Orig. German report avail. from DFVLR, Cologne DM 55.80, [ESTA-TT-260; DLR-MitM-75-11] (STAR) 22P2862, N76-31460, N76-31461 to N76-31467.	STAR	Yes	Reviewed * Article	Socket T/C, Liquid Crystals, Thin Skin	
70. Hours, Y., Measurement of Friction and Heat Transfer at Mach 2 and High Reynolds Numbers, (STAR) 03P0392, N76-12997, (ESA-TT-193), Sept. 1975.	STAR	Uncertain	Reviewed Abstract		Abstract doesn't describe concept (In French)
71. Richards, B.E., Heat Transfer and Pressure Measurement on a Concave Conic Model under Both Steady and Unsteady Hypersonic Flow Conditions, [AD-A069883], (STAR) 21P2763, N79-30150, Nov. 1978.	STAR	Uncertain	Reviewed Abstract	Unknown	Heat transfer measurements at m = 15 and 20
72. Siler, L.G. and Deskins, H.E., "Effect of Shock Impingement on the Heat Transfer and Pressure Distributions on a Cylindrical Leader Edge Model at Mach 18," (STAR), N65-12042, 02 P 0358, AEDC-TDR-64-228, AD-451128, Nov. 1964.	STAR	Uncertain	Reviewed Abstract	Unknown	Abstract doesn't describe concept
73. Meckler, L., "Heat Transfer Measurements at Mach 8 on an Aerodynamically Controllable Winged Reentry Configuration," (STAR) N65-14323, 04P0525, FDL-TDR-64-142, AD-608830, Sept. 1964.	STAR	Uncertain	Reviewed Abstract	Unknown	Testing of Delta Wings
74. Grey, J., "Thermodynamic Methods of High Temperature Measurement," WPAFB, 1964, Contract AF33(657)-9962, N65-15782, 06P0995, ARL-64-179; AD-609977.	STAR	No	Reviewed Abstract	Enthalpy Probes	Probes for measuring high enthalpy gasses
75. Whitehead, A.H. and Dunavant, J.C., "A Study of Pressure and Heat Transfer over an 80° Sweep Slab Delta Wing in Hypersonic Flow," (STAR) NASA-TN-D-2708, N65-19279, 09P1364, March 1965.	STAR	Uncertain	Reviewed Abstract	Unknown	Abstract doesn't describe concept
76. Picken, J., "Free Flight Measurements of Pressure and Heat Transfer in Regions of Separated and Reattached Flow at Mach up to 4," (STAR), N65-27414, 16P2852, ARC-CP-706; RAE-AERO-2643.	STAR	Uncertain	Reviewed Abstract	Unknown	Abstract doesn't describe concept

*Have copy.

TABLE A-4. MISCELLANEOUS (Continued)

REFERENCE	SOURCE	APPLICABLE	REVIEWED	SENSOR	SUMMARY
77. Rumsey, C.B. and Lee, O.B., "Heat-Transfer Measurements on a Blunt Spherical Segment Nose to a Mach of 15.1 and Flight Performance of the Rocket-Propelled Model to Mach of 17.8," (STAR), N65-28448, 17P3028, NASA-TM-X-77, November 1959.	STAR	Uncertain	Reviewed Abstract	Unknown	Abstract doesn't describe concept
78. Ledford, R.L., et al, "Recent Developments in Heat-Transfer Rate, Pressure and Force Measurements for Hot Shot Tunnels," (STAR), N67-23357, 11P1857, AEDC-TR-66-228, AD645764.	STAR	Uncertain	Reviewed Abstract		Abstract doesn't describe concept
79. Stalling, R.R. and Burbank, P.B., "Heat Transfer and Pressure Measurements on a Concave-Nose Cylinder for Mach 2.49 to 4.44," (STAR), N67-32134, 18P3188, NASA-TM-X-221, October 1959.	STAR	Uncertain	Reviewed Abstract		Abstract doesn't describe sensor
80. Edward, J.B.W., "Heat Transfer and Pressure Measurements on the Upper Surface of a Delta Wing at Incidence at Mach 2.0 and 3.6," (STAR), N68-13550, 04P0436, ARC-R&M-3469, RAE-TR-65144, ARC-27235, 1967.	STAR	Uncertain	Reviewed Abstract		Abstract doesn't describe sensor
81. Ellison, J.C., "Experimental Stagnation Point Velocity Gradients and Heat Transfer Coefficients for a Family of Blunt Bodies at Mach 8 and Angles of Attack," N69-22554, 11P1802, NASA-N-D-5121, April 1969.	STAR	Uncertain	Reviewed Abstract		Abstract doesn't describe sensor
82. Wollenberger, H.J., "Problems of Heat Transfer in Solid State Body Calorimetery," N70-30406, 15P2778, JUL-621-FN, November 1969.	STAR	Uncertain	Reviewed Abstract		Sensor error analysis (In German)
83. Owen, F.K., "Transition Experiments on a Flat Plate at Subsonic and Supersonic Speeds," AIAA J., Vol. 8, No. 3, p. 518, March 1970.	AIAA	No	Reviewed Article	Thin Film	Pt. thin film on pyrex to
84. "High Temperature Heat-Transfer Measurements."	Aerospace				
85. Everhart, P.E., "Heat Transfer Measurements on a Low-Fineness-Ratio Cylinder at a Mach No. of 10.4...Angles of Attack From..." NASA-TM-X-1400, N67-36743, 17P3176, July 1967.	Aerospace	Uncertain	Reviewed Abstract		Abstract doesn't describe concept
86. Pappos, C.C., "Measurement of Heat Transfer in the Turbulent Boundary Layer on a Flat Plate in Supersonic Flow and Comparison with Skin-Friction Results," NACA TN 3222, June 1954.	Aerospace				
87. "Model Instrumentation Techniques for Heat Transfer & Force Measurements in a Hypersonic Shock Tunnel," AD97238.	Aerospace				

TABLE A-4. MISCELLANEOUS (Continued)

REFERENCE	SOURCE	APPLICABLE	REVIEWED	SENSOR	SUMMARY
88. Xerikos, S. and Sterger, H.H., Experimental Investigation of Heating Due to Differential Antenna Windows - Heatshield Ablation Occurring at Hypersonic Speeds, MDAC Paper WD2568, Presented at 11th U.S. Navy Symposium on Aeroballistics, 22-24 August 1978.	Aerospace	Yes	Reviewed* Article	IR Scanner, Phosphors,	Excellent example of using instrumental concepts, their applications, data reduction and measurement comparison
89. Smotherman, W. E., Recent Developments in Heat-Transfer-Rate, Pressure and Fource Measurements for Hotshop Tunnels. AEDC-TR-66-228, AD-645-764, January 1967	DDC	No	Reviewed Abstract		Development of transducers
90. Bate, J., Temperature Measurements in Wind Tunnels, RAE-1736, AD-922-12D, June 1974	DDC	Uncertain	Reviewed Abstract	Direct Measure	Thermistors, Resistance elements, T/C.
91. Naysmith, A., Measurement of Aerodynamic Heat Transfer in Intermittent Wind-Tunnels, ARC-CP-780, AD-B-D28-398, January 1964	DDC				
92. Morgan, C.C. and Andrews, J. S., "Morgandyne" Heat Transfer Transducer and Flame-Torch Calibration Technique for Hypervelocity Wind Tunnels AEDC TR-60-1, AO-232-236, February 1960	ODC	Uncertain	Reviewed Abstract	Thermistor	
93. Trussell, D. H., et al, A Radiant Heater to Simulate Aerodynamic Heating in a Wind Tunnel, NASA TN D-53D, AD-245-413, November 196D.	DDC				
94. Brower, E. M., Instrumentation Survey for a Hypersonic Low-Density Wind Tunnel, AO-255-924, May 1961.	DDC				
95. Kaufman, L. G. and Meckler, L., Pressure and Heat Transfer Measurements at Mach 5 and 8 for a Fin-Flat Plate, AD-406-724, April 1963.	DDC				
96. Kubota, H., "A Study of the Interaction Between a Glancing Shock Wave and a Turbulent Boundary Layer", Cranfield Institute of Technology, Aug 1980.	AFWAL				
97. Thomann, H., "Measurements of Heat Transfer and Recovery Temperature in Regions of Separated Flow at M=1.8", FFA Report 82, 1959	AFWAL				

*Have copy.

TABLE A-4. MISCELLANEOUS (Continued)

REFERENCE	SOURCE	APPLICABLE	REVIEWED	SENSOR	SUMMARY
98. Laumann, G.A., "A Steady-State Heat Meter for Determining Heat-Rate of a Cooled Surface." (STAR), N63-18868, 18Pi356, JPL 1963, NASA-CR-50626.	AFWAL	No	Reviewed Abstract	Wafer T/C	Teflon wafer
99. DDC AD-BD22-958, Misc. heat flux gages	AFWAL				
100. Unknown author, "Thermal Effects of Shockwave Turbulent Boundary Layer Interaction at Mach 3 and 5", North American Aviation, Columbus, NA62H-795, Nov 68.	AFWAL				
101. Charwat, A. F. and Redekopp, L. G., "Supersonic Interference Flow Along the Corner of Intersecting Wedges" Rand Corp. Memo RM-4863-FR July 1966	AFWAL				
102. Unknown author, "Heat Transfer and Recovery Temperatures on a Sphere with Laminar, Transitional and Turbulent Boundary Layers at M=2.0 and 4.15", NACA TN 4125, 1956	AFWAL				
103. DeRose, C. and Yee, L., "Tech. for Producing Wind-Tunnel Heat Transfer Models," NASA Tech Brief B72-10349-03, ARC-10659, Dec. 1972	DM-89	Uncertain	Reviewed Abstract	Thin Skin	
104. Collins, D. J., "An Inexpensive Technique for the Fabrication of Two-Dimensional Wind Tunnel Models" Rev. Sci. Instrum. Vol 44, No. 7, p. 855, July 1973.	DM-89	No	Reviewed Article	Pressure	Pressure measurements on air foils
105. Bynum, D. S., "Instrumentation for the AEDC/VKF 100 inch Hotshot (Tunnel F), AEDC -TR-209, Jan 67.	DM-89				
106. Ledford, K. L., et al, "Recent Developments in Heat Transfer Rate, Pressure, and Force Measurements for Hotshot Tunnels", AEDC-TR-66-220, Jan 67.	DM-89				
107. Bodgon, L., "Instrumentation Techniques for Short-Duration Test Facilities", Cornell Aero.Lab. Aerosciences Div. Report WTH-D30, March 1967	DM-89				
108. Czysz, P. A. and Kendall, D. N., "Improved Methods in Wind Tunnel Technology", McDonnell Co. Report F938, April 1968	DM-89				

TABLE A-4. MISCELLANEDUS (Continued)

REFERENCE	SOURCE	APPLICABLE	REVIEWED	SENSOR	SUMMARY
109. Saltveld, J.R., "Survey of Temperature Measurements", At. Energy Can Ltd., AECL Report No. 5394, March 1979, 43 p.	EI	Uncertain	Reviewed Abstract	Various	Survey of measurement techniques
110. Hall, J., "Guide to Temperature Monitoring," Instrum. Control System, V. 51, N. 6, June 1978, p. 57-61.	EI	No	Reviewed* Article	Various	General review of temperature instrumentation
111. Griffing, B.F. and Shivashankas, S.A., Use of Light-Emitting Diodes as Temperature Sensors," Rev. Sci. Instrum., Vol. 48, No. 9, September 1977, p. 1225-6.	EI	Uncertain	Reviewed* Article	LED	LED chip good from 4 to 300°K
112. Kraabel, J.S., "Isothermal Heat Flux Sensor," ASME Paper No. 78-WA/HT-14, December 1978, 6p.	EI	Uncertain	Reviewed Abstract		Accuracy to 2%
113. Goldstein, R.J., "Some Measurement Techniques in Heat Transfer," Int. Heat Transfer Conf., 6th, Toronto, Dnt., 7 Aug. 1978, Publ. by Nat'l. Res. Council of Canada, Avail from Hemisphere Publ. Corp., Washington, DC, Vol. 6, p. 495-505.	EI	No	Reviewed Abstract	Mass Transfer and Optical Interf.	Naphthalene mass transfer analogy and extrapolation using optical interferometry
114. Hall, J., "Applying Temperature Sensors," Instrum. Control Sys., Vol. 53, No. 6, June 1980, p. 24.	EI	No	Reviewed* Article	Various	References other articles
115. Hudson, R.P., "Measurement of Temperature," Rev. Sci. Instrum., Vol. 51, No. 7, July 1980, p. 871-881.	EI				
116. Mackenzie, D.M., "Review of Temperature Measurement Techniques - Part 1: Optimizing the Sensor/Instrument Interface," Instrum. Tech., Vol. 23, No. 9, Sept. 1976, p. 43-48.	EI	Yes	Reviewed* Article	Various	Detailed review of TC, resistance, thermistor, IR devices
117. Bloomer, M.D., "Survey of Temperature Sensors," Proc. Electron Components Conf, 30th, San Francisco, CA, April 1980, Publ. by IEEE (Cat. No. 80 CH1568-5).	EI	Uncertain	Reviewed Abstract	Various	General survey of temperature instruments
118. Lassagne, B. and Kirsch, G., "Theoretical Analysis of the Errors Due to Stray Heat Transfer During the Measurement of Surface Temperature by Direct Contact," Int. J. Heat Mass Transfer, Vol. 23, No. 9, Sept 1980, p. 1207-17	EI	Unable to Ascertain*			(In French)

*Have copy.

TABLE A-4. MISCELLANEOUS (Continued)

REFERENCE	SOURCE	APPLICABLE	REVIEWED	SENSOR	SUMMARY
119. "Temperature: Its Measurement and Control in Science and Industry Vol. 4, Sym. on Temp. Str Proc., Washington, DC, June 21-24, 19[illegible], Publ. by ISA, Pittsburg, PA, Vol. [illegible], 2 Parts, 2383p.	EI (No. 005564)	Yes	Reviewed Abstract	Various	IR camera and scanners, phosphors and pt. films
[illegible] Sutrisno, M., "Measurement of Temperature with Optical Fibers," ISA Trans., Vol. 19, No. 4, 1980.	ISA	No	Reviewed Article	Optical Fiber	Refractive index dependent on temp.
121. Hall, J., "The Highs and Lows of Temperature Monitoring," Instrum. & Control Syst., June 1979, p. 25.		No	Reviewed Article	Various	General and brief review of T/C, resis., optical methods
122. Barber, P., "Non-Contact Temperature Measurement of Metal Surfaces in the Open," ISA Advances in Instrum., V. 33, p.1, p.417, 1978.	ISA	Uncertain	Reviewed Article	IR	Review of criteria for selecting pyro.
[illegible] Fluke Manu. Co., "New Temperature Scanner is Accurate and Inexpensive, "Electronic Design, Vol. 28, Feb. 1980, P. 165.	ASTI	No	Reviewed Article	Scanner	Scanner for temperature meas. of multiple T/C or RTD
124. "Buyers Guide to Temperature Measuring Devices," Instrum. & Control Systems, Vol. 46, Part 2, 1973.	EI	Yes	Reviewed* Article	Various	Buyers guide with vendor list
125. Neumann, R. D., "Corrections to Final Report, Contract Rosello-Gu-C-Sy[illegible]," AFWAL FIMG, letter dated 5 February 1982.					

APPENDIX B. COMPUTER MODEL

A computer code was generated to predict the temperature response of candidate sensor concepts. The code models two dimensional axissymetric - heat conduction in the radial and axial direction using finite difference techniques. The four sensor geometries of Figure B-1 can be analyzed. Four different materials, including the air void for sensors 1 and 2 of Figure B-1, can be included in the analysis. Twenty radial and ten axial nodes (200 total nodes) can be used to define the sensor. Half nodes are used on the front surface. Radiation and convective boundary conditions can be applied at the front surface. Resistance heating of the metalic skin or wafer is modeled using Eqn 4. Convective, adiabatic and constant backface temperature boundary conditions can be used at the back surface. An adiabatic condition is assumed on the circumference of the last radial nodes. Program input is defined in Table B-1.

The thermal properties that were used to analyze candidate sensor systems are presented in Table B-2. The properties were obtained from Reference DM-89.

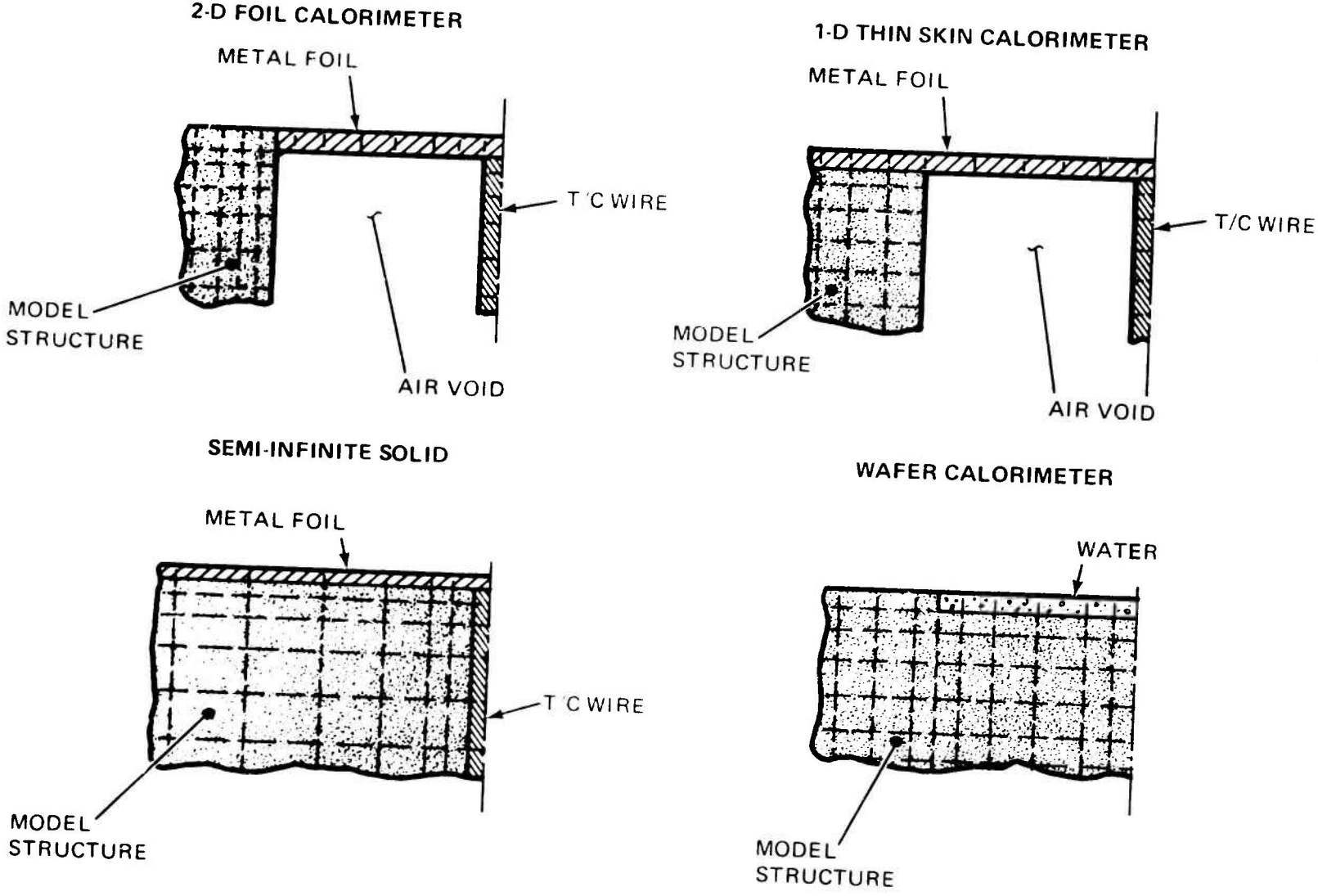

Figure B-1. Sensor Options of Computer Model

TABLE B-1. 2-D CONDUCTION PROGRAM INPUT

QCW(I) = Cold Wall Heat Flux for Node Columns 1 to NRAD, Btu/ft^2-sec.

HR = Recovery Entholpy, Btu/lb

QRS = Incident Radiation Heat Flux, Btu/Ft^2-sec.

TQRI = Time QRI Starts

TWT = Tunnel Wall Temperature, ^{o}R

IFLUID = If IFLUID = 1 Then Internal Fluid Heating; If = 2 No Internal Fluid Heating

TFLUID = If IFLUID = 1 Then Use Fluid Temp., ^{o}R; Otherwise Input Dummy, IFLUID = 1 Only for Model = 3 and 4

RTC = T/C Radius (In)

DXTC = T/C Node Thickness for Model = 2 Only. No. T/C Nodes = NIN. Model = 3. DXTC is not used.

NRAD = No. of Radial Nodes (20 Max.)

NIN = No. of Indepth Nodes (10 Max.)

DR(I) = Radial Width of Columns 1 to NRAD, Inches

DX(I) = Indepth Thickness of Node Rows 1 to NIN, Inches

In The Following, The Last Letter J is Replaced by F for Foil, TC for T/C and S for Structure:

CDJ = Thermal Conductivity, Btu/ft-sec-^{o}R

CPJ = Specific Heat, Btu/lb^{o}R

RHOJ = Density, lb/ft^3

EMIF = Surface Emissivity

EMIS = Structure Emissivity

MODEL = 1 is for 2-D Foil, = 2 is for 1-D then Skin, = 3 is for Semi-Solid and = 4 is Wafer.

NFOIL = No. Foil Nodes for 2-D Foil

= No. of Last Skin Node that is Unsupported in 1-D Thin Skin

= No. of Wafer Nodes

TEMP = Initial Temp, ^{o}R

DTF = Time Step Constant, Usually 1/2

TFIN = Final Time, sec.

TPRNT = Print Interval, sec.

TABLE B-2. MATERIAL THERMAL PROPERTIES

MATERIAL	THERMAL CONDUCTIVITY (Btu/ft sec ^{o}R)	SPECIFIC HEAT (Btu/lb ^{o}R)	DENSITY (lb/ft^{3})
Stycast 2762FT	$2.2X10^{-4}$	0.2	131.
Stycast 1095	$3.0X10^{-5}$	0.25	50.
Stycast 2850KT	$6.9X10^{-4}$	0.2	175.
Electroless Nickel (Niculoy 22)	$9.1X10^{-4}$	0.13	512.
Chromel	$3.0X10^{-3}$	0.11	545.
Constantan	$3.4X10^{-3}$	0.094	557.
Barium Titanate	$4.8X10^{-3}$	0.12	374.

APPENDIX C. SENSOR DESIGN DRAWINGS

Design and fabrication drawings were generated for the four candidate sensor systems recommended for cold wind tunnel application. Table C-1 identifies the sensor system with the applicable design drawings included as attachments to this report. Fabrication procedures are presented in the noted paragraph numbers.

TABLE C-1. SENSOR - DESIGN DRAWING IDENTIFICATION

Sensor	Assembly Drawing	Component Design Drawing	Report Paragraph with Fabrication
Wafer Thermopile (Sensor 4)	SK44309	SK44308, Model Structure SK44307-1, Water Seal Cap SK44306, Replica Model SK44305, Model Mold	3.4
2-D Foil (Sensor 2)	SK44311	SK44310, Model Structure SK44307-4, Water Seal Cap	3.2
Liquid Crystal (Sensor 10) and Thermal Phosphor (Sensor 11)	SK44313	SK44312, Model Structure SK44306, Replica Model SK44305, Model Mold	3.10 and 3.11

The critical stress loads on the model include 1) the aerodynamic loads induced by angle-of-attack testing and 2) internal pressure loads resulting from the flow of heating water in the wafer and 2-D foil sensor systems. At the maximum tunnel supply pressure (570 psia) and with the model at a 10^{0} angle-of-attach, the pressure differential from the windward to leeward sides vary from 3.2 atm at the 0.1 station (distance from stagnation point) to 0.4 atm at the 9 inch station. The resulting bending moment at the base of the 0.700 inch

diameter wafer, SK44308, is 230 in-lb. This induces a maximum stress of 8500 psi which is 3.5 times lower than the 30000 psi yield strength of 304 stainless steel. The model diameter of 0.650 inches for the liquid crystal and thermal phosphor sensors was selected to result in the same maximum stress (i.e., 8500 psi). The 2-D foil model, SK44311, has, relative to the wafer model, a larger moment of interia and therefore a lower maximum stress.

Internal water pressure is required in the wafer and 2-D foil models. At a tunnel supply pressure of 570 psia, the average cold wall heat flux over the model surface is approximately 80 Btu/ft^2 sec, see Figure 2. With a model recovery temperature of 480^o R, a water flow rate of approximately 0.08 lb/sec and an inlet temperature of 660^o R is required to maintain the model surface temperature between 600 and 640^o R. The dynamic pressure of the water in the center of the steel inlet tube is 23 psi. The pressure drop from the water inlet to the outlet is estimated to be 90 psi. Using the 3.5 factor of safety in the bending moment, the internal pressure in the model is 315 psi. In comparison to the bending loads, the hoop and tensile stresses induced by the internal water pressure are negligible.